

DECIPHERING SOURCE AND LITHOSPHERIC IMPRINTS ON MAGMAS FORMED IN A
CONTINENTAL FLOOD BASALT PROVINCE USING PETROLOGICAL AND
GEOCHEMICAL INDICIES: NW ETHIOPIAN LOW-TI FLOOD BASALT PROVINCE

By

Susan R. Krans

A DISSERTATION

Submitted to
Michigan State University
in partial fulfillment of the requirements
for the degree of

Geological Sciences—Doctor of Philosophy

2021

ABSTRACT

DECIPHERING SOURCE AND LITHOSPHERIC IMPRINTS ON MAGMAS FORMED IN A CONTINENTAL FLOOD BASALT PROVINCE USING PETROLOGICAL AND GEOCHEMICAL INDICIES: NW ETHIOPIAN LOW-TI FLOOD BASALT PROVINCE

By

Susan R. Krans

Continental Flood Basalt (CFB) provinces typically erupt low-Ti (LT) and high-Ti (HT) lavas. LT lavas typically dominate the erupted volume in CFBs; however, their magmatic origin is not well understood. This is in part because CFB lavas are not primary magmas; rather they are differentiated products which result from large volumes of melt migrating and stalling in the lithosphere prior to eruption. In addition, the magmatic plumbing systems that feed continental flood basalts are complex networks of intrusive magma bodies in the crust undergoing frequent cycling of inputs (magma recharge, assimilation), outputs (fractional crystallization, eruption), and mixing/mingling of magmas. A temporal sequence of lava flows exposed at the surface does not represent an evolving magma chamber, but rather snapshots of individual plumbing system pathways at a given point in time. For this reason, geochemistry of lava flows observed in a stratigraphic context will result in an apparently inconsistent liquid line of descent. Developing a more complete understanding of the overall system that creates CFB provinces first requires insight into how lithospheric processes impact the geochemical evolution of these magmas, and a relatively complete flow sequence is needed to accurately evaluate how the magma system evolves over time.

The Ethiopian LT flood basalt province is an ideal location to probe the lithospheric processes that impact CFB magmas because the flow-stratigraphy is well-preserved and the geochemical distinctions between LT basalt and HT basalt are well characterized. In this body

of work, 190 lava samples were collected from the LT province and analyzed by a combination of methods including petrographic analysis, bulk rock geochemical analysis, and Sr-Nd-Pb-Hf isotope analysis.

The approach of this dissertation is to use stratigraphic, petrographic, and bulk-rock geochemical datasets to first evaluate the role of lithospheric processes on the geochemical evolution of the LT province. Chapter 1 provides the theoretical framework on how magma evolves in the lithosphere and how different processes (fractional crystallization, assimilation, magma recharge, and magma evacuation) impact the liquid line of descent. Chapter 2 establishes the temporal framework, the petrographic taxonomy, and broader magmatic processes impacting the LT lavas from flood basalt initiation to termination. The results of this work establish 3 main divisions and 3 subdivisions within the LT province based on petrologic transitions observed in the stratigraphy. The transitions in the petrostratigraphic groups indicate a shallowing of the magmatic plumbing system over time. Chapter 3 evaluates the geochemical evolution of the LT basalts within the main phase of volcanism using the petrostratigraphic subdivisions determined in Chapter 2. Geochemical models are then used to constrain the depth of magma storage and relative contribution of recharge, evacuation, assimilation of crust, and fractional crystallization acting upon the plumbing system over time.

After establishing the lithospheric imprint on the LT magma evolution, a multi-component melt source is evaluated using Sr-Nd-Pb-Hf isotopic data (Chapter 4). Mixing models and assimilation and fractional crystallization models illustrate that the LT magmas originated from a multi-component melt source which includes depleted upper mantle, a known regional plume component, and a lithospheric component. It is also shown that the relative contribution of each component varies over time, from flood basalt initiation toward flood basalt termination.

I dedicate this work to my mother, Kathleen Krans and my late father, Richard Krans. My parents fostered my curiosity for the natural world and taught me how to persevere in spite of a multitude of socio-economic barriers. I would also like to dedicate this work to my incredible partner in life, Timothy Grinold, who has been unconditionally supportive in the final years of my degree—making tremendous sacrifices to give me the time and space I needed to succeed. In addition, I dedicate this to my children of another species: Lucy, Bemo, Juniper, and the late Kiki—you have each given me unconditional love and support and taught me patience and balance between work and life. Lastly, but certainly not least, I dedicate this work to everyone who ever believed in me, supported me, and to anyone inspired by what I have accomplished. Life will always present obstacles—what you do with those obstacles is up to you.

ACKNOWLEDGEMENTS

This work was supported by the United States National Science Foundation [EAR-1219647, EAR-1219459, BCS-0921009], and the support of the Michigan State University Department of Earth and Environmental Sciences.

This work was made possible through the collaborative efforts of John Kappelman, Guillaume Girard, Jasper Konter, Val Finlayson, Gezahegn Yirgu, Dereje Ayalew, and the invaluable assistance of Gabre Meskel and other members of the field team in Ethiopia, and the detailed efforts of the geochemistry sample preparation lab at Michigan State University. This work was also made possible with the guidance from my esteemed committee members, Dr. Tyrone Rooney (advisor), Dr. Julie Libarkin, Dr. Michael Velbel, and Dr. Allen McNamara.

TABLE OF CONTENTS

LIST OF FIGURES	viii
1. INTRODUCTION AND BACKGROUND	1
1.1 INTRODUCTION.....	1
1.2 MAGMA DIFFERENTIATION.....	5
1.2.1 Fractional Crystallization	7
1.2.2 Assimilation.....	10
1.2.3 Recharge-Eruption-Assimilation-Fractional Crystallization.....	11
1.3 DECIPHERING LITHOSPHERIC IMPRINTS ON MAGMA CHEMISTRY	13
1.4 APPROACHING THE SOURCE OF LT BASALTS	16
2. FROM INITIATION TO TERMINATION: A PETROSTRATIGRAPHIC TOUR OF THE ETHIOPIAN LOW-TI FLOOD BASALT PROVINCE.....	18
2.1 INTRODUCTION.....	18
2.2 BACKGROUND.....	20
2.2.1 Stratigraphy	21
2.2.2 Spatial Compositional Variability	22
2.3 METHODS.....	25
2.3.1 Stratigraphic Sampling.....	25
2.3.2 Petrography	29
2.3.2.1 Textures	29
2.3.2.2 Modal Mineralogy	30
2.3.2.3 Glomerocrysts and Megacrysts	34
2.4 RESULTS.....	35
2.4.1 Stratigraphy of the NW LT Flood Basalts.....	35
2.4.1.1 Lower Flood Basalts (540 – 940 masl).....	36
2.4.1.2 Middle Flood Basalts (850 – 1844 masl).....	38
2.4.1.3 Upper Flood Basalts (1844 – 2175 masl)	40
2.5 DISCUSSION	43
2.5.1 Decoding Magmatic Processes from Petrography and Stratigraphy.....	43
2.5.2 Conceptual Model for the Evolution of LT Flood Basalts.....	44
2.5.2.1 Lower Flood Basalt: Deep fractionation and early evolution.....	46
2.5.2.2 Middle Flood Basalt: Cyclicity, polybaric fractionation, and increasing flux	48
2.5.2.3 Upper Flood Basalt: The death of a flood basalt	53
2.5.3 Comparison with Other CFBs	55
2.6 CONCLUSIONS	58
3. MAGMA EVOLUTION DURING MAIN-PHASE CONTINENTAL FLOOD BASALT VOLCANISM: A CASE FOR RECHARGE-ERUPTION-ASSIMILATION-FRACTIONAL CRYSTALLIZATION IN THE ETHIOPIAN LOW-TI PROVINCE.....	60
3.1 INTRODUCTION.....	60

3.2 BACKGROUND.....	63
3.3 SAMPLES AND METHODS	67
3.4 RESULTS.....	68
3.4.1 Major and Trace Element Analysis.....	68
3.4.2 New Geochemical Groups.....	74
3.5 DISCUSSION	81
3.5.1 Insights from the Magmatic Stratigraphy.....	83
3.5.2 MELTS Modeling	87
3.5.3 Recharge, Evacuation, Assimilation, and Fractional Crystallization.....	90
3.5.3.1 REAFC Model Construction.....	90
3.5.3.2 Model Results.....	93
3.5.4 Improved Conceptual Model for LT Magma Evolution	97
3.6 CONCLUSIONS	101
4. MODELING THE ORIGIN OF THE ISOTOPIC SIGNATURE FOR LT MAGMAS IN THE ETHIOPIAN CONTINENTAL FLOOD BASALT PROVINCE.....	104
4.1. INTRODUCTION AND BACKGROUND.....	104
4.2. METHODS.....	108
4.3. RESULTS.....	109
4.4. DISCUSSION	114
4.4.1. Assimilation-Fractional Crystallization (AFC).....	114
4.4.2. Mixing	118
4.4.3. Temporal Variation in Source Components.....	122
4.5. CONCLUSIONS	125
APPENDICES	126
APPENDIX A: Detailed sample information.....	127
APPENDIX B: Major and trace element data and standards	128
APPENDIX C: Trace element modeling parameters.....	129
APPENDIX D: Sr-Nd-Pb-Hf isotope data and standards.....	133
APPENDIX E: Isotope modeling parameters.....	134
REFERENCES	135

LIST OF FIGURES

<i>Figure 1.1. Map of study area.</i>	3
<i>Figure 1.2. Simplified schematic of magma evolution by fractional crystallization (FC).</i>	9
<i>Figure 1.3. Simplified schematic of magma evolution by assimilation with fractional crystallization (AFC).</i>	11
<i>Figure 1.4. Simplified schematic of magma evolution by recharge, eruption, assimilation, and fractional crystallization (RE AFC).</i>	13
<i>Figure 2.1. Sample location map.</i>	24
<i>Figure 2.2. Field photos.</i>	28
<i>Figure 2.3. Photomicrographs of representative textures and modal mineralogy in the LT flood basalts.</i>	32
<i>Figure 2.4. Petro-stratigraphic column for flood basalt transects in this study.</i>	41
<i>Figure 2.5. Simplified petro-stratigraphic column of Ethiopian NW plateau LT flood basalts.</i>	45
<i>Figure 2.6. Model for magmatism in Lower flood basalt.</i>	48
<i>Figure 2.7. Model for magmatism in Middle flood basalt.</i>	52
<i>Figure 2.8. Model for magmatism in Upper flood basalt.</i>	55
<i>Figure 3.1. Sample location map.</i>	66
<i>Figure 3.2. Bivariant geochemical plots.</i>	70
<i>Figure 3.3. Chondrite normalized variation diagrams.</i>	73
<i>Figure 3.4. Primitive mantle normalized variation diagrams.</i>	76
<i>Figure 3.5. Chemostratigraphy of Middle and Upper LT basalts from the NW Ethiopian Plateau.</i>	79
<i>Figure 3.6. MELTS model results.</i>	89
<i>Figure 3.7. RE AFC Model results for shallow and deep fractionating systems within Middle group A, Low Nb/La lavas.</i>	95

<i>Figure 3.8. REAFC versus AFC and FC model results for Middle groups A, B, and C Low Nb/La lavas.</i>	96
<i>Figure 3.9. Revised conceptual model for LT magma evolution in Ethiopia.</i>	99
<i>Figure 4.1. Stratigraphic sampling of select Lower, Middle and Upper LT lavas for Sr-Nd-Pb-Hf isotope analysis.</i>	109
<i>Figure 4.2. Sr-Nd-Pb-Hf isotopic plots for Ethiopian LT lavas.</i>	111
<i>Figure 4.3. Sr-Nd-Pb-Hf isotopic plots for Ethiopian LT lavas as a function of MgO (wt. %).</i>	112
<i>Figure 4.4. Sr-Nd-Pb-Hf isotopic plots for Ethiopian LT lavas as a function of Nb/La.</i>	113
<i>Figure 4.5. Isotope AFC models for Ethiopian LT lavas.</i>	117
<i>Figure 4.6. Isotope mixing models for Ethiopian LT lavas.</i>	121
<i>Figure 4.7. Temporal changes in $\epsilon_{\text{Hf}}-^{206}\text{Pb}/^{204}\text{Pb}_{\text{initial}}$ isotopic space from Lower to Middle to Upper LT flood basalts.</i>	124

1. INTRODUCTION AND BACKGROUND

1.1 INTRODUCTION

Continental Flood Basalts (CFBs) are among the largest volcanic deposits on Earth with extrusion rates that far exceed observed historical eruptions, and yet the origin of these voluminous lavas is among the least constrained (Bryan et al., 2010). Though the lavas are dominantly basaltic, they are by no means primary magmas (the original melt composition derived from the mantle) (Cox, 1980; Hawkesworth et al., 1988; Lightfoot et al., 1993; Pik et al., 1998; Xu et al., 2001; Sheth et al., 2004; Ivanov et al., 2008). The magmatic plumbing systems that feed continental flood basalts are complex networks of intrusive magma bodies in the crust undergoing frequent cycling of inputs (magma recharge, assimilation), outputs (fractional crystallization, eruption), and mixing/mingling of magmas (Miller and Ripley, 1996, 1996; Bohrson and Spera, 2001; Spera and Bohrson, 2001; Ernst et al., 2001; Vanderkluysen et al., 2011). Unlike oceanic large igneous provinces (LIPs), continental LIPs to which CFBs belong, are considerably more difficult to interpret in terms of lithospheric imprints on magmatism (Bryan et al., 2010). For this reason, it has been difficult to constrain the origin and melt parameters responsible for producing CFBs (Baker et al., 1996b; Pik et al., 1999; Bohrson and Spera, 2001; Kieffer et al., 2004; Melluso et al., 2006; Ivanov et al., 2008).

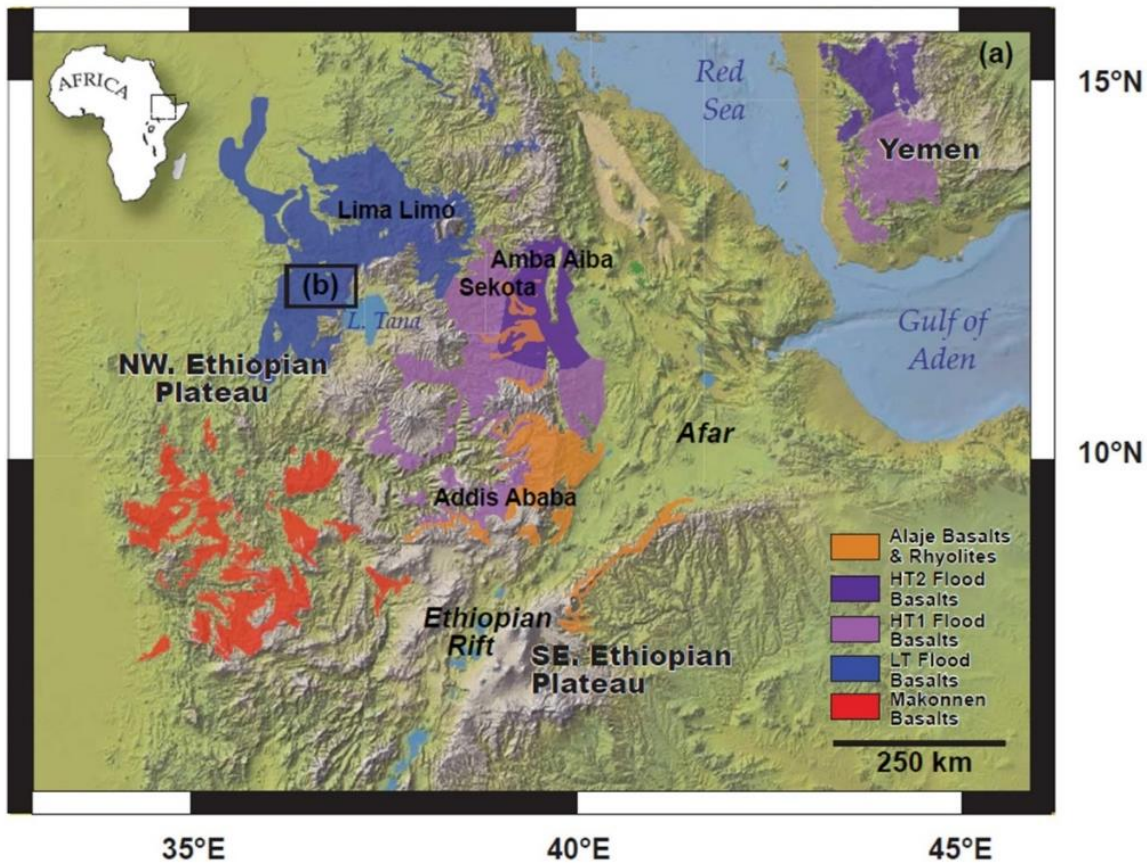
Continental flood basalt (CFB) provinces typically erupt two distinct basalt compositions—Low-Ti basalts and High-Ti basalts (Hawkesworth et al., 1988; Lightfoot et al., 1993; Sweeney et al., 1994; Melluso et al., 1995; Gibson et al., 1995; Pik et al., 1998; Xu et al., 2001; Jourdan et al., 2007; Ivanov et al., 2008; Peate and Hawkesworth, 1994). High-Ti and

Low-Ti provinces can either be temporally or spatially divided; the Ethiopian Flood Basalt province is among the latter (Pik et al., 1998, 1999). The origin of High-Ti basalts has typically been attributed to plume derived sources whereas the origin of Low-Ti basalts remains unclear (Hawkesworth et al., 1988; Lightfoot et al., 1993; Peng et al., 1994; Sweeney et al., 1994; Gibson et al., 1995; Pik et al., 1999; Xu et al., 2001; Kieffer et al., 2004; Ivanov et al., 2008). Low-Ti basalts are thought to be easily susceptible to enrichment of incompatible elements by crustal contamination due to the overall depletion in incompatible elements in the magmas themselves (Hawkesworth et al., 1988; Lightfoot et al., 1993; Pik et al., 1999). The large volume of erupted Low-Ti lavas with nearly homogeneous composition (Peate and Hawkesworth, 1994; Pik et al., 1998; Ivanov et al., 2008) requires an efficient magma plumbing system with continuous magma recharge and evacuation (Bryan et al., 2010; Lee et al., 2014). There are three prevailing interpretations to the origin of Low-Ti basalts in LIPs: 1) melt-crust interaction (Peng et al., 1994; Pik et al., 1999; Meshesha and Shinjo, 2007), 2) melt-subcontinental lithospheric mantle interaction (Hawkesworth et al., 1988; Lightfoot et al., 1993; Sweeney et al., 1994; Ivanov et al., 2008), or 3) heterogeneities in the melt source (Kieffer et al., 2004; Beccaluva et al., 2009).

Prior work shows that the Ethiopian Flood Basalt Province is spatially divided into separate, geochemically distinct, low-Ti (LT) and high-Ti (HT) provinces (Pik et al., 1998, 1999; Kieffer et al., 2004) (Figure 1.4). The clear distinction between LT and HT lava types has led to investigations of their magmatic origins using geochemical and isotopic datasets (Pik et al., 1999; Kieffer et al., 2004; Beccaluva et al., 2009; Natali et al., 2016). While the source of HT lavas has been attributed to melting of the Afar plume (Pik et al., 1999; Natali et al., 2016) or

destabilization of metasomatized lithosphere (Furman et al., 2016), the origin of LT lavas remains a topic of debate (Pik et al., 1999; Kieffer et al., 2004; Beccaluva et al., 2009).

Figure 1.1. Map of study area. a) Map of Oligocene basalts in Ethiopia and Yemen (modified from Rooney, 2017). The HT flood basalt provinces (purple) are restricted to the eastern half of the NW plateau and Yemen. The LT flood basalt province (blue) is restricted to the western half of the Ethiopian plateau. Previous studies of LT basalt are from the Lima Limo section in the north and have been reported at the base of the flood basalt sequence near Sekota (Pik et al., 1998, 1999; Kieffer et al., 2004). This study is focused west and northwest of Lake Tana (inset b). b) Inset shows location of new samples collected and studied in this work.



Relative depletion of Nb, Ta, and Ti, along with relative enrichment in Ba and Pb are observed in Ethiopian LT lavas. While some interpret this geochemical signature as evidence of crustal contamination (Pik et al., 1998), others suggest this signature can be derived from heterogeneities in the melt source (Kieffer et al., 2004; Beccaluva et al., 2009). Fractional

crystallization models using normative mineralogy (Wright and Doherty, 1970) have been used to suggest that LT magmas were derived through shallow fractionation processes (Pik et al., 1998). Subsequent trace element and isotopic analyses were used to propose a two-stage AFC process for LT magmas, indicating a lower crustal and upper crustal component influencing the geochemical trends (Pik et al., 1999). The process of assimilation of continental crust has been previously assessed using trace element ratios (Nb/La, Ce/Pb, Ba/Th) and isotopic tracers (Sr-Nd-Pb systems) (Pik et al., 1999; Kieffer et al., 2004). While some studies attribute the low Nb/La and low $^{206}\text{Pb}/^{204}\text{Pb}$ of LT magmas to crustal contamination (Pik et al., 1999; Meshesha and Shinjo, 2007) others suggest the low Nb/La and low $^{206}\text{Pb}/^{204}\text{Pb}$ could reflect source composition (Kieffer et al., 2004; Beccaluva et al., 2009). Thus, the melt source origin for LT lavas in Ethiopia remains unresolved.

The approach of this dissertation is to use stratigraphic, petrographic, and bulk-rock geochemical datasets to evaluate the role of lithospheric processes on the geochemical evolution of the LT CFB province in Ethiopia. The first of the following three chapters (Chapter 2) will establish the temporal framework, the petrographic taxonomy, and broader magmatic processes impacting the LT lavas from flood basalt initiation to termination. The next chapter (Chapter 3) will evaluate more precisely the impact of multiple lithospheric processes on the magmatic system by focusing on the most continuous lava sequence-- the middle or main-phase of flood volcanism. In this chapter, the evolution of the TL magmas will be modeled first using crystallization-only models (Rayleigh, 1896; Gualda et al., 2012), followed by more complex assimilation and fractional crystallization models (DePaolo, 1981), and finally by recharge-evacuation-assimilation-fractional crystallization models (Lee et al., 2014). The parameters estimated for magma evolution of LT basalt in chapter 3 will be used as independent constraints

while exploring a multi-component source for LT lavas in chapter 4. Chapter 4 will emphasize the importance of Sr-Nd-Pb-Hf isotopic compositions in identifying the potential origin of LT magma in Ethiopia. Potential source components have previously been defined for Ethiopian flood basalts in Sr-Nd-Pb isotopic space (Pik et al., 1999; Rooney et al., 2012a). This final chapter will evaluate the relative contribution of these previously defined source components using an assimilation and fractional crystallization model (DePaolo, 1981) and a series of binary mixing models (Powell, 1984). To understand how each chapter builds upon the preceding chapter, the next section provides fundamental background on how a magma transitions from source to surface by differentiation.

1.2 MAGMA DIFFERENTIATION

Lavas produced in LIPs are physical products of the differentiation processes that acted upon the magmatic system as it traversed the lithosphere (Cox, 1980). The ability to model the relative contribution of each of these processes and how they impact the evolution of a magma is an essential first step in tracing the original source of melt (O'Hara and Herzberg, 2002). Understanding the degree to which a magma has been imprinted by a differentiation process allows us to mathematically correct for that process to arrive at a melt composition close to primary (DePaolo, 1981; O'Hara and Herzberg, 2002; Lee et al., 2014; Bohron et al., 2014). The most common of these corrections applied is for fractional crystallization, in which the least differentiated magma is targeted and early forming mineral phases are added to back-calculate the original primary liquid composition (Wright and Doherty, 1970; Herzberg and Asimow, 2008). For this correction to be successful, one would need to assume that the influence of all other differentiation processes (assimilation, recharge-eruption, and mixing) is insignificant

(O'Hara and Herzberg, 2002). So how does one evaluate the relative contribution of these differentiation processes?

Petrographic observations reveal direct evidence of mineral phases in equilibrium with the magma at the time of eruption (i.e., crystallization; Morse, 1980), foreign materials transported by and interacting with the host magma (i.e., assimilation; Grove et al., 1988)(assimilation), and interactions between magmas (i.e., mixing/mingling; Jerram et al., 2018). Specifically, the nature of the boundary between a crystal or aggregate of crystals (solid material) and the groundmass (the liquid portion of the magma prior to eruption) in a rock can reveal a wealth of information regarding the processes that brought the magma to the surface (Jerram et al., 2018). For example, the mineral phases that crystallize from the magma are a direct result of the pressure-temperature-composition of the magma (Ghiorso and Sack, 1995). Textures, such as size of minerals, spatial distribution of minerals, and boundaries between mineral-mineral and mineral-groundmass reveal how fast the magma ascended, if it stalled for a significant period of time in the crust (residence time), and if it interacted with another magma or host rock (mixing and assimilation)(Bennett et al., 2019).

Geochemical data provide cryptic evidence of cumulative differentiation processes that acted upon the magma over time; these processes include fractional crystallization, recharge, mixing, eruption (Rayleigh, 1896; DePaolo, 1981; Powell, 1984; Lee et al., 2014; Bohron et al., 2014). Geochemical patterns in cogenetic suites of intrusive and volcanic rocks from LIPs are commonly used to identify these processes as potential influences on the magma evolution (Cox, 1980; Lightfoot et al., 1990; Pik et al., 1998; Mahoney et al., 2000; Kieffer et al., 2004; Ivanov et al., 2008; Jean, 2013; Rooney et al., 2018). Extensive experimental and empirical observations have led to the development of mathematical models used to evaluate the role of fractional

crystallization, assimilation, mixing and recharge on the major element, trace element, and isotopic ratios in these systems (Rayleigh, 1896; Anderson and Greenland, 1969; O'Hara, 1977, 1977; DePaolo, 1981; O'Hara and Mathews, 1981; Powell, 1984; Albarede, 1985; Bohrsen and Spera, 2001; Spera and Bohrsen, 2001; Nishimura, 2009, 2013). More recent work focuses on the role of evacuation/eruption coupled with recharge, assimilation, and fractional crystallization has been recognized as an important influence on the evolution of LIPs (Lee et al., 2014; Yu et al., 2015; Grant et al., 2020; Davis et al., 2021).

These two datasets (petrographic and geochemical) are not mutually exclusive and should be analyzed in tandem to reveal a more comprehensive history of the magmatic evolution of LIPs. More importantly, these observations need to have temporal constraints to give meaningful insight as to how LIPs evolve if we are to ever understand their source.

1.2.1 Fractional Crystallization

When a mineral begins to crystallize in a magma, the composition of that newly formed phase is subtracted from the initial magma composition, and the remaining liquid is called the “residual liquid” (Morse, 1980). This process, in which the crystallization of mineral phases drives the residual liquid composition away from the initial starting composition of the magma is called “fractional crystallization”, and the geochemical path formed by the evolving residual liquid is called the “liquid line of descent” (Bowen, 1928). A cogenetic suite of lavas that range from parental to evolved composition is thus needed to evaluate the liquid line of descent for a magmatic system (Bowen, 1928; Cox, 1980). The suite of lavas is typically plotted on several bivariate diagrams with a common indicator of differentiation on the x-axis (e.g., MgO decreases with evolution, SiO₂ increases with evolution). It is common practice to use major element geochemistry to track the removal of mineral phases during equilibrium or fractional

crystallization since the relative proportion of these elements are stoichiometrically fixed in the mineral structure (Ghiorso and Sack, 1995). Trace element concentrations in the residual liquid are also affected by crystallization, and the preference of any given trace element to prefer a mineral over the liquid phase is known as a partition coefficient (K_d), where K_d is equal to the concentration of an element in the mineral divided by the concentration of that same element in the liquid (McIntire, 1963). We can use the weighted sum of partition coefficients for multiple phases acting upon a liquid to estimate how fractional crystallization will influence the concentration of a trace element in the residual liquid using the Rayleigh Law (Rayleigh, 1896):

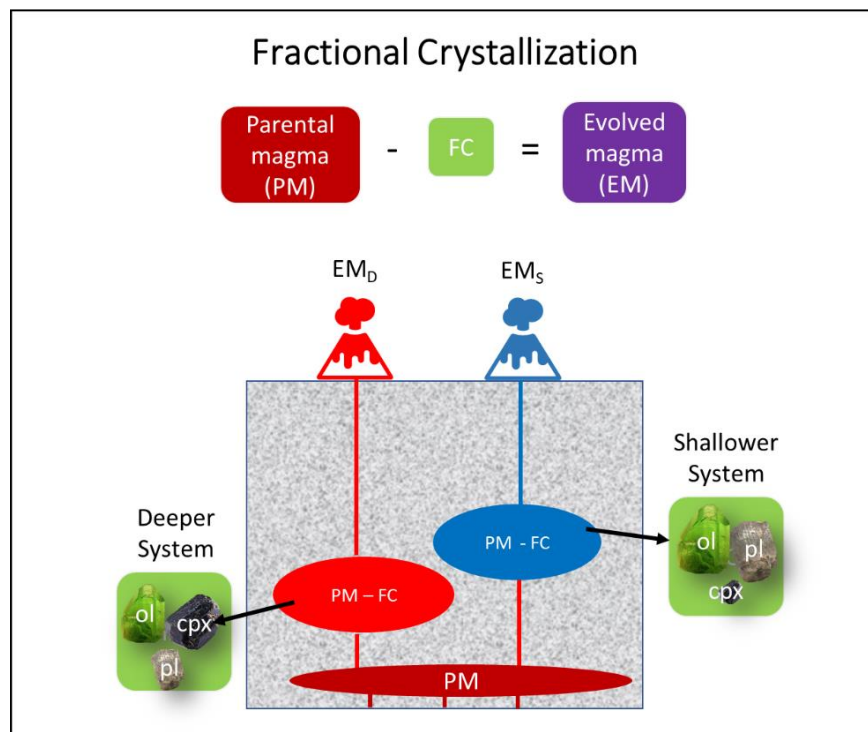
$$C_L/C_0 = F^{(D-1)} \quad \text{Eq. 1}$$

where (C_L) is the concentration of the element in the liquid, (C_0) is the initial concentration of the element in the parental liquid, (F) is the fraction of melt remaining, and (D) is the bulk distribution coefficient of the fractionating phases. If we find the most parental lava in a volcanic suite and assume that fractional crystallization is the dominant processes by which the magma differentiates, then applying this model should predict the observed liquid line of descent.

A parental melt is typically the least differentiated lava among a suite, and may be selected based upon bulk rock geochemical indicators that most closely approach a magma in equilibrium with a peridotite - a primary magma (Roeder and Emslie, 1970; Green, 1971: Mg# 66 – 75 Ni > 400 -500 ppm, and Cr > 1000 ppm). If we assume that the most parental lava in a suite of basalts has only been modified by removal of mineral phases by fractional crystallization, then the lava composition can be corrected to the primary melt composition by adding back in the composition of the phases which are assumed to have been removed (Wright and Doherty, 1970; Herzberg and Asimow, 2008). Ideally, only olivine would need to be added to a basaltic lava composition to arrive at the primary melt composition, but more complex methods have been applied when

the parental magma is suspected of having multiple phases removed (e.g., olivine +clinopyroxene; Herzberg and Asimow, 2008). In either a single-phase or multi-phase correction, the assumption that the magma composition has only been modified by removal of those phases rarely applies to the more complex magmatic provinces such as CFBs (Cox, 1980). The inability to satisfy this assumption has complicated our ability to understand the origin of melt in some of the largest magmatic provinces on Earth, and requires additional parameters to model alongside fractional crystallization. (Cox, 1980; DePaolo, 1981; Lee et al., 2014; Bohrson et al., 2014).

Figure 1.2. Simplified schematic of magma evolution by fractional crystallization (FC). Model inputs include a parental magma composition (PM) and composition of mineral phases removing a proportion of elements from the magma chamber by the process of fractional crystallization (FC). Model output is the evolved magma composition (EM) as a function of crystallizing phases removing a proportion of elements from the magma chamber. A basaltic magma chamber will crystallize olivine (ol) regardless of depth, however the crystallization of clinopyroxene (cpx) is favored over plagioclase (pl) in systems deeper than 0.5 GPa (Morse, 1980). Therefore, the evolved magma resulting from a shallow crustal magma chamber (EM_S) will have a different composition than an evolved magma resulting from a deeper crustal magma chamber (EM_D).



1.2.2 Assimilation

The heat of a magma intrusion coupled with the latent heat of crystallization has the potential to incorporate modal and cryptic signatures of the neighboring host rock (Bowen, 1928). The concentration of a trace element in a system undergoing assimilation-fractional crystallization (AFC) can be modeled if the starting concentration of the magma and concentration of the element in the wall rock assimilant are known (DePaolo, 1981):

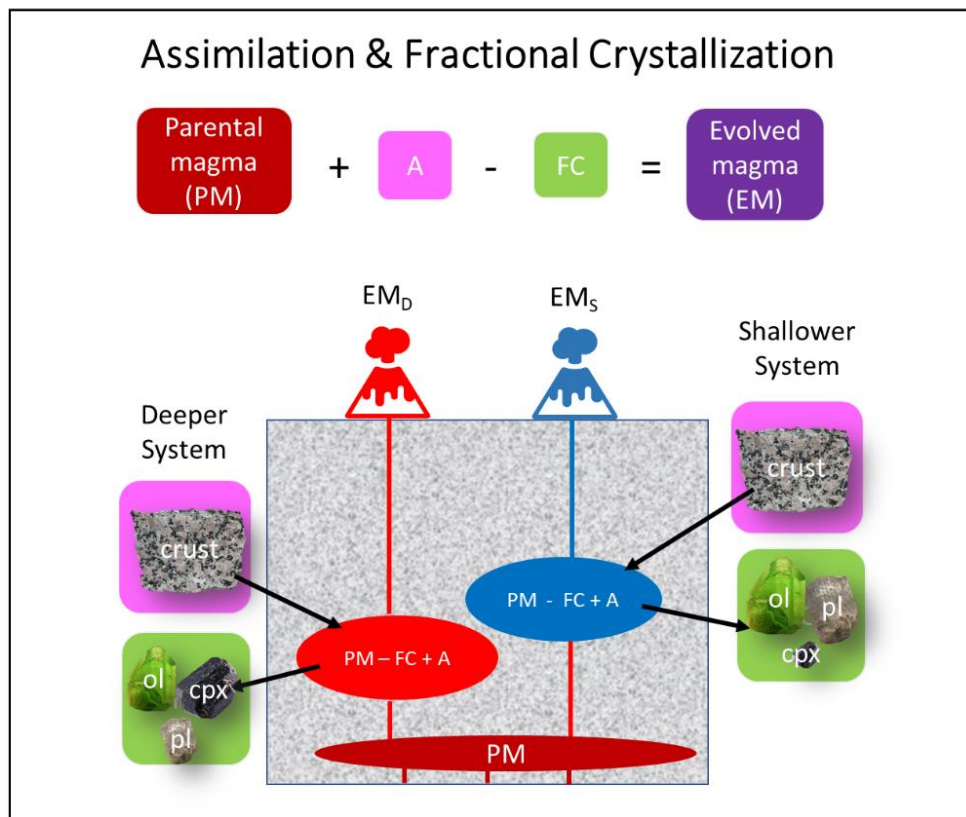
$$C_L/C_0 = f' + \frac{r}{(r - 1 + D)} \cdot \frac{C_A}{C_0} (1 - f') \quad \text{Eq. 2}$$

The ratio of the concentration of the element in the liquid (C_L) over the initial concentration of the element in the parental liquid (C_0) is a function of the concentration of the element in the parental liquid (C_0), the concentration of the element in the wall rock being assimilated (C_A), the bulk distribution coefficient of the crystallizing phases (D), the ratio of the rate of assimilation over the rate of crystallization (r), and the fraction of liquid remaining (f') (DePaolo, 1981; Rollinson, 1993). In cases where the concentration in the parental liquid and wall rock assimilant are similar, the effects of AFC will be virtually indistinguishable, therefore a strong contrast in element behavior is necessary to decipher AFC processes (Rollinson, 1993).

There is considerable geochemical and petrographic evidence to suggest that CFB magmas stall in the crust at various depths and undergo crustal assimilation in addition to fractional crystallization within the crust (Cox, 1980; Bryan et al., 2010). For this reason, AFC models are commonly used to assess the relative contribution of crustal assimilation in the evolution of CFB magmas (Peng et al., 1994; Baker et al., 2000; Xu et al., 2001; Kieffer et al., 2004; Jourdan et al., 2007). Isotopic compositions of the magma and host rock can be modeled using AFC and used as an independent check of trace element AFC modeling (DePaolo, 1981).

Even still, some challenges remain—For example, how does magma composition evolve as a consequence of cyclic recharge (new magma enters the system) and evacuation (old magma leaves the system)?

Figure 1.3. Simplified schematic of magma evolution by assimilation with fractional crystallization (AFC). Model inputs include a parental magma composition (PM), composition of crustal material adding a proportion of elements to the magma chamber by the process of assimilation (A), and composition of mineral phases removing a proportion of elements from the magma chamber by the process of fractional crystallization (FC). All other symbols are the same as in Figure 1.2.



1.2.3 Recharge-Eruption-Assimilation-Fractional Crystallization

The general concept behind the REAFC model presented by Lee et al. (2014) is that the concentration of an element in a magma chamber will eventually achieve steady state as a result of ongoing recharge. When the mass of inputs (recharge and assimilation) is balanced by the

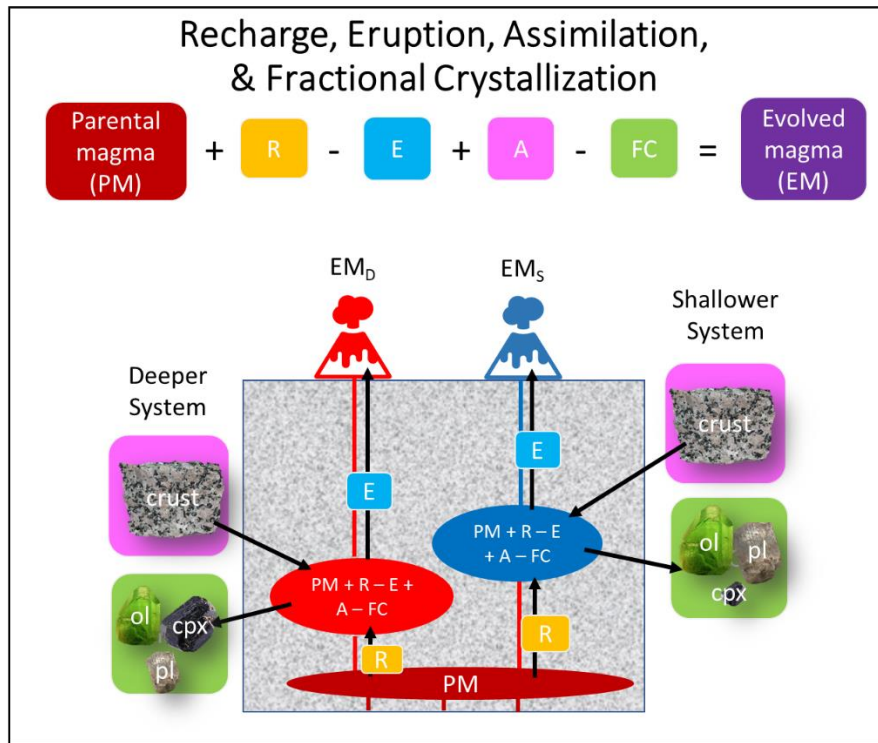
mass of outputs (evacuation and fractional crystallization), a constant mass magma chamber model can be applied.

The behavior of a trace element in a magma undergoing REAFC can be modeled using the following equation defined by Lee et al, (2014):

$$C_{ch}^{REAFC} = \frac{C_{re} + \alpha_{cc}C_{cc}}{D\alpha_x + \alpha_e} - \left[\frac{C_{re} + \alpha_{cc}C_{cc}}{D\alpha_x + \alpha_e} - C_{ch}^0 \right]^{[-\Delta\bar{M}_{re}(D\alpha_x + \alpha_e)]} \quad Eq. 3$$

where (C_{ch}^{REAFC}) is the concentration of an element in a magma chamber that has undergone REAFC, (C_{ch}^0) is the initial starting composition of the magma chamber, (C_{cc}) is the concentration of the element in the assimilate, (C_{re}) is the concentration of the element in the recharging magma, (α_x), (α_{cc}), (α_e) are the relative proportions of crystallization, assimilation, and evacuation (respectively), and ($\Delta\bar{M}_{re}$) is a time-integrated step-function as a system approaches steady-state. Specific details of this model are further discussed in chapter 3 and Appendix B, but the general take-away is that the REAFC equation allows us to track the mass balance of trace elements entering and leaving the magmatic system, and the primary take-away is that some elements may become more enriched or more depleted in a seemingly parental magma than previously thought. The consequence of the operation of REAFC is that the primary melts previously estimated for CFB provinces using other methods may not provide an accurate indication of primary magma composition. In this dissertation I explore a more comprehensive way to address this issue by combining petrographic observations and geochemical observations in a temporal framework.

Figure 1.4. Simplified schematic of magma evolution by recharge, eruption, assimilation, and fractional crystallization (RE AFC). Model inputs include a parental magma composition (PM), recharging magma composition (R), proportion of magma expelled by eruption from the magma chamber, composition of crustal material adding a proportion of elements to the magma chamber by the process of assimilation (A), and composition of mineral phases removing a proportion of elements from the magma chamber by the process of fractional crystallization (FC). All other symbols are the same as in Figure 1.2.



1.3 DECIPHERING LITHOSPHERIC IMPRINTS ON MAGMA CHEMISTRY

Chapter 2 will establish the dominant lithospheric processes the LT magmas have been exposed to enroute to the surface by evaluating variations in modal mineralogy (what phases are crystallizing) and micro textures (if phases are in equilibrium with the magma). The observed mode and textures in basalt are necessary pieces of information for constraining fractional crystallization and equilibrium crystallization models used to evaluate chemical evolution of parental magmas in a magmatic plumbing system. In addition, textural evidence of phases that are not in equilibrium with the host lava reveal information about how magma moves through

the lithosphere. For example, the presence of cumulates indicates magma is stalling, crystallizing, and re-mobilizing previously crystallized phases (Passmore et al., 2012; Óskarsson et al., 2017); this is direct evidence that recharge and evacuation occurred in the magma plumbing system.

The NW Ethiopian plateau offers a well-preserved stratigraphic sequence from flood basalt initiation to termination and is thus an important target for study of CFBs. Chapter 2 examines modal observations within a stratigraphic framework and places these observations within the context of the magmatic evolution of the Ethiopian CFB province. The petrostratigraphic data demonstrate multiple pulses of magma recharge punctuated by brief shut-down events, with initial flows fed by magmas that experienced deeper fractionation (lower crust). Broad changes in modal mineralogy and flow cyclicity are consistent with fluctuating changes in magmatic flux through a complex plumbing system, indicating pulsed magma flux and an overall shallowing of the magmatic plumbing system over time. The composition of plagioclase megacrysts suggests a constant replenishing of new primitive magma recharging the shallow plumbing system during the main phase of volcanism, reaching an apex prior to flood basalt termination.

The results of chapter 2 provide constraints for modeling recharge (R), eruption (E), and fractional crystallization (FC) in chapter 3 that could not have been determined through bulk rock chemistry alone. In particular, the results provide quantified ratios of mineral phases that crystallized in the magmas at a given time (FC over time), cumulate evidence for a polybaric magma plumbing system (R, E, and FC occur at multiple level in the crust), and changes in dominant modal mineralogy over time (changes in rate or R, E, and FC over time). Having constraints on the R, E, and FC parameters limits the amount of non-unique solutions when attempting to resolve these processes combined with assimilation (A).

Chapter 3 focuses on the main phase of volcanism in the NW Ethiopian Plateau, where the flow-stratigraphy is relatively young (~30Ma) and well-preserved. Bulk rock geochemistry is examined within the petrostratigraphic framework established in Chapter 2. MELTS models are applied to infer the depths of a polybaric magmatic plumbing system. In addition, recharge-evacuation-assimilation-fractional crystallization (RE AFC) models are used to capture the differentiation trends observed in the LT lavas. This chapter focuses primarily on the lavas that erupted during the EFB main phase of volcanism because the stratigraphy is the most complete (flow by flow) and they share a similar parental melt (as shown in Chapter 3).

Both deep and shallow magmatic plumbing systems are active throughout the main phase of LT volcanism in Ethiopia. MELTS models show that LT lavas are erupted from mid-crustal (~0.6 GPa) to shallow crustal (<0.2 GPa) depths during the main phase of volcanism. The pressure predicted by MELTS are in agreement with previous interpretations from modal mineralogy (Pik et al., 1998; Krans et al., 2018; Chapter 2).

RE AFC models show that the main phase of LT flood volcanism began with lower relative proportions of evacuation from both the deep and shallow system in Middle group A, followed by an increase in evacuation in both the deep and shallow system in Middle group B, and finally a loss of evacuation from the deep system in Middle group C. As the magma plumbing system matures, the shallower systems contribute more to eruptions than deeper systems. The combined results of the MELTS and RE AFC modeling results suggest that the LT magma plumbing system is shallowing over time as the system begins to transition toward the waning stage of volcanism. These results are consistent with petrostratigraphic observations made by Krans et al. (2018; Chapter 2). The RE AFC models also indicate that the amount of crustal contamination needed to produce the trace element enrichment patterns observed in LT lavas is less than

previously predicted from isotopic models: 4 – 10 % (Chapter 3), as opposed to the 12-25% (Baker et al., 2000; Kieffer et al., 2004).

The combined effects of lithospheric processes (REAFC) with regards to incompatible element enrichment of a magmatic system have profound implications for future investigations into the origin of LT lavas in CFB provinces, especially with regards to the role of continental crust on the geochemical imprints of LT magmas. For instance, CFBs are indeed the products of magmatic systems undergoing continuous or pulsed magma recharge and eruption in addition to fractional crystallization \pm assimilation (Bryan et al., 2010), and therefore there is a need to model these systems using a combined process model such as REAFC. Furthermore, it has been shown that the effects of recharge and eruption on magma evolution can enrich a magma in incompatible trace elements at higher MgO concentrations than typically predicted using FC, or AFC alone (O'Hara, 1977; O'Hara and Mathews, 1981; Albarede, 1985; O'Neill and Jennar, 2012; Lee et al., 2014). In this case, the primary magmas previously presumed for LT basalts may have been overestimating the concentration of incompatible elements in the primary liquid, making the search for the melt source composition, and related pressure and temperature conditions of melting difficult.

1.4 APPROACHING THE SOURCE OF LT BASALTS

Chapter 4 will evaluate the relative contribution of different potential melt/contamination sources for the LT magmas using Sr-Nd-Pb-Hf isotopes. The potential sources that will be evaluated are a depleted mantle source (DM), an enriched mantle plume source (Afar Plume), the sub-continental lithospheric mantle (SCLM), and the Pan African lithosphere (PAL). Parental and evolved lavas are used in this study from the lower, middle and upper portions of the LT stratigraphy and will be used to assess degree of contamination and source mixing over time.

After evaluation of the LT lavas in isotopic/trace element space, an SCLM component is precluded from modeling since the lavas do not deviate from the mantle array as would be expected with contribution from the SCLM. A binary mixing model (Powell, 1984) is then used to assess the relative contribution of a DM component and Afar Plume component in the source melt, and the results of this model are entered in to a second mixing model that uses PAL as a third mixing component. Finally, an assimilation with fractional crystallization (AFC) model (DePaolo, 1981) will be used to evaluate the relative influence of the PAL on melts from a mixed mantle source. Estimates for crustal assimilation determined from REAFC modeling (Chapter 3) are used as a constraint while modeling isotopic AFC in Chapter 4.

The results of this study show that the variability in the LT flood basalt isotopic compositions of the LT flood basalt is better explained using a three-component mixing model than a two-component mixing model, or AFC model. The results of the isotopic mixing models show that the relative contribution of the Afar Plume component on melt source decreases over the eruptive sequence (20 – 30 % in the lower flood basalt sequence and 10 – 20 % in the upper flood basalt sequence), while the relative contribution of the depleted mantle component increases. This shift away from the Afar Plume component toward more DM component is consistent with thermochemical erosion of the lithospheric mantle by the impinging plume head, as suggested by others. In addition, the contribution of Pan African lithosphere is greatest during the Middle flood basalt sequence (10-20 % during the main phase of volcanism) and lowest during the Upper flood basalt sequence (<10 % during the waning phase of volcanism). The exact lithospheric component driving LT magmas away from a two-component DM-Afar Plume mixed source, either by AFC or by source mixing, is yet to be constrained. However, a lower crustal origin may be likely.

2. FROM INITIATION TO TERMINATION: A PETROSTRATIGRAPHIC TOUR OF THE ETHIOPIAN LOW-TI FLOOD BASALT PROVINCE

Reprinted by permission from Copyright Clearance Center: Springer Nature, Contributions to Mineralogy and Petrology, From initiation to termination: a petrostratigraphic tour of the Ethiopian Low-Ti Flood Basalt Province, S. R. Krans et al, 2018

2.1 INTRODUCTION

The most significant manifestation of the interaction between an upwelling thermo-chemical anomaly and the continental lithosphere is the formation of a continental flood basalt (CFB) province (Ernst, 2014). CFBs are voluminous outpourings of dominantly basaltic lava (> 100,000 km² area, \geq 1 km thick) that erupt over geologically short time intervals (1 – 5 Ma, with the greatest volume erupted over ~1 Ma) (Self et al., 1997; Jerram and Widdowson, 2005). Much focus has been placed on constraining the intensive and extensive parameters of melt generation associated with upwelling plumes (Kogiso et al., 2003; Davaille et al., 2005; Herzberg and Asimow, 2008; Kimura and Kawabata, 2015). However, lavas erupted in CFBs are rarely primary, and exhibit geochemical evidence of extended residence time in the continental crust (Cox, 1980; Villiger, 2004). It is thus apparent that CFB lavas, which are preserved as well-constrained temporal sequences, reveal insights into the development of the magmatic plumbing system of a large igneous province (LIP), and by extension, the mechanisms of plume-lithosphere interaction.

Constraints as to the processes active within the plumbing system of CFBs has relied upon the extensive geochemical datasets that now exist within most LIPs (Lightfoot et al., 1990; Arndt et al., 1993; Peng et al., 1994; Pik et al., 1998, 1999; Baker et al., 2000; Mahoney et al.,

2000; Walker et al., 2002; Wolff and Ramos, 2013). These geochemical datasets provide broad constraints on the processes that control magma evolution in CFBs, namely – recharge, assimilation, and fractional crystallization (RAFC) (Lee et al., 2014; Bohrson et al., 2014). In a complex magma plumbing system, with multiple pathways of differentiation, it becomes increasingly difficult to interpret the relative influence of RAFC on magma evolution. Indeed, an assessment of existing phase assemblages and evaluation of which phases are in equilibrium with the liquid is needed to elucidate these processes. Thus, despite the utility of geochemical datasets in inferring magma differentiation processes within the magmatic plumbing system of LIPs, further refinement of these models is dependent on alternate constraints. The petrographic properties of a lava, which provide direct confirmation of phases present during the evolution of a given magma, provides such constraints.

While the utility of petrographic constraints in assessing CFB magma evolution is clearly evident, there remains a paucity of such datasets within the literature. Given the new geochemically defined frameworks for flood basalt provinces, it is timely to examine how petrographic datasets can enhance and refine conceptual models of magmatic plumbing systems in these environments. In this paper we present a petro-stratigraphic reconstruction of the western portion of the Ethiopian-Yemen flood basalt province with a detailed, flow-by-flow petrographic analysis from initiation to termination. Modal analyses indicate evidence of two fractionation regimes, one near the base of the crust (dominated by the crystallization of clinopyroxene cumulates in the absence of plagioclase), and a second in the mid- to shallow crust (dominated by plagioclase cumulates). The distribution of these cumulates through the flood basalt section facilitates a reconstruction of the magmatic plumbing system. We see distinct cycles in the evolution of the magmatic plumbing system which, over time, result in the

shallowing of magma storage from flood basalt onset to termination. Our model has broad application beyond the Ethiopian-Yemen flood basalts and provides an explanation for the frequent observation in CFBs of an initial phase of largely picritic flows followed by a main phase of compositionally homogenous flows, and which is terminated by explosive silicic volcanism.

2.2 BACKGROUND

Cenozoic plume-dominated magmatism in East Africa, extends from Turkana in the south, the southeastern Ethiopian plateau in the east, Yemen in the northeast, Ethiopia and Eritrea in the north, and Sudan in the west, and preserving a rich stratigraphic record of magmatism over the past 45 Ma (Rooney, 2017). Basaltic magmatism is divided into three time periods: Eocene initial phase (45 – 34 Ma), Oligocene trap phase (~33.9 – 27 Ma), and the Early Miocene resurgence phase (~26.9 – 22 Ma) which is later followed by bimodal lavas and silicic volcanism (Rooney, 2017). During the Eocene initial phase, volcanism was restricted to southern Ethiopia and northern Kenya and dominantly basaltic (George and Rogers, 2002; Furman et al., 2006; Rooney, 2017). Estimated magmatic flux from the Eocene initial phase is significantly lower than the Oligocene trap phase ($\sim 3 \times 10^{-4} \text{ km}^3/\text{yr}$ vs. $6 \times 10^{-2} - 1.5 \times 10^{-1} \text{ km}^3/\text{yr}$, respectively) (Ebinger et al., 1993; George et al., 1998; Rooney, 2017). During the Oligocene trap phase, the eruption of the Ethiopian-Arabian plateau flood basalts significantly increased the aerial extent of volcanism to include northern Ethiopia and Yemen (Baker et al., 1996a; Hofmann et al., 1997; Rochette et al., 1998; Rooney, 2017). There is some ambiguity as to the earliest onset of flood basalt activity in the Ethiopian-Yemen province, estimated at ~33 Ma in Turkana (Zanettin et al., 1983; Morley et al., 1992), 31.2 Ma (± 1.2 Ma) in NW Ethiopia (Hofmann et al., 1997; Rochette et al., 1998; Ukstins et al., 2002) and 30.9 Ma (± 0.24 Ma) (Baker et al., 1996a), and it could be

even earlier (Ukstins et al., 2002), The largest volume was extruded between 30 – 29 Ma (Baker et al., 1996a; Hofmann et al., 1997; Abbate et al., 2014). Following the termination of the flood basalts, volcanic activity is relatively rare except for focused activity in Turkana (Brown and Mcdougall, 2011) and sparse silicic activity and diking along the evolving Ethiopian-Yemen rift margin (Peate and Bryan, 2008; Rooney et al., 2013). In the early Miocene, a resurgence in basaltic activity occurred in the form of shield building activity in the NW Ethiopian plateau, fissure eruptions on the SE Ethiopian plateau, and increased eruptions in the Turkana region (Kieffer et al., 2004; Furman et al., 2006; Brown and Mcdougall, 2011; Rooney, 2017). Recent estimates for total lava volumes erupted from 45 – 22 Ma in the African Arabian LIP are $\sim 720,000 \text{ km}^3$, placing this province between Emeishan and Deccan LIPs in terms of overall volume (Rooney, 2017).

2.2.1 Stratigraphy

Initial stratigraphic studies, centered on the Northeastern region of the Ethiopian plateau, divided the Ethiopian flood basalts into four-divisions from oldest to youngest: Ashange basalt, Aiba fissure basalt, Alaji basalts and rhyolites, and the Termaber basalts (Zanettin et al., 1980). The Ashange is characterized by thin ($\sim 5 \text{ m}$) dipping flows restricted to only a few kilometers in extent. These flows are locally zeolitized and are unconformably overlain by flat-lying flows. The Aiba Formation is characterized by massive flows (up to 100 m when ponded) that are generally olivine basalt with columnar jointing common. Locally, sparse interbedded pyroclastic deposits of varying thickness are observed in this Formation at Amba Aiba. This Formation is overlain by the Alaji and Termaber Formations which are characterized by ignimbrites with sparsely interbedded basalt flows, and shield volcanism, respectively (Mohr and Zanettin, 1988). This initial stratigraphic division between the lower Ashange and upper Aiba was recognized as

being of limited regional utility due to the local characteristics of the type sections (deformed beds overlain by an unconformity) which are not observed elsewhere (Mohr, 1983). Subsequent research by Hoffman et al. (1997) uses the 1950 m thick Lima-Limo section north of Lake Tana to divide the Province into upper and lower units based on morphological boundaries: 1) a lower 900 m thick section of lavas capped by 150 m of differentiated products forming a significant regional terrace; and 2) an upper 1000 m thick section intercalated with silicic tuffs forming another erosional terrace. The work of Kieffer et al. (2004) assesses the transition from main-phase LT and HT flood basalt through the development of Miocene shield volcanoes, including a lower 1470 m thickness of flood basalt and nearly 300 m of overlying shield flows from three regions on the plateau. Kieffer et al. (2004) adopt the “lower” and “upper” stratigraphic divisions of Hoffman et al. (1997) and do not report significant compositional heterogeneity over time.

2.2.2 Spatial Compositional Variability

A spatial division based on geochemical differences has been assigned for flood basalts of the northwest Ethiopian plateau and includes a western Low-Ti (LT) sub-province (the focus of this study), and an eastern High-Ti (HT) sub-province (Pik et al., 1998). The LT basalts are tholeiitic with characteristically low TiO_2 (1 – 2.6 wt. %), low Nb/La (0.55 – 0.85), and higher SiO_2 (47 – 51 wt. %) (Pik et al., 1998). The LT basalts are characterized petrographically as having hypocrystalline coarser-grained (intergranular and aphyric-ophitic) textures, 0 – 10% phenocrysts that are predominately plagioclase \pm olivine, and often glomerophyric (Pik et al., 1998; Beccaluva et al., 2009; Natali et al., 2016). Groundmass contains plagioclase, interstitial clinopyroxene (colorless in PPL), and Fe-Ti oxides (Pik et al., 1998); these characteristics are consistent among tholeiitic magmas. The HT basalts are further subdivided into HT1 and HT2, where HT1 lavas represent a continuum between LT and HT2 magma types. The HT1 basalts are

aphyric to ol-phyric and range from microcrystalline to coarser-grained textures. Plagioclase is rare as a phenocryst phase and tends to exhibit sieve texture when present. Olivine is common in the groundmass, along with pinkish clinopyroxene (in PPL) and abundant Fe-Ti oxides, consistent with more alkaline magmas with respect to LT magmas. HT2 lavas are transitional basalts and picrites with higher TiO₂ (2.6-5 wt. %), higher Nb/La (1.1 – 1.4), and lower SiO₂ (44 – 48.3 wt. %) (Pik et al., 1998). HT2 basalts are typically porphyritic with olivine as the dominant phenocryst phase ± pinkish Ti-rich clinopyroxene, Cr-spinel, and rare plagioclase, again consistent with transitional to alkaline lavas (Pik et al., 1998). The groundmass contains similar phases plus Ti-magnetite with rare alkali feldspar and phlogopite (Beccaluva et al., 2009).

The clear distinction between LT and HT lava types has led to investigations of their magmatic origins using geochemical and isotopic datasets (Pik et al., 1999; Kieffer et al., 2004; Beccaluva et al., 2009; Natali et al., 2016). While the source of HT lavas has been attributed to melting of the Afar plume (Pik et al., 1999; Natali et al., 2016), the origin of LT lavas remains a topic of debate (Pik et al., 1999; Kieffer et al., 2004; Beccaluva et al., 2009). Fractional crystallization models using normative mineralogy originally proposed by Pik et al. (1998) suggested that LT magmas were derived through shallow fractionation processes. Subsequent trace element and isotopic analysis proposed a two-stage AFC process for LT magmas, indicating a lower crustal and upper crustal component influencing geochemical trends (Pik et al., 1999). Assimilation of continental crust has been assessed using trace element ratios (Nb/La, Ce/Pb, Ba/Th) and isotopic ratios (Sr-Nd-Pb systems) (Pik et al., 1999; Kieffer et al., 2004). While some studies attribute the low Nb/La and low ²⁰⁶Pb/²⁰⁴Pb of LT magmas to crustal contamination (Pik et al., 1999; Meshesha and Shinjo, 2007) others suggest the low Nb/La and

unradiogenic Pb could reflect source composition (Kieffer et al., 2004; Beccaluva et al., 2009). The issue regarding the origin of LT magmas remains largely unresolved due to the difficulty of constraining AFC processes using whole rock geochemistry. We present petrography of individual flows within the LT stratigraphy of the NW Ethiopian plateau and use these datasets to evaluate magma-lithosphere interactions.

Figure 2.1. Sample location map. a) Map of Oligocene basalts in Ethiopia and Yemen (modified from Rooney, 2017). The HT flood basalt provinces (purple) are restricted to the eastern half of the NW plateau and Yemen. The LT flood basalt province (blue) is restricted to the western half of the Ethiopian plateau. Previous studies of LT basalt are from the Lima Limo section in the north and have been reported at the base of the flood basalt sequence near Sekota (Pik et al., 1998, 1999; Kieffer et al., 2004). This study is focused west and northwest of Lake Tana (inset b). b) Topographic relief map showing sample locations in this study including exposure of the underlying Pan African granite (basement) and tuff near base of sequence. Symbols represent different stratigraphic transects. The upper limit of the Tana escarpment is shown by dashed line. Gondar graben boarder fault near Aykel town (solid line) as noted in Mège and Korme (2004). The division between the escarpment and lowlands occurs just below 1000 masl.

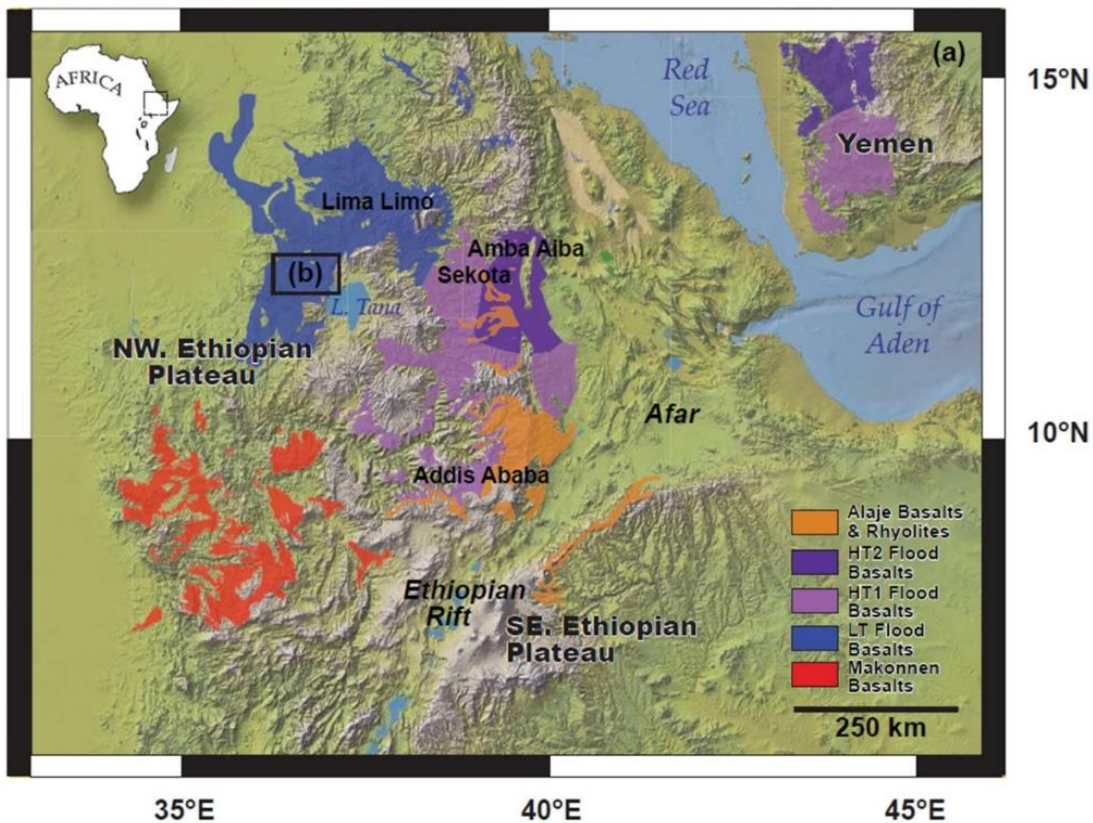
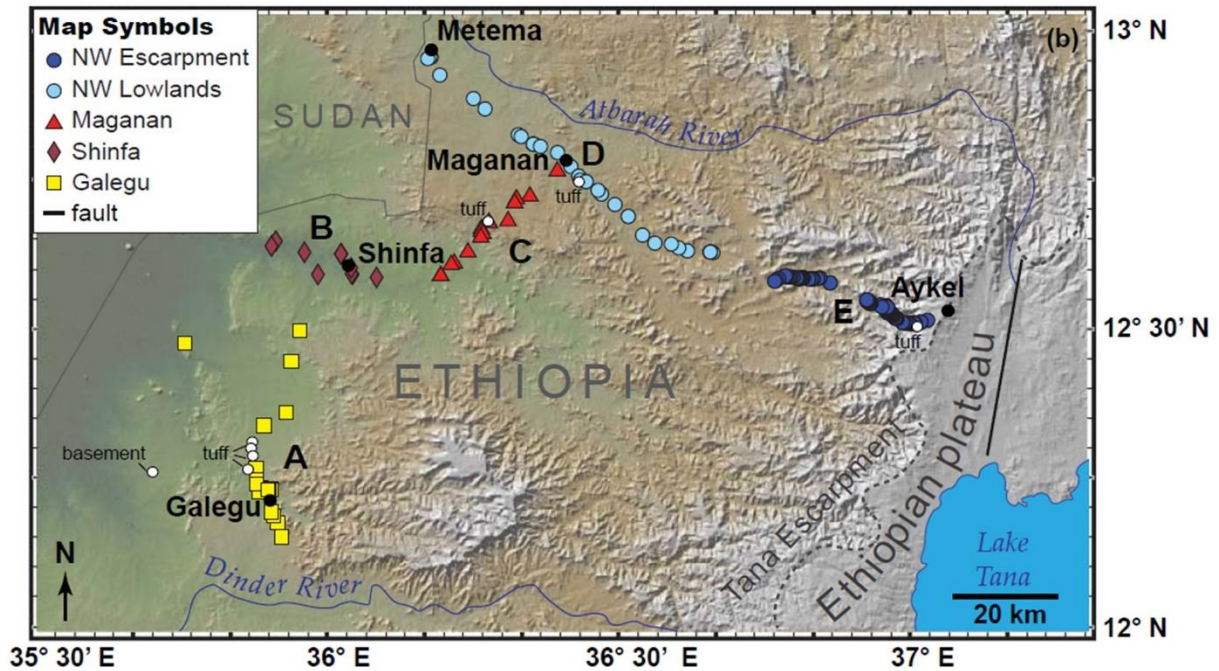


Figure 2.1. (cont'd)



2.3 METHODS

2.3.1 Stratigraphic Sampling

Samples were collected from the far western region of the northwest Ethiopian plateau erosional escarpment and lowlands over the course of two field seasons (2010 and 2014; Figure 2.1a and 2.1b). Because flood basalt in this region is predominately flat lying (Figure 2.2a), the superpositional relationship of individually sampled flows was clear, especially when stacks of flows could be traced from one exposure to another, sometimes over several 100 m. Sample sites were recorded with a handheld GPS (see Supplementary Table A.1 in Appendix A). Elevation was also recorded and used as a proxy to log stratigraphic sequences over short distances at the outcrop scale; however, given the large error ($\sim\pm 10$ m) inherent with most handheld GPS units, elevation was used as a rough proxy within a new series of exposed flows,

and this value was paired with visual confirmation between flow contacts and height estimates of individual flows in the field over outcrop scales.

Continuous sampling of individual flows within the 1635 m thick sequence was performed at generally fresh road-cuts along five transects (Figure 2.2.1b). At higher elevations (> 950 masl), the deeply eroded upper flood basalt sequence forms steep competent slopes and cliffs along the Tana escarpment (see Kappelman et al., 2014, Figure 2.2). Flood basalt flows are also found exposed across the top of the plateau but faulting near Aykel town and north of Lake Tana disrupt the stratigraphic relationship of these flows (Chorowicz et al., 1998; Mège and Korme, 2004). For this reason, we elect to use the western top of the escarpment as the upper boundary of our stratigraphic transects. The NW-SE trending NW Escarpment transect covers ~30 km from 2175 masl near Aykel town, down the erosional escarpment to 987 masl at the start of the lowlands. This section is well-preserved and exposes >1100 m of lava flows over ~30 kms in length. At ~1260 masl there is a relatively flat segment that extends for ~ 8 km along this transect; continuity in lava flows was traced along this segment and no samples were collected. At lower elevations (< 950 masl), the slope is much more gradual, and outcrops are usually isolated (Figure 2.2 1b; also see Kappelman et al., 2014, Figure 2.2). The NW Lowlands transect continues west for another 65 km from 940 to 720 masl, ending just east of the Ethio-Sudan border. The Maganan transect trends NE-SW and covers ~ 30 km of lowland flows from 900 – 610 masl. The Shinfa transect trends E-W and covers ~21 km of the lowest flood basalt exposure (589 – 540 masl). The Galegu transect trends N-S and covers ~38 km from 932 – 564 masl.

A total of 190 of the freshest basalt lava flows were sampled from the LT province. A sledgehammer was used to break through exposed surfaces, and this sampling protocol served to avoid areas of alteration and weathering rinds. Flow facies mostly resemble compound-braided

sequences of competent lobes in weathered vesicular basalt (Figure 2.2b) with rare thick tabular flow facies with columnar jointing observed between 1770-1870 masl (Figure 2.2c). Less vesicular, competent portions of flows (e.g., solid lobe cores or massive horizons) were preferentially sampled within highly vesicular flows to avoid alteration. Flow contacts were commonly seen as continuous red horizons within competent portions of flow stacks and typically resemble pahoehoe flow tops (Figure 2.2d and 2e). In rare cases, rubbly flow tops (*aa*, or agglomerate) were observed. Thicker horizons of red, friable material were interpreted as weathering horizons. Similar red horizons seen in the Columbia River basalt province have been identified as paleosols (Sheldon, 2003). Unlike the weathering horizons in the Columbia River basalts, we did not observe root structures or fossils, but we still use the term paleosol (*psol*) to describe these horizons since they are thick (>30) cm and composed of clay-size material with hackly jointing (Figure 2.2f). These paleosols vary in color from red to green to tan. Because the basalts in some sections were more vesicular and weathered than others, flow contacts were not always preserved. In these cases, sampling occurred when changes in flow morphology, texture, and mineralogy were observed. In the lowlands, where outcrops were more isolated, sampling occurred whenever there was fresh exposure.

Proterozoic basement (Pan African granite) is exposed ~20 km west of Galegu at 622 masl but its surface varies in elevation. A thorough inspection of the far western landscape and especially the bottoms of the river channels that are exposed only during the dry season permitted the collection of a dozen flood basalt samples between 540 - 622 masl with these representing the base of the sequence.

Figure 2.2. Field photos. a) View of the Upper and Middle flood basalts exposed on the NW Escarpment looking east. Note that flows are flat lying. Photo was taken at an elevation of ~1560 masl near sampling location of 3495. b) Complex braided flow facies with inflated lobe structure with solid cores and vesicular rims. Photo taken from Middle Group A along NW Escarpment at ~ 980 masl in unsampled portion just below sample 3380. Note hammer for scale. c) Columnar jointing observed in tabular flow facies near top of Middle flood basalt sequence. Photo taken along NW Escarpment from sampling site of 3362. Note person for scale. d) Pahoehoe flow surface with hammer for scale. This photo was taken during the second field season at a location along a more southern transect (not reported here) and resembles flow surfaces observed in the NW Escarpment. e) Red flow contacts in stacked 1 m thick flows from Middle Group B in the NW Escarpment (~1465 masl). f) Red paleosol (psol) at 1844 masl dividing the Middle Group C and Upper flood basalt sequences in the NW Escarpment. The paleosol is ~0.5 m thick, overlying sample 3361 and underlying sample 3360.



2.3.2 *Petrography*

Thin sections were prepared for 178 samples and compared in terms of phenocryst abundances, mineralogical assemblages, and micro-textures. The Ethiopian LT flood basalts can be classified into three textural groups, three modal mineralogical groups based on hand sample and thin section observations. Two additional terms describing the presence of glomerocrysts and megacrysts in lava flows are used as modifiers. Many of these petrographic observations (plag-megacrystic, intergranular, aphyric-ophitic, and cpx-cumulophyric) have been reported in other CFBs including the Columbia River Basalts (Bondre and Hart, 2008; Camp et al., 2013), the Mid-continent rift (Annells, 1973; Huber, 1973; Berg and Klewin, 1988), Siberian Traps (Lightfoot et al., 1990; Renne and Basu, 1991), Deccan Traps (Beane et al., 1986; Hooper et al., 1988; Duraiswami et al., 2001), the Ethiopian flood basalt province (Beccaluva et al., 2009) and older CFBs (Anderson and Dunham, 1966; Emeleus and Bell, 2005; Cheng et al., 2014; Sheth, 2016). Existing literature on CFBs reveal a consistent nomenclature is required. For this reason, the nomenclature used to establish petrographic groups in this study is defined as follows:

2.3.2.1 *Textures*

Aphyric-microcrystalline. —A rock that is aphyric in hand sample and microcrystalline in thin section (Figure 2.3a). In hand sample, these rocks appear dark gray and are often glassy in appearance. In thin section they contain few to no phenocrysts (< 3%) with indistinguishable mineralogy in groundmass (plagioclase 0.25mm, other phases < 0.5mm). Groundmass textures vary between felty and trachytic. Rare phenocrysts, when present, are subhedral to euhedral plagioclase less than 1 mm.

Aphyric- intergranular. — A rock that is aphyric in hand sample but having discrete grains of olivine ± pyroxene filling the interstices between larger plagioclase lathes (Figure 2.3b). In hand sample, these rocks appear coarser grained than aphyric-microcrystalline rocks, and similar range in grain size as aphyric-ophitic rocks. Phases often include larger plagioclase (0.3mm – 1mm) and smaller ol + cpx + oxides (0.1 – 0.5mm).

Aphyric-ophitic. — This texture is often gradational with aphyric-intergranular, but the term is used when plagioclase lathes are partially to fully enclosed by larger (> 0.3mm) interstitial clinopyroxene (Figure 2.3c), giving the rock a mottled appearance in thin section that can be visible in hand sample when texture is coarser grain (cpx > 1mm). Porphyritic samples (plag ± ol- phytic) were occasionally observed with aphyric-ophitic groundmass.

2.3.2.2 *Modal Mineralogy*

In this study, porphyritic rocks are termed -phyric when they contain > 3 % phenocrysts in an aphyric matrix. Volume % phenocrysts are approximations from visual inspection of thin sections and hand sample. We define the cutoff range for phenocrysts as 0.3mm to < 1000mm.

Ol-phyric. —Porphyritic rock with > 70% olivine in the phenocryst phase (Figure 2.3g). Total phenocryst abundances are 5 – 15% with groundmass from microcrystalline to intergranular, and in rare cases aphyric-ophitic. Olivines are 0.6mm – 2mm, commonly euhedral, and in rare cases skeletal. In many cases the olivine is partially or completely altered to iddingsite (goethite + smectite). Completely altered olivine was only recognized in cases where the euhedral phenocryst shape was preserved and found pervasively throughout the sample.

Plag-ol-phyric. —Porphyritic rock with nearly equal proportions of plagioclase and olivine in the phenocryst phase (Figure 2.3h). Total phenocryst abundances are 5 – 25% and up to 40% in coarser grained rocks. Groundmass textures alternate between microcrystalline and

intergranular. Plagioclase ranges 0.3mm – 3.5mm, euhedral to subhedral with sieve texture common in larger subhedral grains. Olivine is generally smaller (0.3mm – 1.5mm), euhedral, and partially or completely altered to iddingsite.

Plag-phyric. —Porphyritic rock with > 70% plagioclase in the phenocryst phase (Figure 2.3i). Total phenocryst abundances are 5 – 25% with predominately microcrystalline groundmass with rare intergranular to aphyric-ophitic groundmass textures. Plagioclase range from 0.5mm – 5mm, euhedral to subhedral, and can occur in irregular or radial clusters. Plagioclase composition determined by the Michel Lévy method ranges from andesine to bytownite (An40 – An70). Olivine micro-phenocrysts are sometimes included in larger plagioclase. Strong sieve texture is common in subhedral grains; in rare cases, sieved cores are mantled by euhedral rims.

Figure 2.3. Photomicrographs of representative textures and modal mineralogy in the LT flood basalts. All images are in XPL unless noted otherwise. a) Aphyric-cryptocrystalline texture (3387-2). Sample is Lower flood basalt, NW Lowlands section (742 masl).



Figure 2.3. (cont'd)

b) Aphyric-intergranular texture (3382 T). Sample is from Middle flood basalt Group A, NW Lowlands section (925 – 930 masl). c) aphyric-ophitic texture with interstitial clinopyroxene up to 1 mm (3460 B). Sample is from Middle flood basalt Group B, NW Escarpment (1240 – 1255 masl).



Figure 2.3. (cont'd)

d) Plag-megacrystic texture with cm-size plagioclase with oscillatory zoning (3500). Sample is from Middle flood basalt Group B, NW Escarpment (1605 – 1615 masl). e) Cpx-cumulophyric texture with 5 mm clinopyroxene glomerocrysts (3433). Sample is from Lower flood basalt, Galegu section (710 masl). f) Plag-megacrystic texture in hand sample (3500, same as in 3d). g) Olivine-phyric flow with 1 – 3 mm subhedral olivine in intergranular groundmass (3452). Sample is from Middle flood basalt Group A, NW Escarpment (1160 masl). h) Plagioclase- and olivine-phyric flow with up to 5 mm sieved plagioclase, 0.5 – 1 mm subhedral olivine, and cryptocrystalline groundmass (3477). Sample is from Middle flood basalt Group B, NW Escarpment (1450 masl). i) Plagioclase-phyric flow with up to 3 mm plagioclase glomerocrysts in cryptocrystalline groundmass (3422). Sample is from Middle flood basalt Group A, Maganan section (900 masl). j) Intergranular texture in transitional basalt from Shinfa (3443). Sample is from Lower flood basalt (565 masl). k) Olivine-rich transitional basalt from Shinfa (3515 A). Sample is from Lower flood basalt (561 masl). l) Same image as 3j, but in PPL. Note the pinkish-brown interstitial titaniferous augite and abundant Fe-Ti oxides.

2.3.2.3 Glomerocrysts and Megacrysts

Glomerocrystic material and megacrysts are found in several lava flows in this study.

Glomerocrysts are either clinopyroxene-rich ± olivine or plagioclase-rich ± olivine, while megacrysts are usually plagioclase. Below is a detailed description of these modifying terms:

Plag-megacrystic. —This term is used as a modifier to describe flows containing megacrystic plagioclase > 1 cm and up to 4 cm in length (Figures 3d and 3f). Flows containing megacrystic plagioclase are between 25 – 35 volume % phenocrysts. Plagioclase megacrysts are mostly euhedral to subhedral and exhibit extensive oscillatory zoning. Mineral and melt inclusions, when present, occur along growth zones. Sieve texture, when present, also occurs along growth zones and rarely in the core of plagioclase. The megacrysts can occur isolated or clustered and lack preferred orientation. In rare cases, clusters of plagioclase megacrysts are radial. Plagioclase composition for megacrysts determined by Michel Lévy are mostly labradorite (An₆₄ – An₇₂) (see Supplementary Table A.2 in Appendix A). Occasionally, clinopyroxene and olivine were observed within clusters of plagioclase megacrysts.

Cpx-cumulophytic. —A term used when glomerocrysts of clinopyroxene \pm olivine is observed (Figure 2.3e). These glomerocrysts range in size from 1-4 mm in diameter, are dominantly clinopyroxene with characteristic augite twinning, and clear in PPL. The glomerocrysts do not appear to be in equilibrium with the groundmass (resorbed edges, undulose extinction, recrystallization). This term is used as a modifier since these glomerocrysts are found in a variety of flow modes and textures.

2.4 RESULTS

The majority of flows are petrographically consistent with LT magmas (as described in section 2.2 above). Only a few intermittent flows (7 in total) restricted to the lower 200 meters of the stratigraphy did not fall into the above categories (Figure 2.3j-1). These flows are rich in euhedral to skeletal olivine that lacks alteration to iddingsite. They tend to have intergranular textures with pink-ish brown clinopyroxene (in PPL) and abundant Fe-Ti oxides. These observations are consistent with the more transitional-alkaline compositions of HT magmas (described in section 2.2) and are hence-forth referred to as transitional basalts.

2.4.1 *Stratigraphy of the NW LT Flood Basalts*

The petro-stratigraphic column is coded using the petrographic nomenclature described above, where color denotes mode and symbols denote textures (Figure 2.4 and Supplementary Table A.2 in Appendix A). The earlier published distinction between the Ashange, Aiba, Alaji, and Termaber flood basalts (Mohr and Zanettin, 1988) is not entirely clear in these new data, probably because the characteristics used to define the upper and lower units relied on local observations that are not consistent across the entire flood basalt province. The morphological distinction between Upper and Lower flood basalt suggested by Hofmann et al. (1997) is an

improvement but lacked petrological constraint. Based on petrographic differences observed in this study, we define three stratigraphic divisions: Lower, Middle, and Upper flood basalts.

2.4.1.1 Lower Flood Basalts (540 – 940 masl)

The Lower flood basalt sequence consists of 400 m of flows and includes the Shinfa, Galegu, and Maganan sections, and lower half of the NW Lowland section. The precise number of flows is difficult to determine because it is not possible to correlate the flows between and among these widely separated sections. The basal exposures of this sequence reflect the underlying basement topography and the elevation varies among stratigraphic sections (Figure 2.4a-d). For example, and as noted above, the Proterozoic Pan African granite outcrops ~20 km west of the lowest flows at Galegu; both occur at 622 masl (Figure 2.4a), and another flow is found 24 km SW of this area at 564 masl.

Shinfa (540 – 589 masl). —The lava flows of the Shinfa section (Figure 2.4b) are among the lowest elevation flows observed (540 – 589 masl). The number of flows is estimated between 7 – 9 based on the observation of vesicular flow tops, a rare agglomerate flow top, and petrographic variation. A 2-m thick dike crosscuts the flow unit directly below the agglomerate flow. Flow thicknesses are not well constrained due to an absence of exposed contacts but are estimated between 5 – 15 m. Flows at Shinfa are dominantly ol-phyric, and alternate between tholeiitic and transitional magma types. Total phenocryst abundances range from 3 – 7% with intergranular to ophitic groundmass.

Galegu (564 – 932) masl. —The Galegu section includes the exposure of the Pan African basement and serves to illustrate the variable topography that forms the base of the flood basalts (Figure 2.4a). This exposure is one of the few examples where basement is exposed in close proximity (tens of meters) to the lowest exposed flows. The lower flows in this section range

from aphyric (glassy to aphyric-ophitic) to plag-phyric. From 653 – 785 masl, flows are dominantly plag-ol-phyric and sometimes exhibit cpx-cumulophyric texture. A large hill near Galegu exposes over 200 m of continuous section that grades from porphyritic flows to aphyric-ophitic flows separated by thick packages (20 – 25 m) of weathered vesicular basalt and rare aphyric-microcrystalline flows (2 – 5 m thick). The upper portions of the hill (800 – 932 masl) are dominated by thick (10 – 18 m) aphyric-ophitic flows and capped by an eroded aphyric-intergranular flow.

Maganan (610 – 900 masl). —The Maganan section has sparse outcrops because of its undulating topography and is therefore difficult to characterize in terms of flow number, flow thickness, and absolute variation in flow composition and textures (Figure 2.4c). The few exposures below 750 masl alternate between tholeiitic and transitional magma types and are mostly ol-phyric to aphyric with varying coarseness in groundmass (microcrystalline to aphyric-ophitic). The lowest exposure (3408 A) is a rare ol-phyric flow with coarsely aphyric-ophitic groundmass and is nearly identical petrographically to the upper eroded flow at Shinfa (3407). While these two exposures (3407 and 3408 A) are separated by ~ 12 km distance, they are suspected to be the same flow or originate from a similar eruptive event. Flows exposed above 800 masl are dominantly plag-phyric and often display columnar jointing. Two 30 cm paleosols are observed at 686 and 849 masl. A 4-m tuff is also observed at 853 masl and overlies the higher paleosol.

NW Lowlands (720 – 850 masl). —The NW Lowlands are separated by a ~ 50-m covered interval between sample 3405 and 3403 (Figure 2.4d). Below the covered interval, inflated lobe structures are commonly observed with rare columnar jointing. The exact number of flows is difficult to determine due to complex inflated lobe structures, but ~22 flow packages are

estimated based on variation in mode and textures. Flows are usually 2 – 5 m thick, alternating between porphyritic and aphyric-microcrystalline flow packages with rare cpx-rich glomerocrysts. Porphyritic flows are usually plag-phyric to plag-ol-phyric with 8 – 20 % phenocrysts in a microcrystalline groundmass. A tuff of variable thickness (2 – 10 m) is observed at ~776 masl. A thick (0.5 – 1 m) paleosol is observed at 792 masl. The basalts above this paleosol are mostly aphyric flows up until the 50-m covered interval.

2.4.1.2 Middle Flood Basalts (850 – 1844 masl)

The Middle flood basalts are the thickest portion of the LT flood basalts and include nearly 1000 m of flows, including the upper half of the NW Lowlands section (Figure 2.4d) and most of the NW Escarpment section (Figure 2.4e). Plagioclase plag-megacrystic flows first appear above 850 masl (sample 3402); a significant petrological change that defines the start of the Middle flood basalts. The division between Lower and Middle flood basalt occurs roughly at the topographic transition from steep sloping escarpment to gradual sloping lowlands, similar to the morphological boundary in the Lima Limo section described by Hofmann et al. (1997). The covered interval in the NW Lowlands section makes it difficult to place a precise division between Lower and Middle flood basalt, and therefore an extrapolation is made using the neighboring Maganan section, beginning ~ 3 km south of the NW Lowlands section. In the Maganan section, a tuff and paleosol occur just 10 m below the elevation of the plagioclase plag-megacrystic basalt observed in the NW Lowlands section (Figure 2.4c and d). We have chosen to draw the division within the covered interval so that it coincides with the elevation of this tuff and paleosol.

The NW Escarpment consists of ~1200 m of flood basalts with preserved flow contacts exposed in fresh road cuts that were densely sampled (Figures 2a and 4e). Variation in flow

thickness, mineralogy, and textures does not appear to vary systematically over short vertical intervals but can be grouped over large (250 – 350 m) intervals throughout the section. The boundary between Middle and Upper flood basalts occurs in this section at 1844 masl. We define three flow groups within the Middle flood basalts based on the presence of glomerocrysts and megacrysts, modal cycling of flows, and flow thicknesses.

Group A occurs between 863 – 1212 masl and is defined by the first appearance of plagioclase plag-megacrystic basalt followed by alternating ol-phyric to plag-phyric basalt. Group A includes the upper portion of the NW Lowlands section above the covered interval (Figure 2.4d) up through the lower 1000 m of flows in the NW Escarpment (Figure 2.4e). Flow thicknesses are usually between 2 – 16 m but can be as thick as 24 m. Packages of thin (1 – 2 m thick) stacked flows and highly vesicular packages with solid cores are common. At the base of this group is a 25 m thick plagioclase plag-megacrystic flow overlying a thin aphyric-microcrystalline flow at ~860 masl (3403). Above the plagioclase plag-megacrystic flow, flows are thinner (2 – 5 m), ol-phyric to aphyric with coarser groundmass textures (intergranular to aphyric-ophitic) and separated by 10 – 20 m covered intervals with no exposed flows. Cpx-cumulophyric texture is more common between 1000 – 1040 masl, but then disappears. Alternating plag-phyric and ol+plag-phyric stacked thin flows and braided pahoehoe flow packages are found in the upper 150 m of this group.

Group B (Figure 2.4e) occurs between 1216 – 1561 masl and is defined by the presence of thick aphyric-ophitic and intergranular basalt alternating with aphyric to porphyritic basalt. Aphyric-ophitic to aphyric-intergranular basalt flows separated by thick (25 – 50 m) packages of weathered vesicular basalt differentiate group B from group A. Plag-phyric, plag-ol-phyric, ol-phyric, and aphyric-microcrystalline basalt are also observed, with groundmass textures varying

from microcrystalline to intergranular and aphyric-ophitic. Cpx-cumulophyric texture occurs in the middle and top of this sequence. Flow thicknesses are usually between 4 – 11 m and up to 19 m, although packages of thin (≤ 1 m) stacked flows are also observed. Multiple 2 – 5 m thick dikes are observed in this sequence. The sequence is terminated by a 30 cm paleosol.

Group C occurs between 1561 – 1844 masl and is defined by the recommencement of plagioclase plag-megacrystic basalt (3496) after the 30 cm paleosol (Figure 2.4e). Thick plagioclase plag-megacrystic basalt and alternating aphyric basalt are common. Cpx-cumulophyric texture is observed in flows directly overlying paleosols. Flow thicknesses in this sequence increase from 4 – 10 m, to 15 – 20 m, to 37 m at the top. The capping flow is columnar jointed with a cpx-cumulophyric agglomerate flow top overlain by a 50 cm paleosol.

2.4.1.3 Upper Flood Basalts (1844 – 2175 masl)

The Upper flood basalt sequence (Figure 2.4e) includes ~330 m of flows and is truncated at the top of the plateau where the stratigraphic relationships are difficult to discern because of faulting north of Lake Tana near Aykel town. This sequence has 21 observed flows and one silicic tuff. The lower boundary of the Upper sequence is defined by the disappearance of cpx-glomerocrysts, coincident with a 50 cm paleosol, and the disappearance of megacrystic plagioclase. Above the 50 cm paleosol (1844 masl), the first flows are thicker (10 – 21 m) and are aphyric-microcrystalline. Continuing up the sequence, flows are consistently 5 – 6 m thick and are dominantly plag-phyric to aphyric-microcrystalline. Coarse groundmass textures (aphyric-ophitic and intergranular) are rare.

Figure 2.4. Petro-stratigraphic column for flood basalt transects in this study. Elevation in masl is listed on the left of column and sample numbers are listed on the right. Sample numbers with an * indicate transitional basalt. a) Galegu section showing basement topography. b) Shinfa section with interbedded transitional basalt flows. A single flow (3408 A) at the base of the Maganan section appears petrographically similar to the uppermost flow of the Shinfa section (3407); they are separated by ~12 km distance. c) Maganan section. Four transitional basalt flows are found interbedded with LT lavas between 650 and 750 masl. The boundary between Lower and Middle flood basalts is extrapolated at ~850 masl (psol and tuff). d) The NW Lowlands section. Middle flood basalt sequence begins approximately when plagioclase plagioclase megacrystic basalt appears (~865 masl).

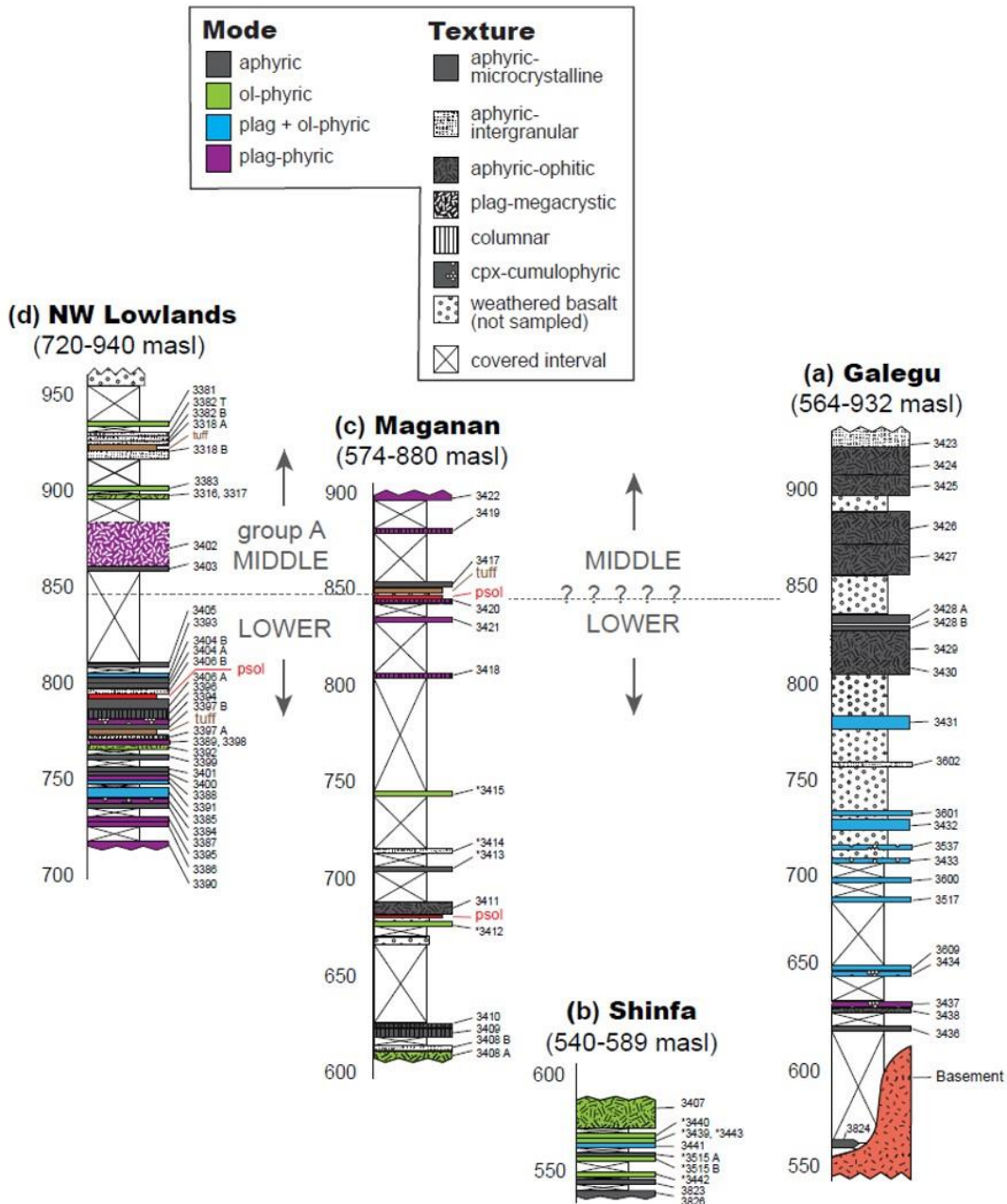
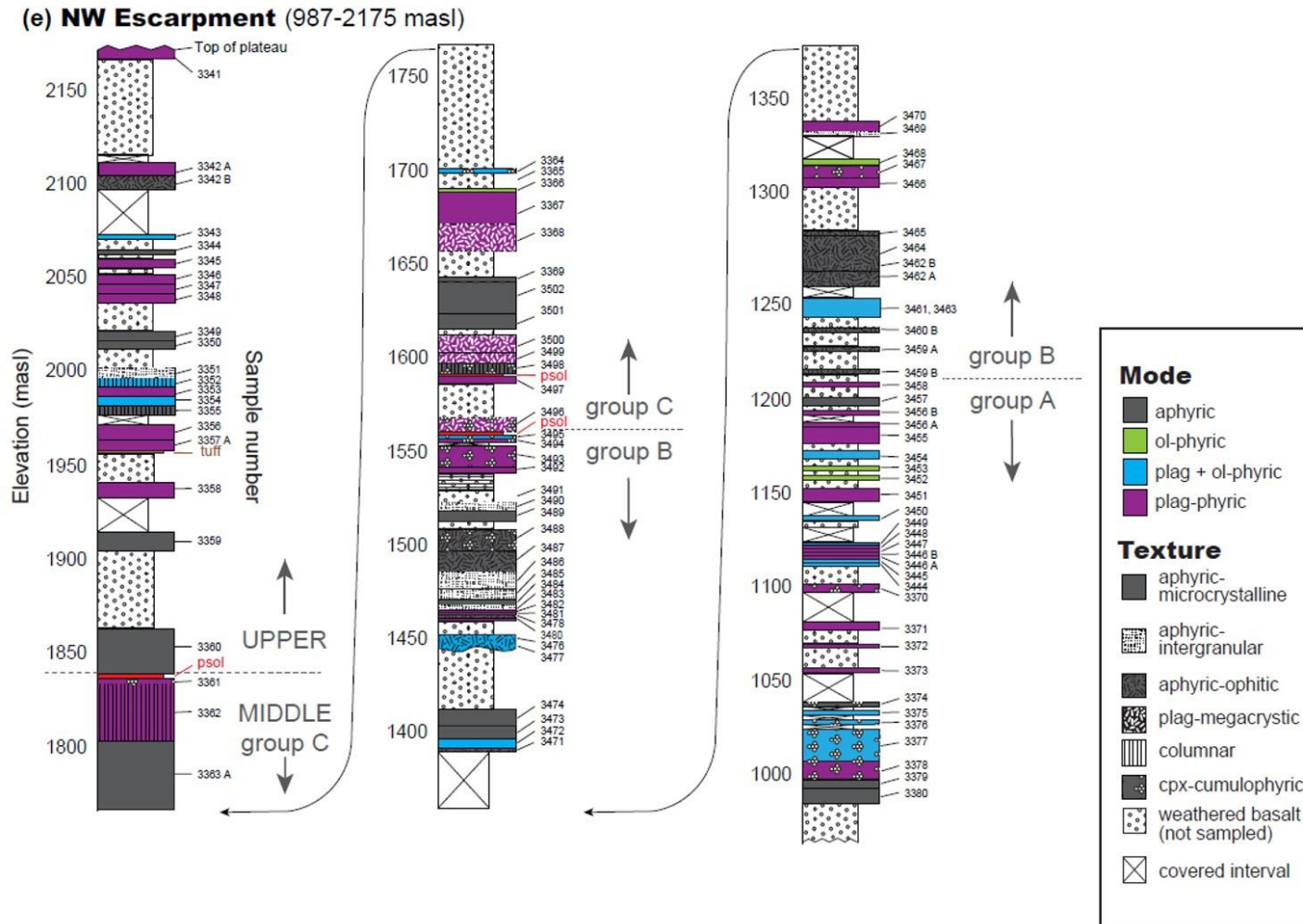


Figure 2.4. (cont'd)

e) The NW Escarpment section. The Boundary between the Middle and Upper flood basalts is observed at 1844 masl (psol). The boundaries within the Middle flood basalt groups occur at ~1210 masl (A – B) and ~1550 masl (B - C) which is separated by a paleosol.



2.5 DISCUSSION

2.5.1 *Decoding Magmatic Processes from Petrography and Stratigraphy*

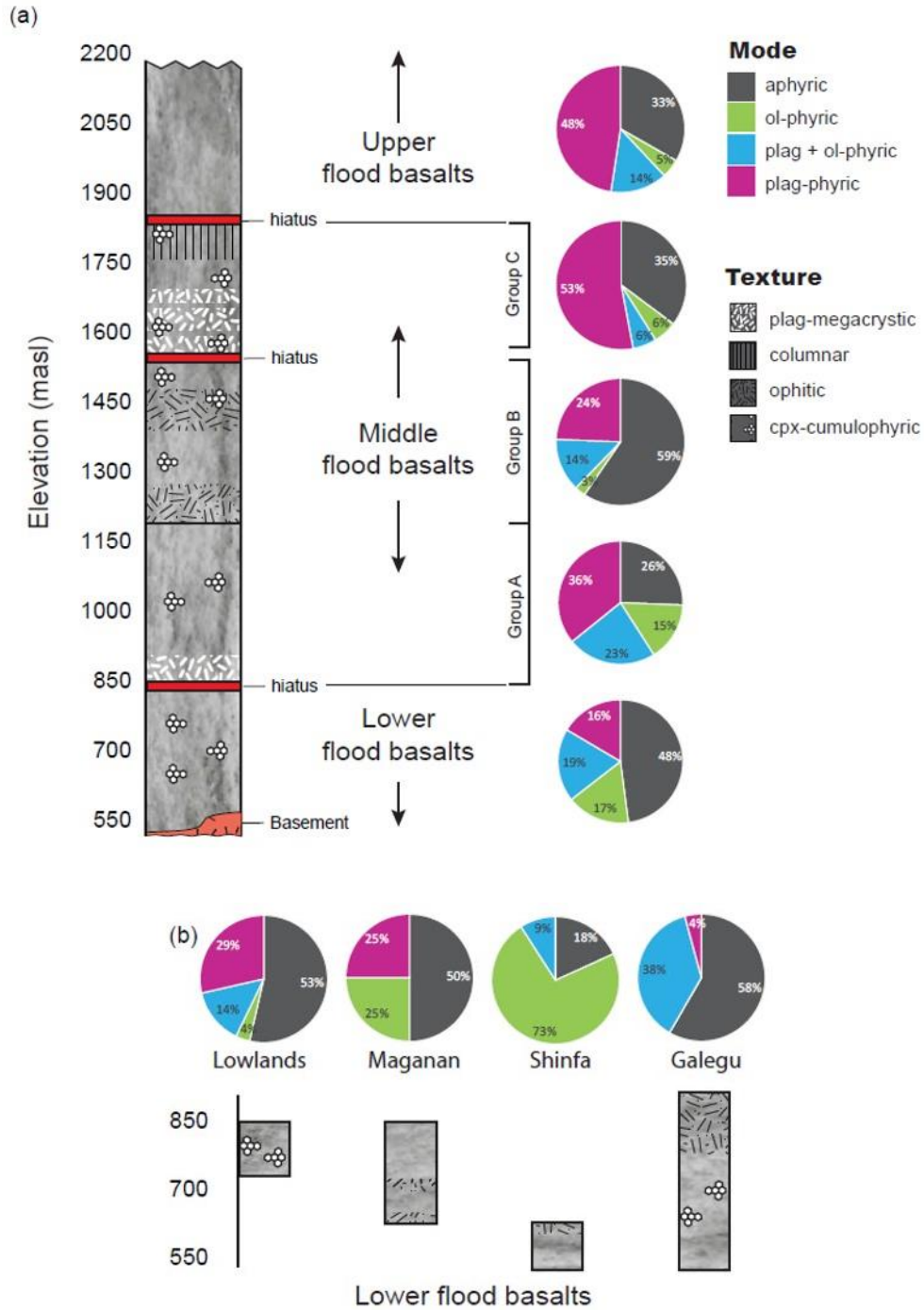
The use of petrography and stratigraphy to evaluate magmatic processes first requires an assessment of the parameters that control crystallization of phases in a basaltic magma. These parameters include: 1) the starting composition of the parental magma, 2) pressure of crystallization, and 3) the presence of volatiles. The composition of the parental magma controls the mode and order of crystallization along the liquid line of descent (Bartels et al., 1991; Shi and Libourel, 1991), thus explaining the observation of ol+plag phenocrysts in LT lavas, and ol+cpx in HT lavas (Pik et al., 1998; Kieffer et al., 2004; Beccaluva et al., 2009; Natali et al., 2016). Within the NW Ethiopian plateau there is a limited diversity in magma compositions – defined by existing literature as either HT or LT provinces which are spatially restricted to the western and eastern half of the NW Ethiopian Plateau, respectively (Pik et al., 1998; Kieffer et al., 2004; Beccaluva et al., 2009). While a thin layer of LT lavas has been found, at the base of a predominately HT1 sequence in the NE portion of the Ethiopian plateau (Kieffer et al., 2004), there is no evidence to suggest cyclicity between HT and LT magma types throughout the duration of flood basalt activity (Pik et al., 1998; Kieffer et al., 2004; Beccaluva et al., 2009), therefore a continuous sequence of flows with similar compositional properties can be treated as a single magma type from a petrographic perspective. On the basis of our current understanding of the behavior of magmas with a broadly basaltic composition, the crystallization of clinopyroxene is favored at higher pressures (10 – 20 kbar), at the expense of plagioclase and olivine (Morse 1980). The same magmas at lower pressures (<5 kbar) will favor the crystallization of plagioclase over clinopyroxene (Morse, 1980). Such observations are valid for relatively dry magmas, as the presence of water (> 3wt. %) can facilitate the crystallization of

clinopyroxene over plagioclase at shallow crustal pressures (Feig et al., 2006). Since the LT flood basalts are reportedly dry (Kieffer et al., 2004), a preferred crystallization of clinopyroxene versus plagioclase can indicate a relative difference in depth of stalled magmas. Within the stratigraphy presented in this paper, the majority of flows are petrographically consistent with LT lavas. Only ten flows, restricted to the lower 200 m of the stratigraphy, are observed as transitional basalts similar to HT lavas. For the purposes of the discussion that follows, only LT lavas will be considered.

2.5.2 Conceptual Model for the Evolution of LT Flood Basalts

Petrographic observations presented in this study demonstrate three divisions within the Ethiopian flood basalt province, defined broadly as the Lower flood basalt which is dominantly ol-phyric with cpx-cumulates, the Middle flood basalt which exhibits plag-megacrystic flows and oscillation between plag-phyric and ol-phyric flows, and the Upper flood basalt which is dominantly plag-phyric and devoid of cumulates (Figure 2.5a). We propose that these distinctive petrographic heterogeneities reflect differences in the depth of fractionation and magnitude of magma flux into the lithosphere.

Figure 2.5. Simplified petro-stratigraphic column of Ethiopian NW plateau LT flood basalts.
a) Relative percentages of modal phases for each unit and group are shown on the right. Percentages for Lower flood basalts are the mean of all stratigraphic sections (Lowlands, Maganan, Shinfa, and Galegu). b) Modal variation between different stratigraphic sections in Lower flood basalts.



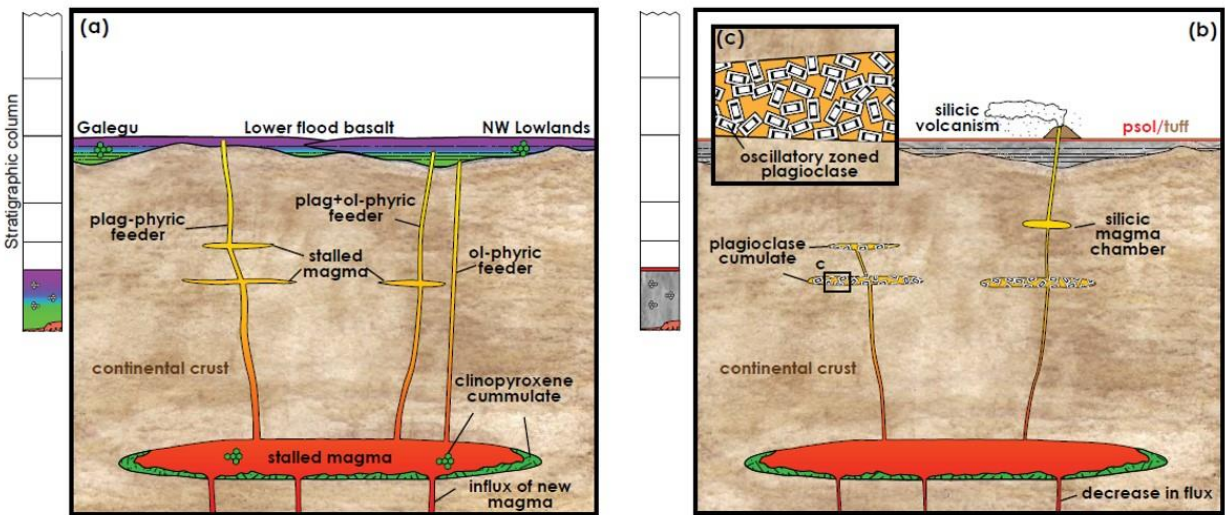
2.5.2.1 *Lower Flood Basalt: Deep fractionation and early evolution*

The most distinctive feature observed in the Lower flood basalt is the presence of ol-phyric flows and clinopyroxene-rich glomerocrysts. Cpx-cumulophyric texture occurs throughout the Lower and Middle flood basalt sequences with no correlation to modal mineralogy or flow texture. The clinopyroxene-rich glomerocrysts contain minor olivine and are devoid of plagioclase. Considering the clinopyroxene-rich glomerocrysts are of LT magma origin, their presence and phase assemblage suggest they crystallized at higher pressures more consistent with mid- deep crust rather than shallow crust. Initial melts derived from the impinging plume head would have migrated up through the sub-continental lithospheric mantle due to their negative buoyancy until the melts reached the density contrast where they would accumulate. The stalled, LT parental magma would begin to crystallize cpx+opx \pm olivine. Existing seismic and gravity data supports the presence of a large mafic cumulate body beneath the NW Ethiopian Plateau (Mackenzie et al., 2005; Cornwell et al., 2006, 2010; Stuart et al., 2006; Mammo, 2013) overlain by large mafic dike swarms (Mège and Korme, 2004). The presence of large mafic cumulates underlying CFBs has been shown in other LIPs (Holm and Prægel, 2006; Ridley and Richards, 2010). Recent petrologic studies of pyroxenite xenoliths from Cenozoic volcanism on the Ethiopian plateau show equilibrium pressures consistent with the crust/mantle boundary and suggest a linkage between opx+cpx-rich cumulates and LT flood basalt magmatism (Rooney et al., 2017). However, the cpx-glomerocrysts observed in this study lack orthopyroxene and are therefore further along the liquid-line of descent. For this reason, we interpret the clinopyroxene cumulates observed in this study as having crystallized from stalled magmas in the lower to middle crust (Figure 2.6). These lower to middle crust staging chambers are fed by more primitive magmas derived from lower in the lithosphere.

The second most distinctive feature is the presence of paleosols that punctuate eruption of lava flows in the Lower flood basalt. The paleosols represent weathering horizons of basalt (and/or silicic tuff) during pauses in flood basalt eruption. These pauses suggest a decrease in magma flux; magma may still be fluxing into the lithosphere, but the rate may not be high enough to cause them to erupt at the surface.

The transition from ol-phyric to plag-phyric flows in the Lower flood basalt sequence appears to be a case for simple fractional crystallization of a single pulse of magmatism. However, paleosols and tuffs are found intercalated with these flows suggesting pulsed magma flux into the lithosphere and lower-volume eruptive events. Likewise, modal variation between local stratigraphy (Figure 2.5b) suggest isolated fractionation paths for magma traversing the lithosphere. It is more likely that the overall transition from ol-phyric to plag-phyric trend observed in the Lower section reflects the early formation of a shallowing magmatic plumbing system in which initial lavas traversed the crust quickly, experiencing limited differentiation and producing ol-phyric flows (Figure 2.6a). Over time, magmas began to stall in the shallow crust where they differentiated to form plag-phyric magmas prior to eruption (Figure 2.6a). A pause in flood basalt extrusion, defined by a 30-cm thick paleosol and 4-m thick silicic tuff, occurs following the Lower flood basalt emplacement (Figure 2.6b).

Figure 2.6. Model for magmatism in Lower flood basalt. a) Lower flood basalt eruptive phase. Isolated eruptive centers exploit pre-existing weaknesses in lithosphere. Low magma flux and low-volume eruptions. Initial flows fill topographic lows and are ol-phyric with transitional basalt characteristics. Cpx-glomerocrysts found in flows are derived from stalled magmas in the mid- to lower crust. Transition toward plag-phyric possibly related to early formation of sill complex in the shallow crust. b) Lower flood basalt hiatus prior to Middle flood basalt phase. Shallow reservoir forms plagioclase mush with oscillatory zoned plagioclase megacrysts during pause in flood basalt eruption. Silicic volcanism (tuff) results from fractionation in shallow reservoir. Paleosol develops due to weathering of flood basalts and/or tuff.



2.5.2.2 Middle Flood Basalt: Cyclicity, polybaric fractionation, and increasing flux

In the Lower flood basalts, we observe an increase in plag-phyric flows interrupted by several pauses. This sequence was succeeded by eruption of the Middle flood basalt. The most striking feature of the Middle flood basalt is the appearance of plagioclase- megacrystic flows with high An-plagioclase megacrysts (mostly labradorite) and strong oscillatory zoning. Sieve texture (although rare) is usually restricted to zones between the core and rim, suggesting some perturbation in equilibrium conditions midway through crystal growth. Thick plagioclase-megacrystic flows often occur above paleosols and alternate with aphyric flows which can contain sparse plagioclase macrocrysts. Despite the high crystal cargo in plag-megacrystic flows

(up to 35 %) these flows are commonly observed with pahoehoe flow tops which suggest they are relatively low viscosity upon emplacement.

The occurrence of plagioclase-megacrystic basalt flows in other CFBs has been attributed to the presence of a shallow magma plumbing system that undergoes periods of longer residence between eruptive episodes (Hansen and Grönvold, 2000; Sen, 2001; Sen et al., 2006; Higgins and Chandrasekharam, 2007; Borges et al., 2014) and the high An-contents of plagioclase megacrysts has been explained by multiple recharge events into the shallow crystal mush zone (Óskarsson et al., 2017). The low viscosity nature of plag-megacrystic flows has been explained by processes related to disaggregation and eruption of the crystal cargo as a result of recharge (Óskarsson et al., 2017). From here on, we propose that the plag-megacrystic flows in this study are evidence of an established shallow mush zone undergoing frequent recharge.

Despite clear evidence of a shallowing fractionation system within the Middle flood basalt, significant complexities in modal abundances require subdivisions of the Middle group in order to resolve differentiation processes within this interval. On the flow-by-flow scale, there is no apparent systematic variation in modal mineralogy or flow thickness over time, indicating the magma plumbing system is too complex to assume simple differentiation by crystallization. However, when comparing large flow packages, a broader shift in plumbing system dynamics can be observed petrographically (e.g., Middle flood basalt Groups A – C). The alternating occurrence of cpx-cumulophyric and plag-megacrystic texture attest to varying contributions from the deeper and shallower staging chambers, respectively. The presence of cpx-glomerocrysts suggests pulses of magma recharge from the deeper staging chamber. Cyclical variation from ol-phyric → plag-ol-phyric → plag-phyric suggests either multiple episodes of magma differentiation due to recharge pulses or that the sequence of flows are tapping magmas

from a variety of differentiation pathways within the magmatic plumbing system. We will attempt to deconvolute the complexity in cyclicity by addressing petrographic patterns observed in each sub-group of the Middle flood basalt sequence.

Group A of the Middle flood basalts represents a new pulse of magmatism that followed the Lower flood basalt hiatus (Figure 2.7a). It began with the extrusion of a thin aphyric flow immediately followed by a 24 m thick plag-megacrystic flow. As the shallow reservoir was perturbed by newly injected magma, it disaggregated and mobilized the plagioclase mush, resulting in a plagioclase megacrystic cargo with up to 35 % plagioclase by volume (Figure 2.7b). Ol-phyric flows were likely fed by dikes that bypassed the crystal mush, while aphyric flows may have bypassed the mush zone or erupted through feeders that previously cleared the loose crystal cargo from mush zones. Clinopyroxene glomerocrysts restricted to flows between 1000 – 1100 masl suggest an increase in magma supply feeding the shallow plumbing system from the lower crustal chamber. Alternating modal mineralogy of flows in this group reflect variation in magma differentiation by crystal fractionation which can either be explained by isolated feeder systems that have independent fractionation paths and/or by frequent injection of new magmas into the plumbing system (Figure 2.7c).

Group B of the Middle flood basalt represents both high magmatic flux and eruptive volume (Figure 2.7d). These flows are predominantly thick, coarser-grained flows (8 – 16 m; intergranular to aphyric-ophitic textures) with stacked, thin, aphyric to plag±ol-phyric flows. Cpx-glomerocrysts are common and occur with increasing frequency toward the top of the flow group, suggesting that magma flux into the lower staging chambers was high while extrusion rates increased as the plumbing system reached maturity (wider conduits and interconnected, homogenized magma plumbing system)(Figure 2.7d). High extrusion rates resulted in thick

flows with slow-cooling textures (intergranular to aphyric-ophitic), compared to the more phyrlic and aphyric-microcrystalline flows of Group A. These characteristics appear to indicate higher flux of magma into the plumbing system and higher extrusion rates than previously erupted groups.

A pause in flood basalt extrusion occurs between Group B and Group C of the Middle flood basalts (Figure 2.7e). During this hiatus, a plagioclase mush developed again in the shallow reservoir and formed oscillatory zoned plagioclase megacrysts. Some of the shallow reservoirs likely froze depending on volume and connectivity. A 30 cm paleosol formed at the surface of the Middle flood basalt- Group B.

Group C of the Middle flood basalt began with a new pulse of magma introduced to the shallow plumbing system from the deeper crustal magmas (Figure 2.7f) and another episode of mush remobilization. This pulse produced alternating flows of plag-megacrystic, aphyric, and plag-phyric basalts. Cpx-glomerocrysts occurred at the beginning and in the middle of this flow group, suggesting there was still new magma recharging the deeper staging chambers. Flow thickness increases over time, from 8 – 10 m to nearly 40 m, with columnar jointing toward the top of the flow group. The dramatic increase in flow thickness seen in this flow group is not seen anywhere else in the stratigraphy presented here and attests to an apex in flood basalt eruption. There is an abrupt cessation in flood basalt eruptions immediately following Group C (Figure 2.8a). During this hiatus, a 50 cm paleosol forms on the uppermost surface of Group C.

Figure 2.7. Model for magmatism in Middle flood basalt. a) Middle flood basalt: Group A. Early eruption of thick plagioclase megacrystic basalt followed by ol-phyric and aphyric flows. Plagioclase megacrystic flows are produced when new dikes from lower crustal magmas are captured by the shallow crystal mush zone which triggers an eruption carrying the megacrystic cargo to the surface. Olivine-phyric flows are fed by dikes that by-pass mush zones. Aphyric flows may be fed by dikes directly from lower crustal magmas or after a pathway through the plagioclase mush zone is cleared. b) Inset showing injection of new magma into plagioclase mush zone, mobilizing zoned plagioclase megacrysts and producing a plagioclase megacrystic flow with up to 30 % plag by volume. c) Middle flood basalt: Group A (continued). Continuing eruptions are fed by isolated fractionation pathways producing alternating flow packages of plag+ol-phyric and plag-phyric. Cpx-glomerocrysts are restricted to flows between 1000 – 1100 masl and suggest a continuing increase in magma flux. The shallow plumbing system continues to mature during influx of new magma. d) Middle flood basalt: Group B. Magmatic plumbing system achieves maturity and becomes an interconnected, homogenized, shallow dike and sill complex. Magma supply to surface is likely rapid to produces thick, insulated flows that form slow-cooling textures (intergranular to aphyric-ophitic). Cpx-glomerocrysts are common in flows and occur in increasing frequency toward the top of this flow group, suggesting that magma recharging the lower crustal system is achieving an apex in flux. e) Middle flood basalt hiatus between Middle flood basalt: Groups B and C. Temporary pause in flood basalt eruption and formation of paleosol. Plagioclase mush develops in shallow reservoir and forms oscillatory zoned plagioclase megacrysts. Some portions of sill complex begin to freeze in the crust and no longer offer pathways for new magma. f) Middle flood basalt: Group C. New magma pulse re-mobilizes and disaggregates plagioclase mush and produces thick plagioclase megacrystic flows interbedded with thin aphyric flows fed by feeders that by-pass the mush zone. Cpx-glomerocrysts observed in this flow group suggest there are still significant volumes of magma recharging the lower crustal magma system. The final eruptions in this group produce very thick (>35 m) aphyric flows with columnar jointing and cpx-glomerocrysts. This event represents the apex of flood basalt volcanism.

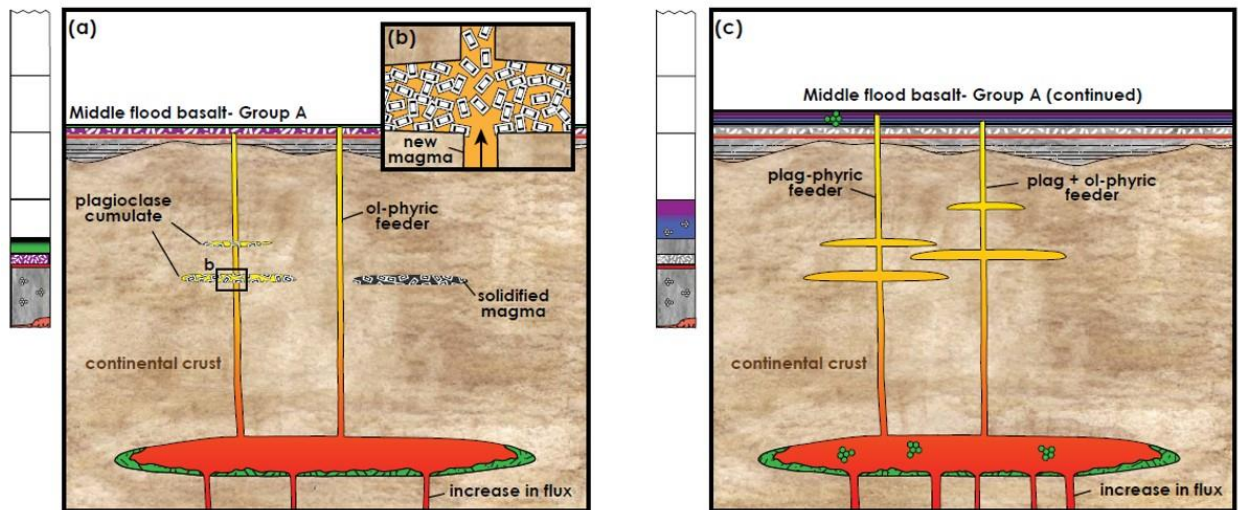
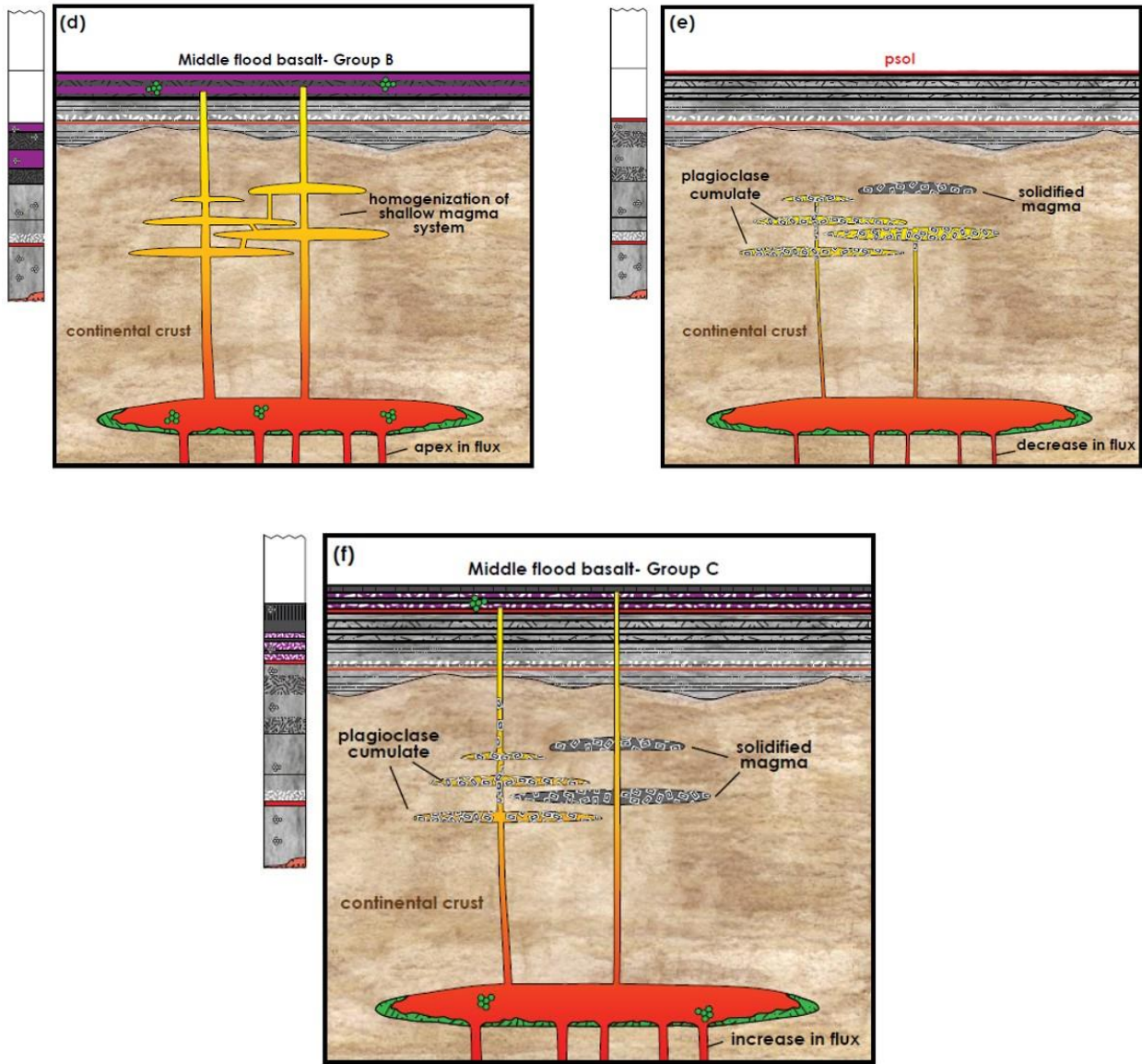


Figure 2.7. (cont'd)

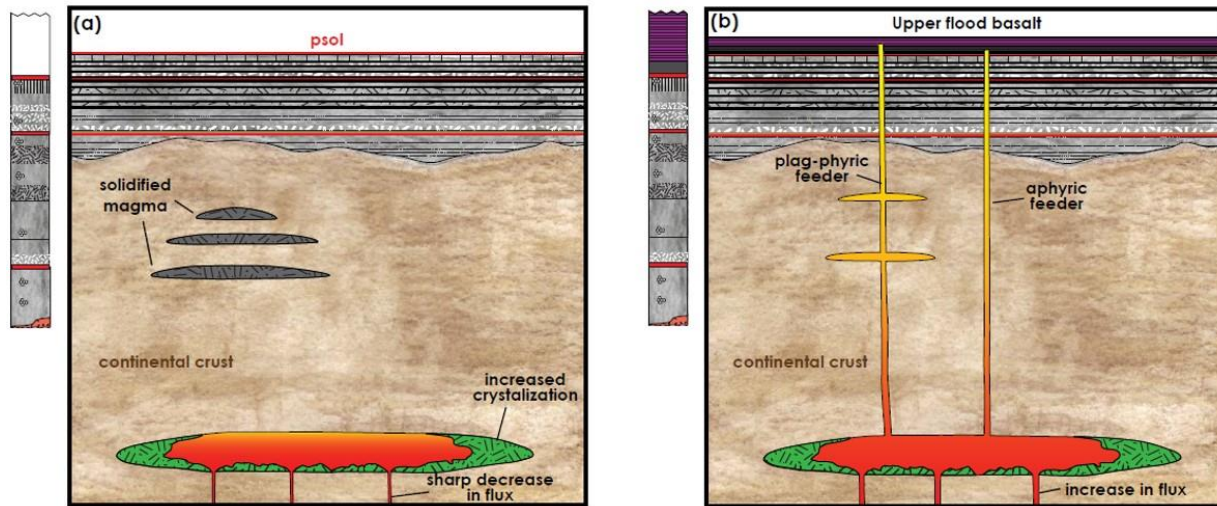


2.5.2.3 Upper Flood Basalt: The death of a flood basalt

Above the 50 cm psol, the Upper flood basalt sequence is characterized by an initial eruption of a 20-m thick aphyric flow followed by predominantly plag-phyric and aphyric flows of consistent thickness (~5 m). The Upper flood basalts began erupting after the hiatus and represent the onset of flood basalt termination (Figure 2.9b). In addition to the fairly uniform

modal composition and thickness, the Upper flood basalts are devoid of cpx-glomerocrysts and megacrystic plagioclase. We hypothesize that lower flux of magma into the lithosphere could no longer produce the recharge volumes necessary to sustain the growth of large megacrystic plagioclase and allowed the shallow mush zones to freeze. The dominance of plagioclase in these flows also suggests lower flux since a decrease in magma recharge would facilitate fractionation of the magmas residing in the lithosphere. The absence of cpx-glomerocrysts may also be explained by a decrease in flux into the deeper staging chambers, since higher volumes of newly injected magma would be more capable of disaggregating cumulate. As flood basalt activity terminated, volcanism transitioned to localized shield building activity across the plateau, beginning with the 30 Ma Simien shield near the LT flood basalts at Lima Limo (Kieffer et al., 2004). The transition from flood basalt eruptions to shield activity is further evidence of the decrease in magma flux associated with flood basalt termination.

Figure 2.8. Model for magmatism in Upper flood basalt. a) Hiatus between Middle and Upper flood basalts. Pause in flood basalt eruptions allows for formation of paleosol. Magma flux into magmatic system has decreased, b) and the lower crustal stalled magmas begins to crystallize. As recharge to the shallow reservoirs shuts down, the plumbing system is no longer capable of sustaining a mush zone and the dike and sill complex freezes completely. c) Upper flood basalt eruptive phase signifies termination of flood basalts. Flows are uniformly thin (~5m), dominantly plag-phyric or aphyric, and devoid of cpx-glomerocrysts and plag-megacrysts. The plagioclase-phyric flows indicate that magma is once again stalling and fractionating in the shallow crust, but not long enough to produce large megacrystic plagioclase.



2.5.3 Comparison with Other CFBs

Continental flood basalt provinces are typically divided into three phases: 1) an initiation phase characterized by low-volume, transitional-alkaline lavas erupted via pre-existing weaknesses in the lithosphere; 2) a main phase characterized by high-flux and large volume, fissure-fed, tholeiitic lavas with approximately 80 – 90% of the erupted volume extruded during this phase; and 3) a waning or termination phase characterized by a rapid reduction in volume and frequency of eruption, intercalated with silicic-explosive eruptions and more widely distributed volcanic centers (Jerram and Widdowson, 2005). The transition between these phases reflects changes in the magmatic plumbing system in terms of the flux of magma entering and leaving the lithosphere.

During the initiation phase, early lavas tend to be more primitive, lower volume (in comparison to main phase), and intercalated with weathering horizons (Beane et al., 1986; Lightfoot et al., 1993; Jerram et al., 2000; Jerram and Stollhofen, 2002; Sheldon, 2003; Jerram and Widdowson, 2005; Zhang et al., 2006; Beccaluva et al., 2009). These characteristics indicate that magma involved in early eruptions 1) experienced limited fractionation in comparison to later predominately plagioclase-phyric flood basalt eruptions, and 2) eruptions occur in short pulses separated by pauses. The observed variability in modal mineralogy found in the Lower flood basalts in this study supports the idea of isolated feeder systems during early development of the magmatic plumbing system. As the magmatic plumbing system evolved, there is evidence of shallow fractionation in concert with evidence for deep fractionation. Geochemical and petrologic studies (Cox, 1980; Mohr, 1983; Lightfoot et al., 1990) provide evidence for polybaric fractionation in the evolution of CFB magmas and suggest that the depth of crustal storage shallows over time (Peate and Bryan, 2008).

The largest volumes of basalt are erupted during main phase volcanism (Self et al., 1997; Thordarson and Self, 1998; Duraiswami et al., 2001; Bondre et al., 2004; Jerram and Widdowson, 2005). This observation has led to debate over the rate of flood basalt eruption which has focused on dating, volume estimates, and flow-morphology (Courtillet et al., 1986; Self et al., 1997; Rochette et al., 1998; Thordarson and Self, 1998; Duraiswami et al., 2001; Bondre et al., 2004; Jerram and Widdowson, 2005; Sen et al., 2006; Chenet et al., 2008; Barry et al., 2010; Reidel et al., 2013). Classic tabular flow facies with rubbly flow tops, thought to indicate high extrusion rates as in the Parana-Etendeka main phase (Jerram and Widdowson, 2005), are generally rare in the NW Ethiopian flood basalt province. Conversely, braided lobe facies observed in the Deccan and Columbia River are thought to indicate prolonged, episodic

eruptions (Self et al., 1997; Thordarson and Self, 1998; Duraiswami et al., 2001; Bondre et al., 2004; Jerram and Widdowson, 2005). Braided lobe facies were more common than classic tabular flow facies in the NW Ethiopian plateau, and an episodic main phase is supported by the oscillation of modal mineralogy and alternating occurrence of glomerocrysts and zoned megacrysts observed in this study. The growth of large, zoned plagioclase megacrysts requires some duration of residence time in between eruptions, but frequent recharge into the mush is necessary to maintain crystal cargo mobility for future transport during eruptions. Similarly, the high An-content commonly observed in plagioclase megacrysts from CFBs requires frequent recharge of more primitive magmas into the mush zone. The occurrence of cpx-rich glomerocrysts is evidence of this recharge. Using the detailed petro-stratigraphic analysis of consecutive flows documents a general increase in magma flux throughout the main phase, as evidenced by the increasing frequency of cpx-glomerocrysts and thicker lava flows that produce the greatest basalt volume prior to flood basalt termination.

During the termination phase, a general transition toward more evolved lavas is typically observed in CFBs; this is consistent with a magma plumbing system that is shutting down. For example, the late-stage eruptions of the Ethiopian-Yemen, Emeishan, and Parana-Etendeka CFBs are interbedded with silicic tuffs (Mohr and Zanettin, 1988; Piccirillo, 1988; Ayalew et al., 1999, 2002; Ukstins et al., 2002; Zhang et al., 2006). In the Upper flood basalts, we observe flows that are dominantly plag-phyric to aphyric and an absence of plagioclase megacrysts and cpx-glomerocrysts. This composition indicates two things: 1) the plumbing system feeding the Upper flood basalt is dominated by shallow fractionation; and 2) recharge of new primitive magma into the shallow plumbing system is significantly reduced in comparison to the Middle flood basalts. The tendency for flood lavas to be more plag-phyric toward the upper part of the

sequence is consistent with observations made throughout the Ethiopian-Yemen CFB province (Mohr, 1983; Pik et al., 1998; Kieffer et al., 2004) as well as the Deccan and Emeishan (Beane et al., 1986; Zhang et al., 2006). A decrease in magma flux is consistent with the transition from flood basalt eruption to shield activity in Ethiopia, and more broadly the termination of CFBs.

2.6 CONCLUSIONS

This study's detailed petrographic analyses of a ~1600 m flow-by-flow stratigraphy provides critical insights into the evolution of the magmatic plumbing system of CFBs. Initial flows are fed by magmas that have experienced deeper fractionation (mid- to deep crust). Overtime, the fractionation became polybaric thus reflecting the stalling of magmas in both the shallow and deeper crust. Overall, the flux of new primitive magma appears to have been continuous throughout the eruption of the Middle flood basalts, but its magnitude changed over time. Changes in flux magnitude control how much lava erupts at the surface as well as hiatuses in eruption. During hiatuses, megacrystic plagioclase with high An-content (labradorite) and oscillatory zoning form, indicating constant feeding of the shallow plumbing system by more primitive magmas. In contrast, the very high extrusion rate witnessed during Group B of the main eruptive phase suggests an apex in magma flux through the lithosphere. Shallowing of the magma plumbing system toward the end of the eruptive phase is consistent with observations of increased silicic volcanism in Ethiopian flood basalt Province and other CFBs. Furthermore, changes in magma flux are consistent with the typical observation that CFBs undergo a transition from fissure-fed flood basalt eruptions to magmatism centered on large volcanic shields.

The data presented here suggest that the main phase of flood basalt eruption is better explained by pulses of high flux, rather than continuous high flux. The origin of these pulses remains enigmatic and may relate to heterogeneities in plume composition, variation in

upwelling rate, or mantle potential temperature. The results of this study provide new petrographic constraints that require revision of existing models of plume-lithosphere interaction in terms of pulsed versus continuous magma flux. Although the details of the magmatic plumbing model presented herein may prove to be unique to the Ethiopian-Yemen CFB province, these petrographic observations and lithologic associations are commonly found in other CFBs. These detailed petrographic analyses, framed within a well-constrained stratigraphy, have provided new geochemical insights into the initiation and evolution of the Ethiopian flood basalt province, and offer a new approach for understanding magma evolution in other CFBs.

3. MAGMA EVOLUTION DURING MAIN-PHASE CONTINENTAL FLOOD BASALT VOLCANISM: A CASE FOR RECHARGE-ERUPTION-ASSIMILATION-FRACTIONAL CRYSTALLIZATION IN THE ETHIOPIAN LOW-TI PROVINCE

3.1 INTRODUCTION

Continental flood basalt (CFB) provinces, including the Ethiopian-Yemen, Paraná-Etendeka, Karoo-Ferrar, Siberian Traps, Deccan Traps, and Emeishan Large Igneous Provinces (LIPs), typically erupt two distinct basalt compositions—Low-Ti basalts and High-Ti basalts (Hawkesworth et al., 1988; Lightfoot et al., 1993; Sweeney et al., 1994; Melluso et al., 1995; Gibson et al., 1995; Pik et al., 1998; Xu et al., 2001; Jourdan et al., 2007; Ivanov et al., 2008). While there is some overlap in composition across these LIPs, there are striking similarities among High-Ti and Low-Ti lavas. In general, High-Ti (HT) basalts usually produce transitional to alkaline liquid lines of descent and are geochemically characterized as having >2 wt. % TiO_2 , higher Ti/Y (> 400), and tend to be more enriched in incompatible trace elements than Low-Ti (LT) basalts (Hawkesworth et al., 1988; Lightfoot et al., 1993; Sweeney et al., 1994; Melluso et al., 1995; Gibson et al., 1995; Pik et al., 1998; Xu et al., 2001; Jourdan et al., 2007). Low-Ti basalts are characterized as having < 2 wt.% TiO_2 , lower Ti/Y (<400), and are less enriched in incompatible trace elements than High-Ti basalts (Hawkesworth et al., 1988; Lightfoot et al., 1993; Sweeney et al., 1994; Melluso et al., 1995; Gibson et al., 1995; Pik et al., 1998; Xu et al., 2001; Jourdan et al., 2007; Ivanov et al., 2008). These geochemical distinctions have been used to support and model a variety of potential origins of CFBs, including thermo-chemical heterogeneities in the asthenosphere, and heterogeneities in the lithospheric mantle (Lightfoot et

al., 1993; Melluso et al., 1995; Gibson et al., 1995; Pik et al., 1998, 1999; Xu et al., 2001; Kieffer et al., 2004; Jourdan et al., 2007; Ivanov et al., 2008; Beccaluva et al., 2009; Heinonen et al., 2016).

Probing the origin of melt in CFBs is complicated by the lack of primitive magmas. The erupted flows that constitute CFB provinces are not primary magmas, having experienced extensive differentiation as a result of large volumes of melt migrating and stalling in the lithosphere prior to eruption (Cox, 1980; Farentani et al., 1996). (Thus, developing a more complete understanding of the overall system that creates CFB provinces requires insight into how lithospheric processes impact the CFB magmas. For example, the relative enrichment and depletion of trace elements in a magma is not only sensitive to the mantle melting conditions (pressure, temperature, and composition of melt source (Herzberg and Asimow, 2008; Kimura and Kawabata, 2015), but also to differentiation processes such as fractional crystallization, crustal assimilation, magma recharge and evacuation (Rayleigh, 1896; O'Hara, 1977; DePaolo, 1981; O'Hara and Mathews, 1981; Albarede, 1985; Lee et al., 2014). A major limitation in evaluating the effects of lithospheric processes on CFB magma evolution are the complexities inherent to their differentiation system (Cox, 1980; Bryan et al., 2010). For example, if the magma plumbing system is undergoing fractional crystallization, but is also periodically recharged over time while simultaneously losing mass due to eruption, the resulting liquid line of descent is no longer linear. A relatively complete flow sequence can more accurately evaluate how the magma system evolves over time, however most CFBs erupt via large dike swarms in the form of fissure eruptions (Ernst et al., 2001), which means a sequence of overlapping flows may represent differentiation trends among several magma pathways, further complicating a temporal analysis of magma evolution.

The NW Ethiopian Plateau is an ideal location to probe the lithospheric processes that control CFB magma evolution, and the potential origin of LT and HT magmas. In this region, the flow-stratigraphy is well-preserved and the separation between LT and HT dike swarms is ~400 km apart, resulting in little to no overlap between the two plumbing systems (Rooney et al., 2018). Moreover, the geochemical distinctions between Low-Ti (LT) basalt and High-Ti (HT) basalt are well characterized (Pik et al., 1998, 1999; Kieffer et al., 2004; Beccaluva et al., 2009). While the origin of HT basalts has been attributed to plume derived sources (Beccaluva et al., 2009; Rooney et al., 2013; Natali et al., 2016), the origin of LT basalts remains unclear, occluded by an overall depletion in incompatible elements (Pik et al., 1998, 1999; Kieffer et al., 2004; Beccaluva et al., 2009; Rooney, 2017) and geochemical indications of crustal contamination (e.g. enriched Ba, Sr and Pb, elevated $^{87}\text{Sr}/^{86}\text{Sr}$, and lower $^{206}\text{Pb}/^{204}\text{Pb}$).

Existing constraints show that the LT lavas are more voluminous than HT lavas, exhibit complex cumulate textures, and exhibit tight grouping on trace element variation diagrams despite the range in MgO (~4 – 12 wt. %). To achieve large volume eruptions of relatively evolved homogeneous lavas containing cumulates requires an efficient magma plumbing system with consistent melt input (Óskarsson et al., 2017). Specifically, geochemical modeling of trace element enrichment by Recharge-Eruption-Assimilation-Fractional Crystallization (RE AFC) has shown that different elements in a magma chamber undergoing recharge and eruption will achieve steady-state at different intervals based on their bulk partition coefficient (Lee et al., 2014).

In this paper, we utilize the existing conceptual petrographic framework to evaluate the origin of geochemical trends of LT lavas from the NW Ethiopian Plateau through time. We explore the possible mechanisms for the trace element characteristics of the LT lavas by

processes of magma differentiation by modeling the following: 1) Equilibrium crystallization using MELTS, 2) Fractional Crystallization (FC) (Rayleigh, 1896), 3) Assimilation with Fractional Crystallization (AFC) (DePaolo, 1981), and finally 4) REAFC (Lee et al., 2014). We find that trace element enrichment patterns in LT lavas from the Ethiopian CFB province can only be achieved at the MgO ranges observed when the effects of recharge and eruption are coupled with AFC processes. The results of REAFC modeling of the Middle LT flood basalt groups support a polybaric magma plumbing system that shallows over time. In addition, REAFC shows that the highest flux occurs midway through the main phase of flood volcanism (Middle group B), where the deeper system increases from 57% to 65% eruption of magma entering the system, and the shallow system increases from 30 % to 55% eruption. Lastly, we find that the amount of assimilation of Pan African Crust based on REAFC modeling ranges between 3-4 % during the highest flux events to as much as 10% as the system begins to shut down.

3.2 BACKGROUND

The Ethiopian-Yemen Large Igneous Province (LIP) comprises the two conjugate rift margins in East Africa (Figure 3.1a). Large-scale basaltic magmatism within the LIP is divided into three time periods: Eocene Initial phase (45 – 34 Ma), Oligocene Traps phase (~33.9 – 27 Ma), and the Early Miocene Resurgence phase (~26.9 – 22 Ma), after which time magmatic activity became more restricted to the evolving East African Rift System (Rooney, 2017). Magmatic activity during the Eocene Initial phase was restricted to southern Ethiopia and northern Kenya. During the Oligocene Traps phase, the eruption of the Ethiopian-Arabian plateau flood basalts expanded volcanism to include northern Ethiopia and Yemen (Baker et al., 1996a; Hofmann et al., 1997; Rochette et al., 1998; Rooney, 2017). After a magmatic hiatus,

renewed volcanism during the Early Miocene Resurgence phase was geographically more widespread but volumetrically less significant than the prior two phases of activity. Recent estimates for total lava volumes erupted from 45 – 22 Ma in the African Arabian LIP are $\sim 720,000 \text{ km}^3$, placing this province between Emeishan and Deccan LIPs in terms of overall volume (Rooney, 2017).

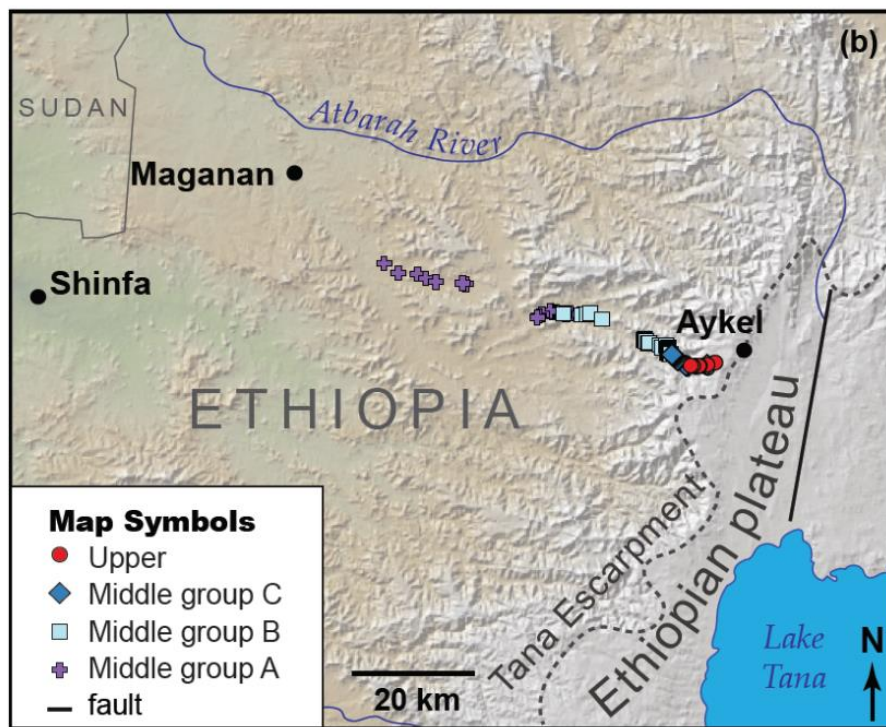
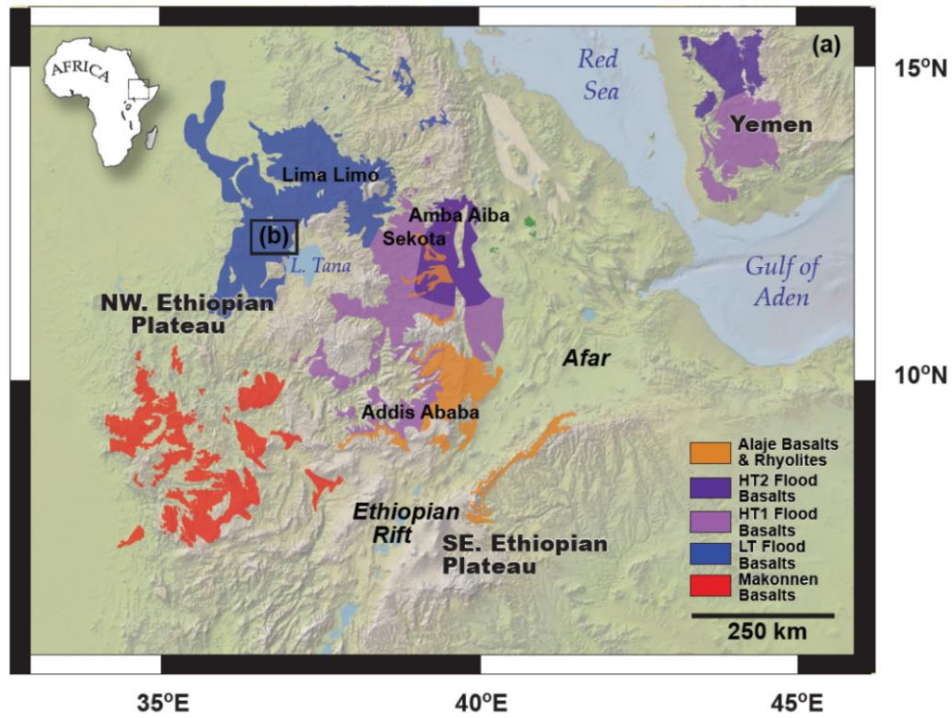
The Oligocene Traps phase flood basalts of the NW Ethiopian plateau have been spatially divided on the basis of two distinct compositions: a western Low-Ti (LT) sub-province (the focus of this study), and an eastern High-Ti (HT) sub-province (Pik et al., 1998). The LT basalts are tholeiitic with characteristically low TiO_2 (1 – 2.6 wt. %), low Nb/La (0.55 – 0.85), and higher SiO_2 (47 – 51 wt. %) (Pik et al., 1998). The LT lavas are enriched in large ion lithophile (LIL) elements like Ba, Sr, and Pb that has been interpreted as evidence of crustal contamination (Pik et al., 1998, 1999; Kieffer et al., 2004), however a mantle component previously enriched by subduction fluids has not been excluded as a possible source of the enrichment (Beccaluva et al., 2009).

The clear distinction between LT and HT lava types has led to investigations of their magmatic origins using geochemical and isotopic datasets (Pik et al., 1999; Kieffer et al., 2004; Beccaluva et al., 2009; Natali et al., 2016; Furman et al., 2016). While the source of HT lavas has been attributed to melting of the Afar plume (Pik et al., 1999; Natali et al., 2016), the origin of LT lavas remains a topic of debate (Pik et al., 1999; Kieffer et al., 2004; Beccaluva et al., 2009). Fractional crystallization models using normative mineralogy originally proposed by (Pik et al., 1998) suggested that LT magmas were derived through shallow fractionation processes. Subsequent trace element and isotopic analysis was used to propose two-stage AFC process for LT magmas, indicating a lower crustal and upper crustal component influencing geochemical

trends (Pik et al., 1999). Assimilation of continental crust has been assessed using trace element ratios (Nb/La, Ce/Pb, Ba/Th) and isotopic ratios (Sr-Nd-Pb systems) (Pik et al., 1999; Kieffer et al., 2004). While some studies attribute the low Nb/La and low $^{206}\text{Pb}/^{204}\text{Pb}$ of LT magmas to crustal contamination (Pik et al., 1999; Meshesha and Shinjo, 2007) others suggest the low Nb/La and nonradiogenic Pb could reflect source composition (Kieffer et al., 2004; Beccaluva et al., 2009). Thus, the origin of LT magmas remains largely unresolved due to the difficulty of constraining AFC processes using whole rock geochemistry in the absence of a petro-stratigraphic framework.

Within the LT province, lava groups have been recently subdivided on the basis of petrographic and stratigraphic similarities (Krans et al., 2018): 1) a Lower flood basalt which is dominantly ol-phyric with cpx-cumulates; 2) A Middle flood basalt which exhibits plagioclase megacrystic flows and oscillation between plagioclase-phyric and ol-phyric flows; and 3) an Upper flood basalt which is dominantly plagioclase-phyric and devoid of cumulates. The Middle flood basalt group is the most continuous flow-series preserved and is further subdivided by Krans et al. (2018) into group A (increasing flux stage), B (the apex of flux stage), and C (the waning stage). By utilizing this petro-stratigraphic framework in the interpretation of whole rock geochemistry, this study provides a novel integrative probe into the evolution of the LT flood basalts.

Figure 3.1. Sample location map. a) Map of Oligocene basalts in Ethiopia and Yemen (modified from Rooney, 2017). b) Location of middle and upper flood basalts lavas used in this study. Figure modified from Krans et al. (2018).



3.3 SAMPLES AND METHODS

In this paper we focus on flood basalt lavas from the NW Ethiopian plateau in order to examine the role of lithospheric process on magma evolution. In particular, this study examines a nearly continuous, 1307-m thick sequence of stratigraphically constrained flows in the LT sub-province. This sequence includes the main phase of flood volcanism and the transition to the termination of flood basalt activity (Figure 3.1). Flow groups, initially defined on the basis of petrographic and stratigraphic similarities (Krans et al., 2018), are retained in this study. The Middle and Upper flood basalt groups are the focus of this study, since they preserve the best stratigraphic continuity, making them ideal to evaluate temporal evolution of the magmatic system.

107 mafic lava samples were prepared for major and trace element analysis. Samples were cut in to ~30g representative billets, avoiding large crystals and alteration. The billets were then polished to remove saw marks and crushed in a steel jaw crusher. The resulting chips were powdered in a Bico disk pulverizer with ceramic plates to minimize contamination. Fused glass disks were prepared from the powder using a lithium tetraborate flux following procedures outlined elsewhere (Rooney et al., 2012b). Major element data were obtained using a Bruker S4 Pioneer XRF at Michigan State University (Supplementary Table B.1). Standards were analyzed as unknowns throughout the data collection period and are presented in Supplementary Table B.2. Following major element analysis, each disk was analyzed three times for trace elements using a Photon Machines G2 excimer laser coupled to a Thermo iCap ICP-MS following the procedures outlined in Rooney et al. (2015). Standard information, relative standard deviation of samples, and full procedural replicates (denoted with suffix *_X*) are presented in Supplementary Table B.3).

3.4 RESULTS

3.4.1 Major and Trace Element Analysis

Geochemical results are presented in Supplementary Table B.1 and are divided on the basis of petrostratigraphic groups as defined in Krans et al. (2018). These groups include Middle groups A-C and Upper flood basalts. All of the flows analyzed in this study are subalkaline and exhibit strong affinity with LT flood basalts observed in Ethiopia (Pik et al., 1998; Kieffer et al., 2004; Beccaluva et al., 2009; Rooney et al., 2018) in terms of major element and trace element variation as a function of MgO (Figure 3.2). Chondrite normalized rare earth element diagrams for all upper and middle flood basalts greater than 6.0 wt.% MgO are relatively flat lying with a mean value of $(La/Yb)_{CN} = 2.6 \pm 0.55$; 1σ ; $n=85$) (Figure 3.2). The chondrite normalized data stack mostly parallel, which is consistent with variation in MgO (Figure 3.3b, suggesting the majority of flows share a similar parental magma. Collectively, extended trace element diagrams show a broadly flat lying profile that follows 10-times primitive mantle enrichment with enrichments in Ba, Pb, and Sr and depletion in P (Figure 3.4). In terms of Cenozoic magmatism in East Africa, these are consistent with Group Ia magma types (Rooney, 2017).

Petrostratigraphic groups show clear distinction between Middle and Upper flood basalts when comparing means $\pm 1\sigma$ standard deviation (Supplementary Table B.4 in Appendix B). The Upper flood basalts exhibit high Nb/La (0.88 ± 0.07), CaO/Al₂O₃ (0.75 ± 0.05), TiO₂/P₂O₅ (12.4 ± 1.21), Ce/Pb (16.8 ± 2.78), Sc (42.3 ± 4.4 ppm), and low SiO₂ (48.4 ± 0.73 wt.%), Ba/La (9.31 ± 2.35). In contrast, the Middle flood basalts exhibit low Nb/La (0.66 ± 0.07), CaO/Al₂O₃ (0.69 ± 0.05), TiO₂/P₂O₅ (9.28 ± 1.11), Ce/Pb (12.3 ± 2.54), Sc (31.6 ± 3.0 ppm), and high SiO₂ (50.5 ± 0.97 wt.%), Ba/La (17.3 ± 3.82). In addition, Upper flood basalts have flatter chondrite

normalized REE slopes $(La/Yb)_{CN}$ (1.61 ± 0.18) compared to Middle flood basalts $(La/Yb)_{CN}$ (2.80 ± 0.33) (Figure 3.2).

Broad, overlapping geochemical shifts are observed within the Middle flood basalt groups (A-C). Most notable is the decreasing Ti/Y from group A (381 ± 26.3) to group B (367 ± 21.5) to group C (353 ± 25.0) and decreasing $(La/Yb)_{CN}$ from group A (2.95 ± 0.33) to group B (2.69 ± 0.27) to group C (2.27 ± 0.01). In addition, Middle group C exhibits the lowest Cr/Ni (1.72 ± 0.75), CaO/Al₂O₃ (0.64 ± 0.07), Ce/Pb (9.01 ± 1.37) and highest Ba/La (20.0 ± 3.34) compared to other Middle Flood basalts. In contrast, Middle group B has the highest Ce/Pb (13.9 ± 1.98) and lowest Ba/La (15.0 ± 3.0).

When plotted against elevation, lava chemistry exhibits distinct changes near the petrostratigraphic boundaries. Among the more notable are the sudden split between more evolved lavas (~4 wt. % MgO, 8 – 9 wt. % CaO, ~100 ppm Cr, <80 ppm Ni, <12 Ce/Pb) and less evolved lavas (~8 wt. % MgO, 11 – 12 wt. % CaO, ~250 ppm Cr, >100 ppm Ni, ≥14 Ce/Pb) at the base of Middle group A, Middle group A-B boundary, and Middle group B-C boundary (Figure 3.5). There is also a distinct shift in lava chemistry in the Upper lavas compared to the Middle, as noted earlier. Another notable change is the clear decoupling of elements such as CaO, TiO₂, Fe₂O₃, Al₂O₃, K₂O, SiO₂, Sc, and Sr between plagioclase-megacrystic flows and associated aphyric flows despite having similar low MgO values of ~ 4 wt. % (Figure 3.5). Finally, some sections appear to show temporal trends in element enrichment and depletion (i.e., Middle Group A and Upper) while in other sections trends are more obscure (i.e., Middle group B and C). These inconsistencies will be explored in more detail in the discussion (3.5.1).

Figure 3.2. Bivariant geochemical plots. a) Variation of select major and elements (plotted on a volatile-free basis with measured Fe_2O_3 Total converted to FeO (85%) and Fe_2O_3 (15%), then normalized to 100%) and compatible trace elements versus MgO as an index for differentiation. Data Sources: Supplementary Table B.1 for this study; all other published LT flood basalt data for Ethiopian Plateau—Pik et al. (1999), Kieffer et al. (2004), Teklay et al. (2005), Beccaluva et al. (2009), Rooney et al. (2018).

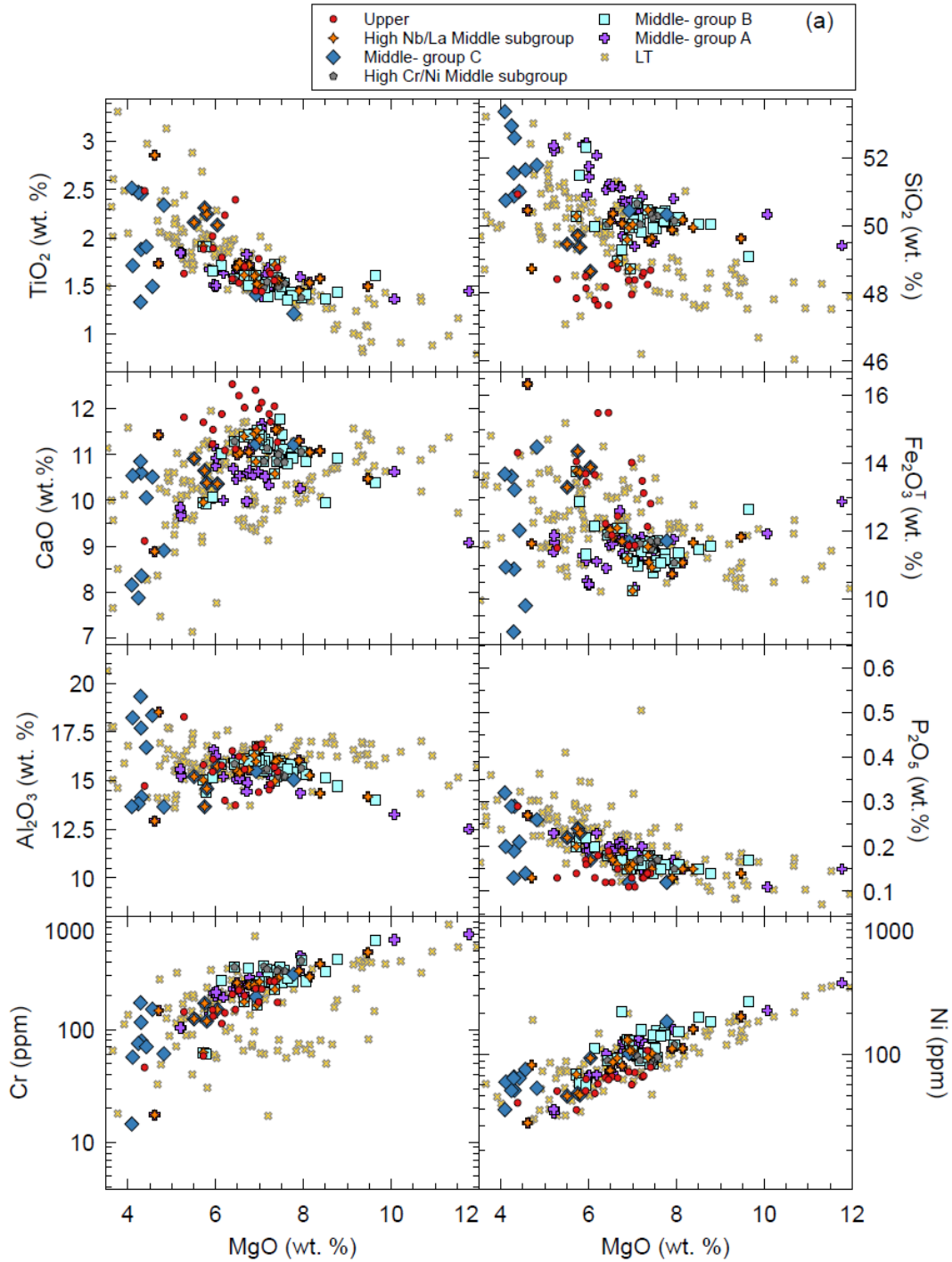


Figure 3.2. (cont'd)

b) Variation of select trace elements in ppm versus MgO in wt.% as an index for differentiation. Data from this study are presented in Supplementary Table B.1. Data sources for LT Flood basalts are the same as Figure 3.2a. c) Variation of select trace element ratios. Data from this study are presented in Supplementary Table B.1. Data sources for LT Flood basalts are the same as Figure 3.2a. The Ti/Y versus Nb/Y plot is used to classify low Ti (LT) or high Ti (HT1 and HT2) basalt in Ethiopia (after Pik et al., 1998).

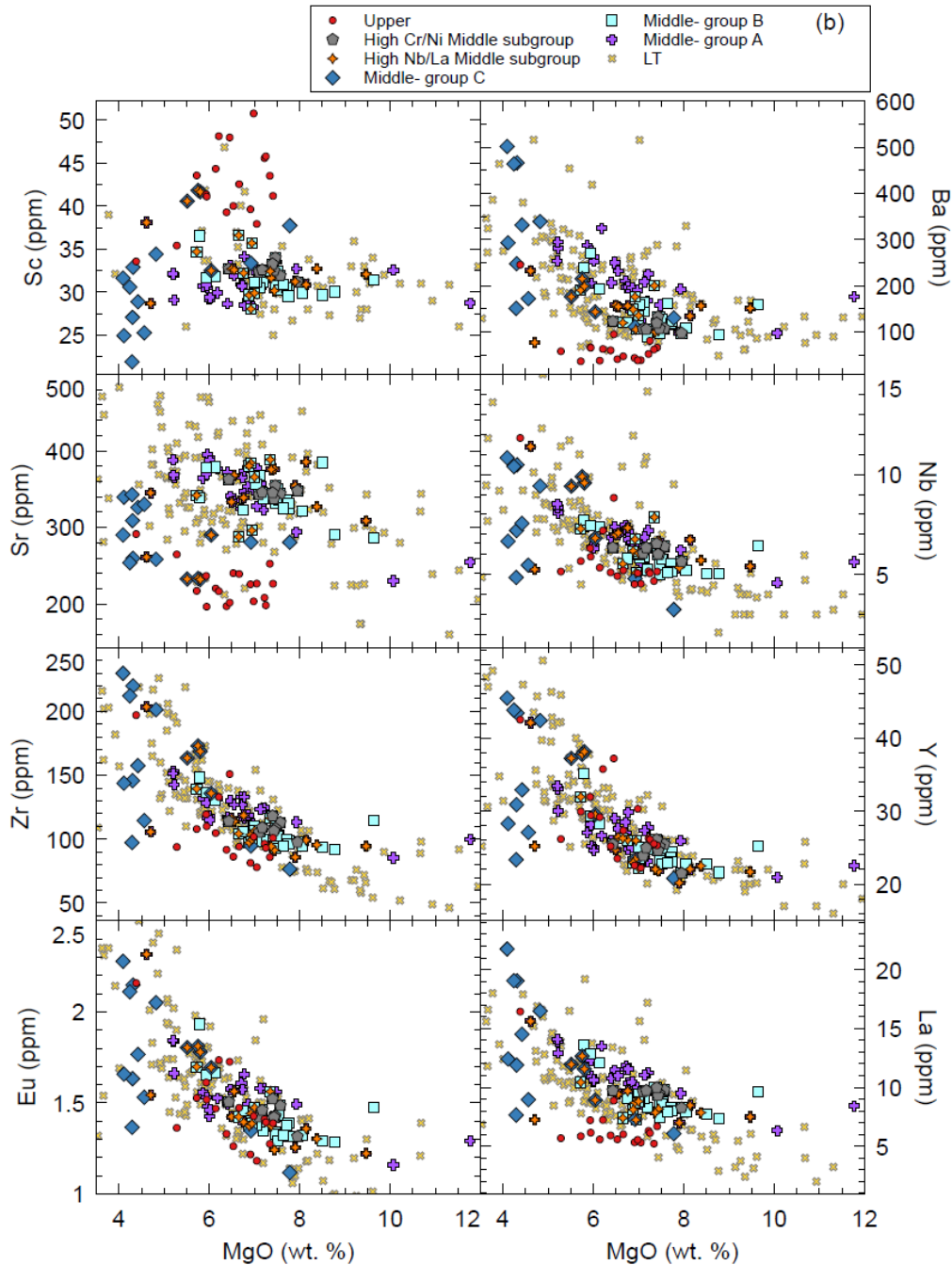


Figure 3.2. (cont'd)

The La/Nb vs. Ce/Pb plot is used to examine potential crustal influence on magmatic rocks (Hofmann et al., 1986). The solid and dashed lines represent the suggested average and standard deviation (respectively) for Ce/Pb in mantle rocks, as suggested by Hofmann et al. (1986). All samples from this study plot within ranges of published Ethiopian LT flood basalts. Note separation of LT basalts coded by petrostratigraphic groups (this study) in various plots—Middle group C has the lowest Ce/Pb and highest La/Nb. Conversely, the Upper flood basalts have the highest Ce/Pb and lowest La/Nb.

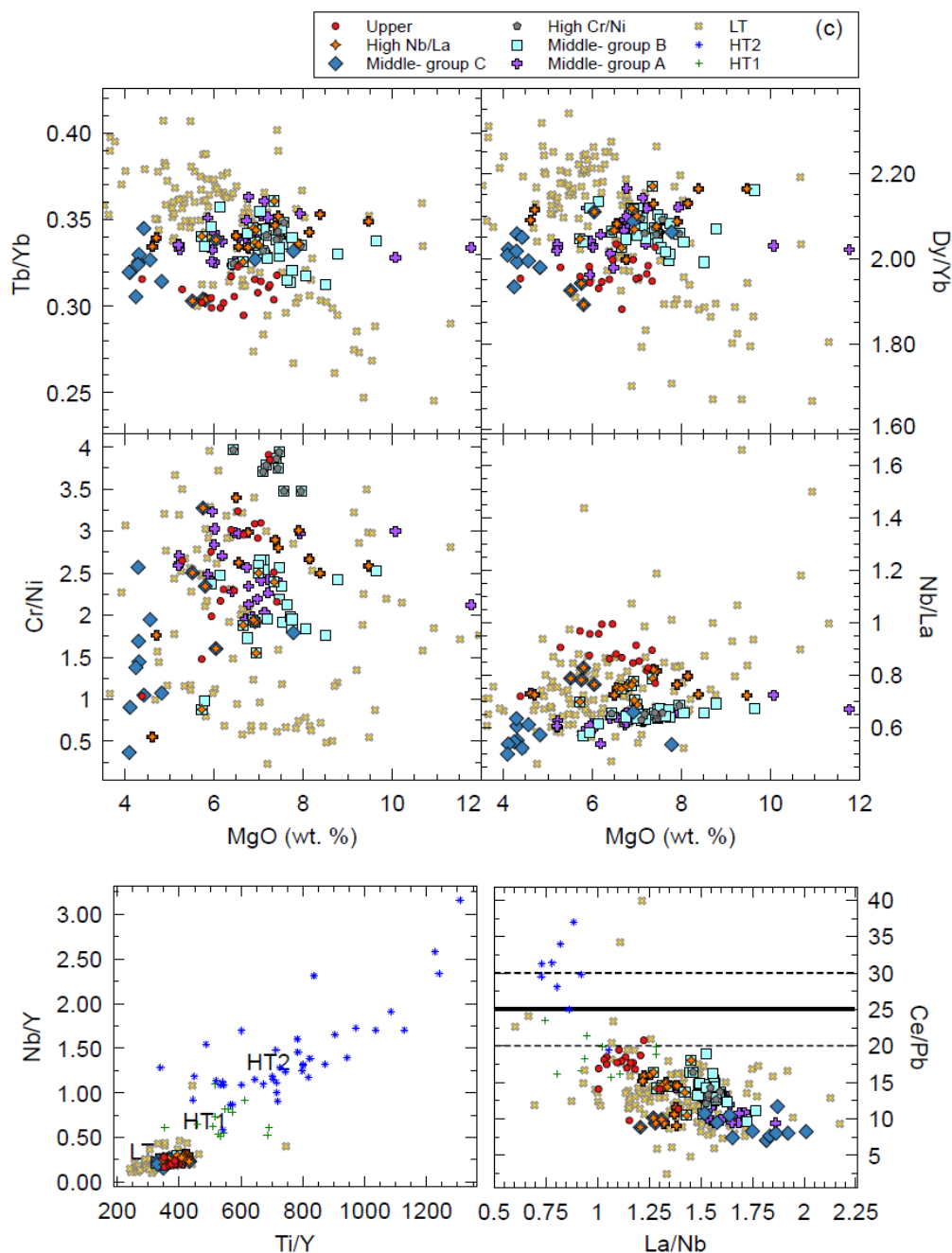


Figure 3.3. Chondrite normalized variation diagrams. Variation diagrams showing the behavior of REEs normalized to chondrite values (Boynnton, 1984) for flood basalt lavas in this study ≥ 6 wt.% MgO. Gray lines represent entire dataset restricted to 6 wt.% MgO and greater from this study. a) Data organized by the original petrostratigraphic groups defined by Krans et al (2018). b) Data organized by the new geochemical groups defined in this paper. $(La/Yb)_{CN}$ values shown to compare steepness/flatness of REE patterns (values reported as mean $\pm 1\sigma$ standard deviation with number of flows in parentheses). Note that within the Middle flood basalt low Nb/La subgroup $(La/Yb)_{CN}$ decreases (becomes flatter) over time (from group A to B to C). The Upper flood basalt have the lowest $(La/Yb)_{CN}$ and are suspected to be from a different parental melt than the Middle flood basalts.

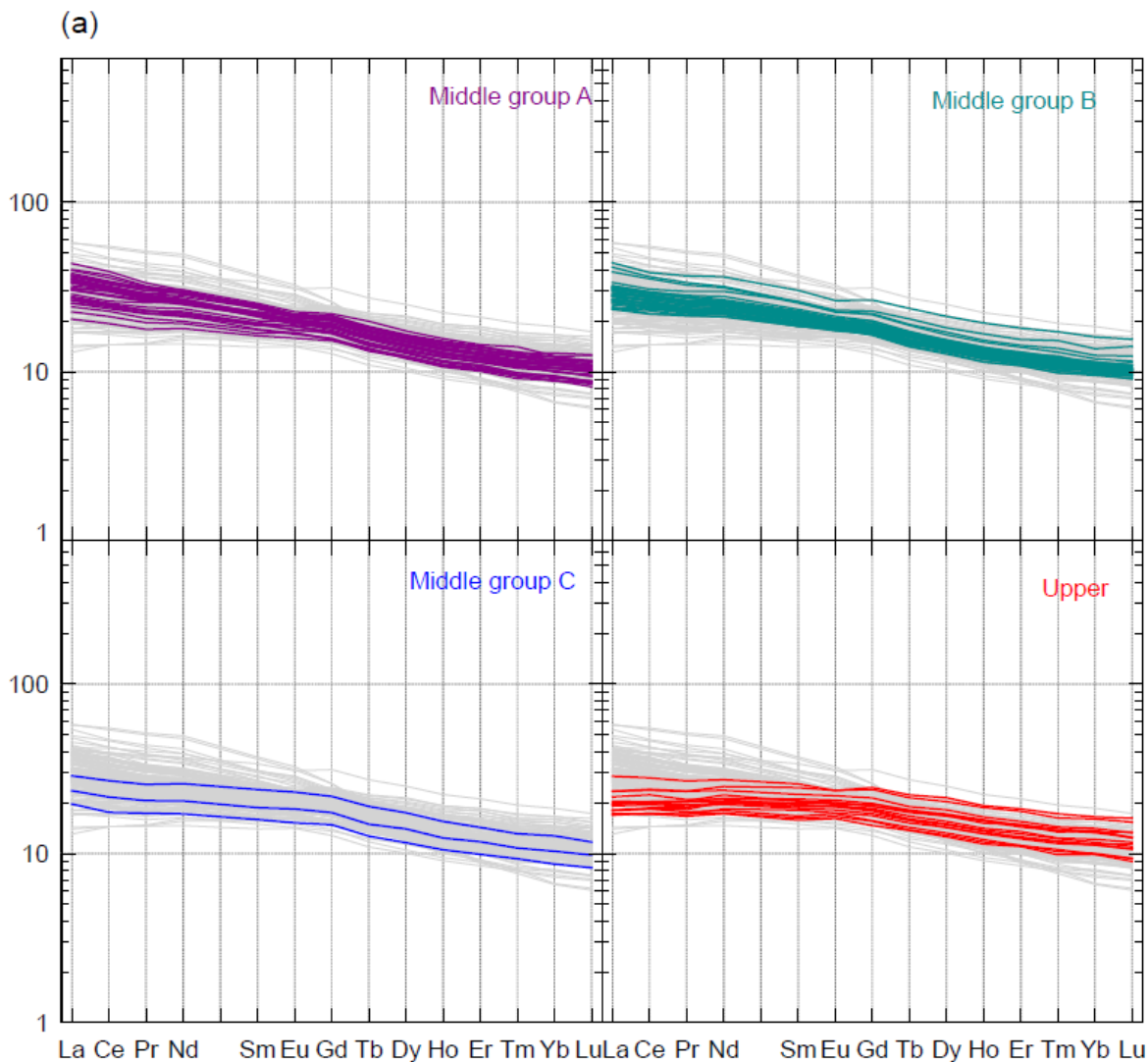
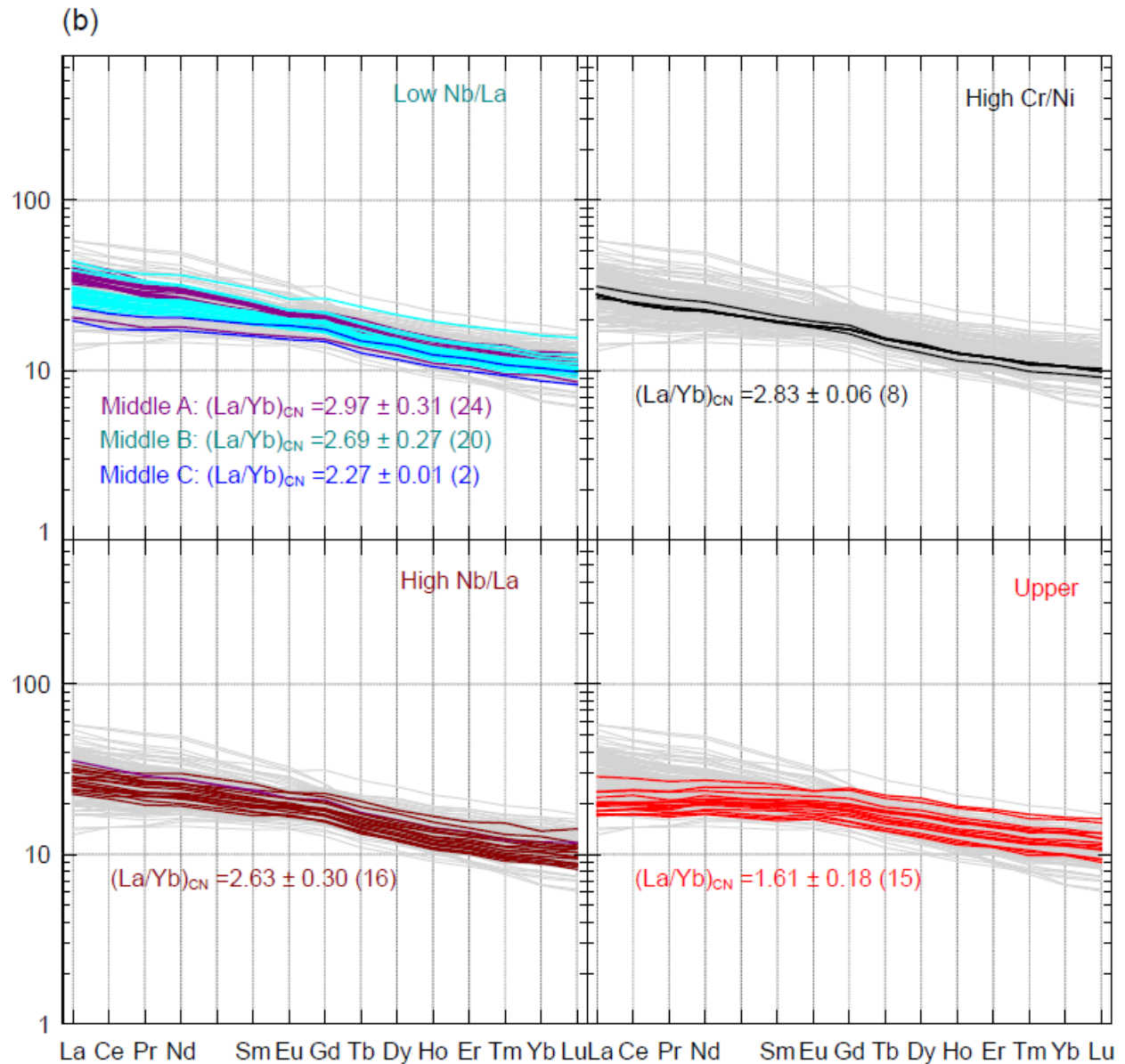


Figure 3.3. (cont'd)



3.4.2 New Geochemical Groups

Systematic variation in major and trace elements is observed within the Middle flood basalts that transgresses the existing petrostratigraphic groupings (Figure 3.5). For this reason, further subdivision of the Middle flood basalt groups has been assigned on the basis of trace

element clustering in bivariate diagrams and in primitive mantle normalized trace element diagrams (Figures 3.3a and 3.3b). The three new geochemical subgroups are: 1) the low Nb/La subgroup; 2) the high Nb/La subgroup; and 3) the high Cr/Ni subgroup.

The majority of flows (n=59) fall within the Low Nb/La subgroup. This subgroup exhibits low Nb/La (0.62 ± 0.07), Ti/Y (361 ± 19.7), $\text{TiO}_2/\text{P}_2\text{O}_5$ (8.87 ± 0.84) and somewhat higher SiO_2 (50.8 ± 0.99 wt.%) when compared to the high Nb/La subgroup (n=22): Nb/La (0.76 ± 0.04), Ti/Y (397 ± 27.6), $\text{TiO}_2/\text{P}_2\text{O}_5$ (10.5 ± 1.07) and lower SiO_2 (49.7 ± 0.57 wt.%). The high Cr/Ni subgroup is nearly identical to the Low Nb/La subgroup except it is higher in Cr/Ni (3.75 ± 0.19) and lower in Ba/La (11.83 ± 1.14), compared to Cr/Ni (2.19 ± 0.57) and Ba/La (18.39 ± 3.72) in the Low Nb/La subgroup.

Figure 3.4. Primitive mantle normalized variation diagrams. Variation diagrams showing the behavior of incompatible trace elements normalized to primitive mantle (Sun and McDonough, 1989) for flood basalt lavas ≥ 6 wt.% MgO (solid lines) and < 6 wt.% MgO (dashed lines). Gray lines represent entire dataset from this study. Thick solid line (yellow) is a Pan-African granite from west of Lake Tana (Rooney et al., 2018). Thick dotted and dashed line (dark red) is the proposed parental magma from Group A (discussed in section 3.5.2).

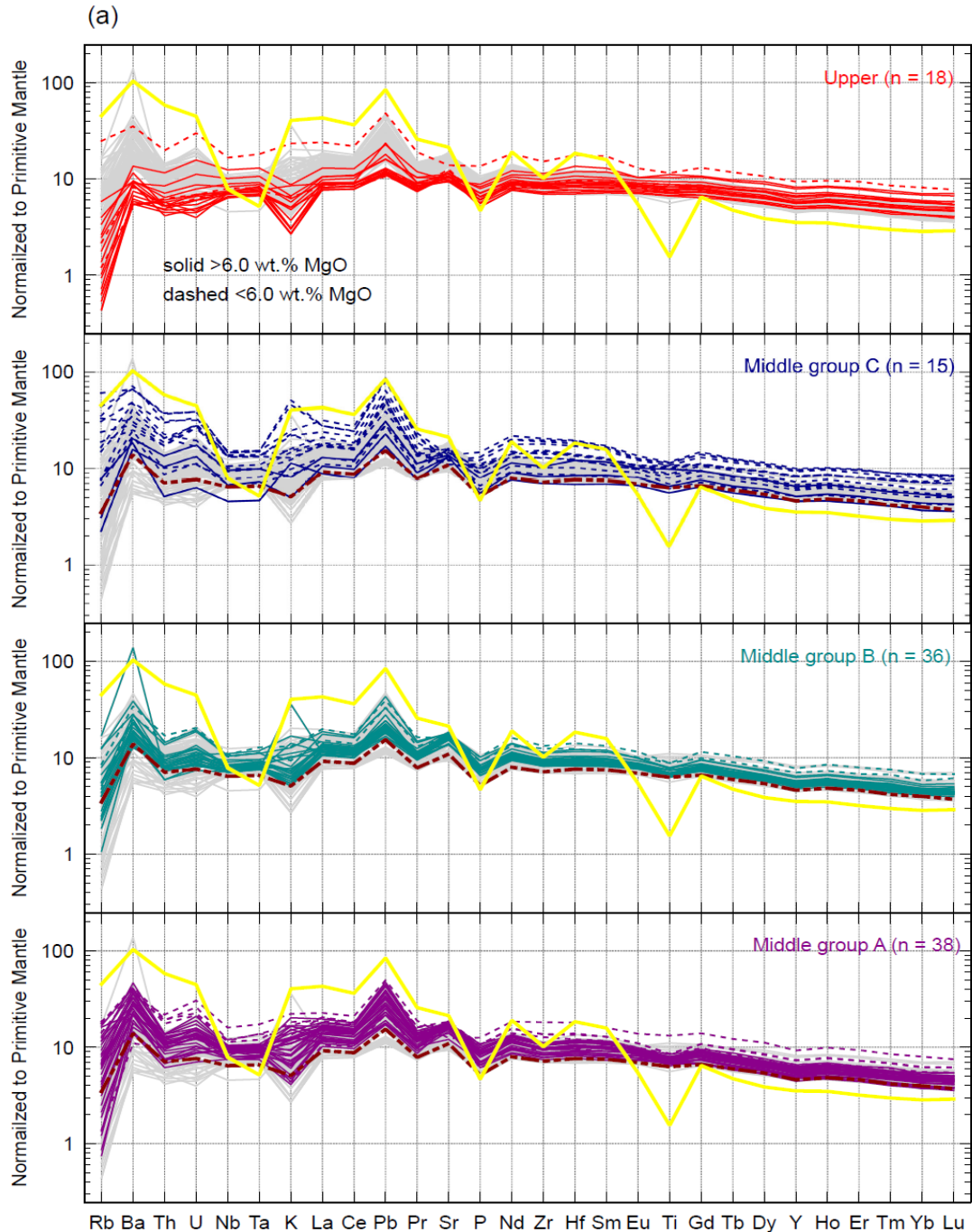


Figure 3.4. (cont'd)

a) Data organized by original petrostratigraphic groups defined by Krans *et al.* (2018). Number of flows given in parentheses. Solid lines are ≥ 6 wt.% MgO and dashed lines are < 6 wt.% MgO.

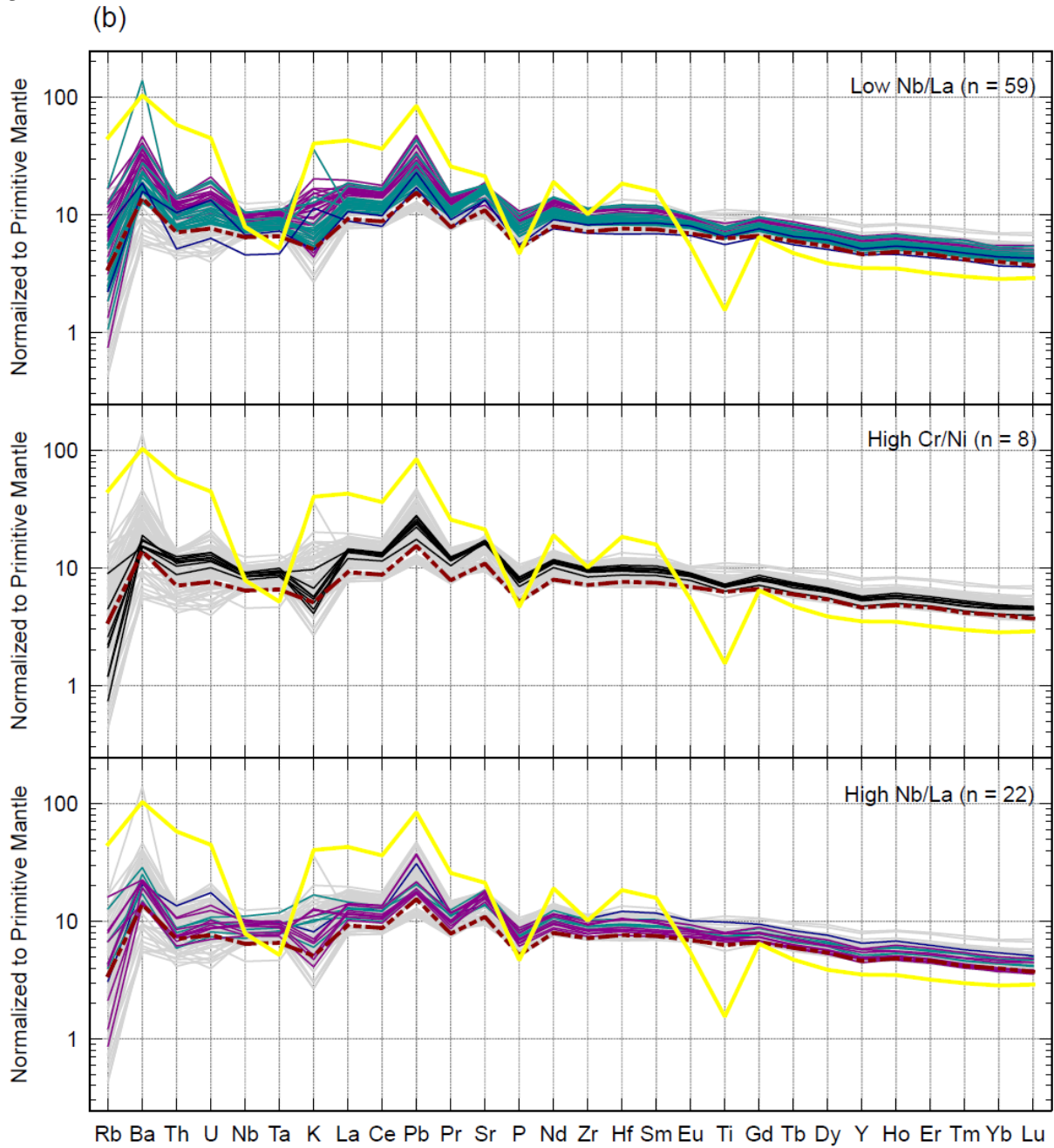


Figure 3.4. (cont'd)

Note that Middle group B has the tightest clustering of data despite having roughly the same number of flows as Middle group A. In contrast, Middle group C has the most range in data, including the most evolved samples. b) New geochemical groups defined in this paper, all are ≥ 6 wt.% MgO. Number of flows given in parentheses. Note the overall patterns between the three geochemical subgroups are similar, which supports the concept that they have a similar parent magma. The distinction between these groups is, however, important when modeling differentiation processes. c) Plagioclase-megacrystic flows (dotted lines) and intercalated aphyric flows from Middle groups A and C. All samples exhibit MgO restricted to ~ 4.4 wt.%. Note the aphyric flows are more enriched than the plagioclase-megacrystic flows, despite having identical MgO values. This suggests interactions between liquid and crystal mush zone are occurring in this system.

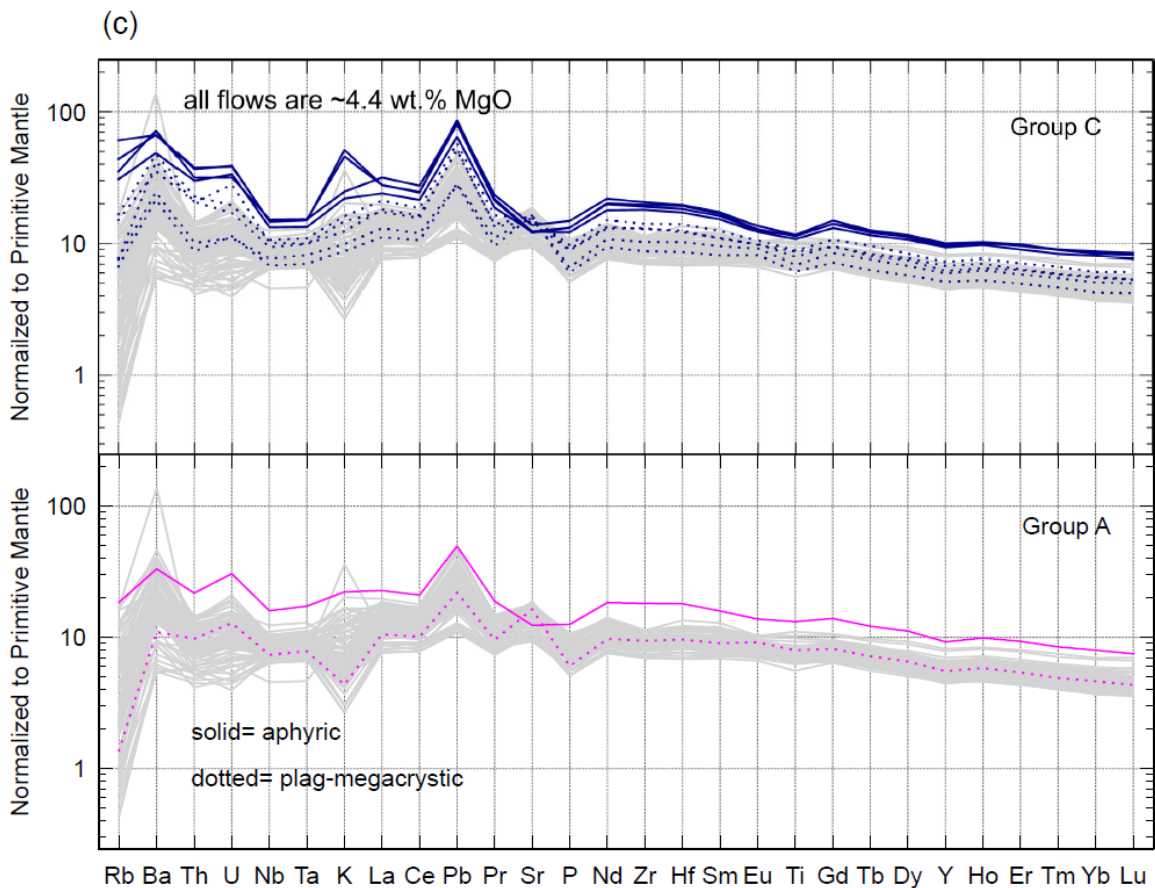


Figure 3.5. Chemostratigraphy of Middle and Upper LT basalts from the NW Ethiopian Plateau. Elevation of flow base is noted in meters above sea-level on the y-axis against select major elements (a) and select trace elements and trace element ratios (b).

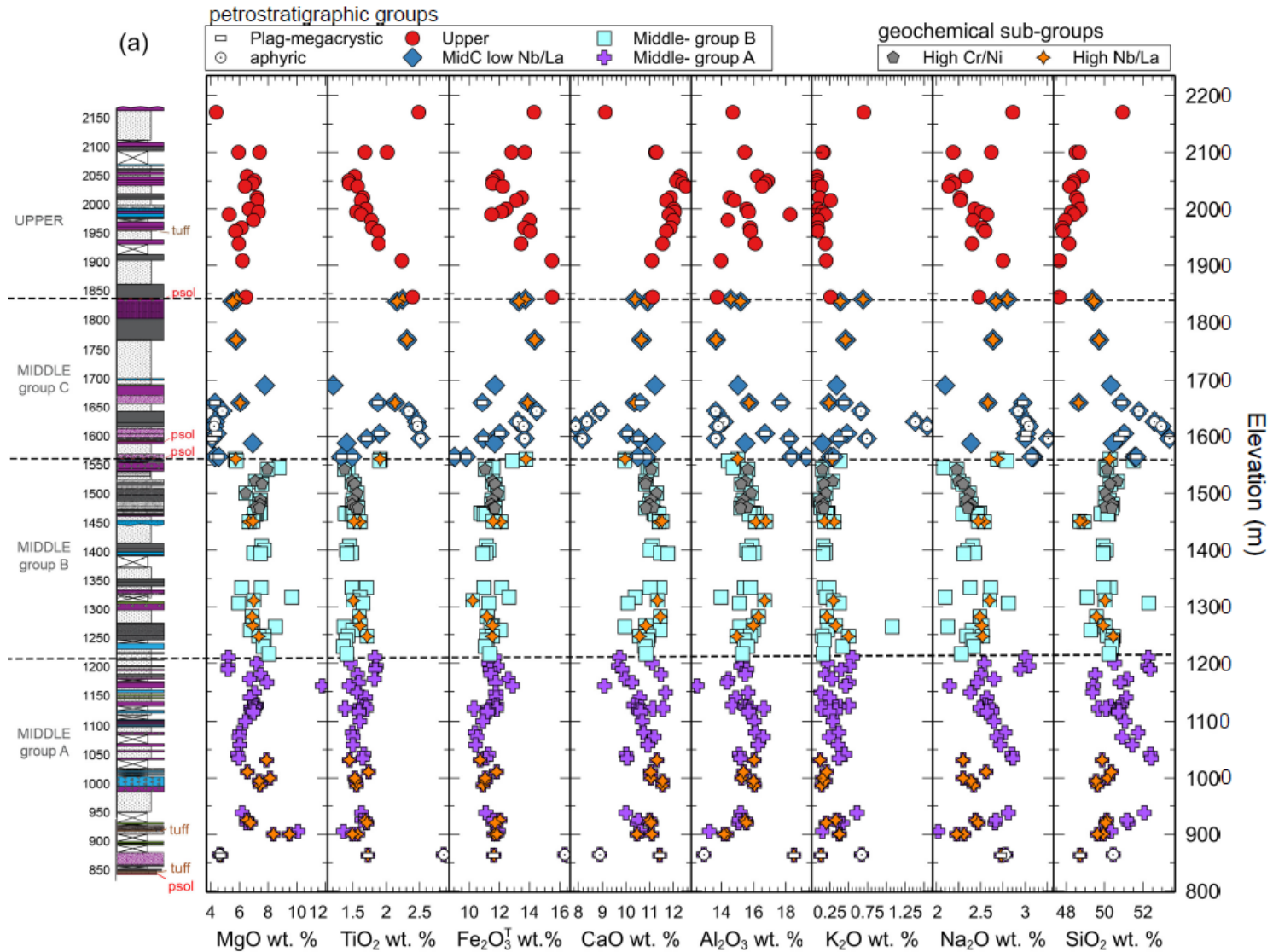


Figure 3.5. (cont'd)

Flow elevation is used as a proxy for time since the flows are flat-lying and lack evidence of tectonic disturbance to sequence (Krans et al., 2018; Chapter 2).

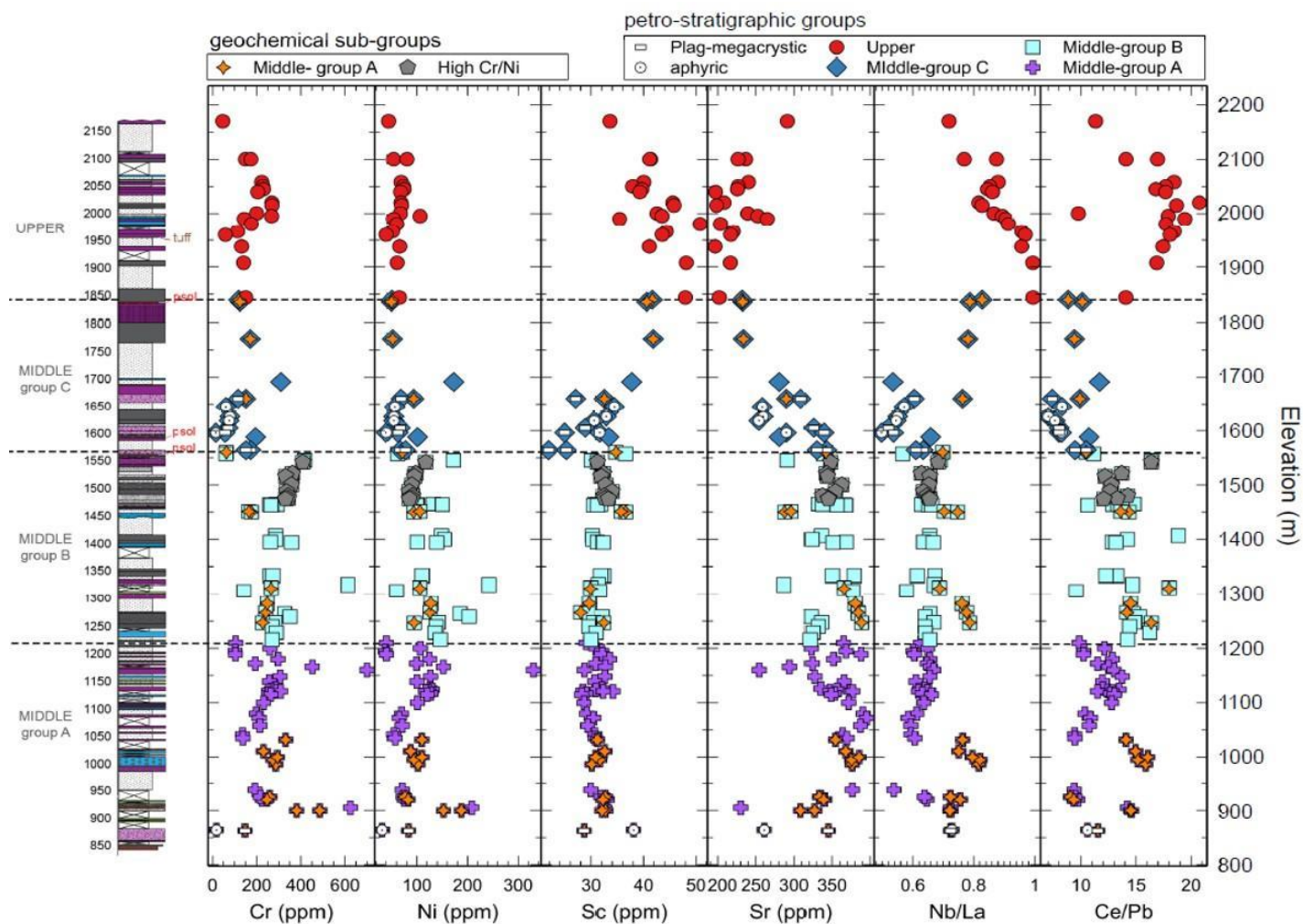


Figure 3.5. (cont'd)

Petrostratigraphic groups are the same as defined in Chapter 2 (Middle-group A, Middle-group B, Middle-group C, and Upper). Plagioclase-megacrystic flows and co-existing aphyric flows are symbolized to show de-coupling behavior in chemistry despite similar low MgO (~4.4 wt. %). New geochemical subgroups within each petrostratigraphic group are emphasized with overlapping symbols for high Nb/La and high Cr/Ni; Low Nb/La lavas have no overlapping symbol. The dashed lines represent the inferred boundary between petrostratigraphic groups as defined in Chapter 2, Figure 2.4. Colors denote primary mineral mode of flow and patterns denote key textural observations as defined in Krans et al., (2018) (See Figure 2.4 in Chapter 2 for higher resolution Petrostratigraphy). Paleosols (psol) and tuffs are labeled to highlight pauses in volcanic activity. Weathered vesicular basalt that was not sampled for geochemical analysis appears as white boxes with dot fill.

3.5 DISCUSSION

Prior work shows that the Ethiopian Flood Basalt Province is spatially divided into separate, geochemically distinct, LT and HT provinces (Pik et al., 1998, 1999; Kieffer et al., 2004). Other than a thin layer of LT lavas found at the base of a predominately HT sequence in the NE portion of the Ethiopian plateau (Kieffer et al., 2004), cyclicity between LT and HT magma types over the duration of flood basalt activity has not been observed.

To date, few studies have evaluated the stratigraphy of the Oligocene LT flood basalt province in Ethiopia (Kieffer et al., 2004; Prave, 2016; Krans et al., 2018). Prave et al. (2016) reports stratigraphy and ages for basalt units in the Lake Tana region, but it is unclear where these samples lie in the context of the LT flood basalt sequence and overlying shield activity. Kieffer et al. (2004) addresses petrogenesis of LT and HT lavas at large with the goal of pointing to source melt conditions and influence from crustal contamination. Kieffer et al. (2004) presents petrostratigraphic logs for various sections in LT and HT provinces, as well as geochemical variations with altitude distinguishing between lower and upper flood basalts in addition to overlying shield lavas. This dataset has been used to establish distinct, spatially separated volcanic centers where shield activity represents a decrease in magmatic flux over time and is

geochemically similar to underlying flood basalts (LT in the west, HT in the east). The Kieffer et al. (2004) dataset has not been used to evaluate the role of lithospheric processes within the upper and lower divisions of the LT sequence. The study by Krans et al. (2018) is the only detailed flow-by-flow analysis of the LT-province that investigates the evolution of the magmatic plumbing system. Krans et al. (2018) further divides the LT basalts into a Lower, Middle, and Upper sequence on the basis of broad petrographic changes in lavas with elevation and proposes a shallowing magma-plumbing system over time.

A two-stage AFC process for LT magma evolution has been suggested by Pik et al. (1999) in which assimilation of crustal components occurs in the lower and upper crust. However, no depth estimates have been made for the proposed polybaric plumbing system, and the lower and upper crustal components involved in assimilation are loosely defined. Furthermore, there is ongoing debate as to whether the chemical signature of LT lavas are the result of melt-crust interactions, melt-SCLM interactions, or related to heterogeneities in the source melt (Pik et al., 1999; Kieffer et al., 2004; Beccaluva et al., 2009).

The factors that limit resolution of this debate include trace element and isotopic compositions that are non-unique to any one case. In particular, the observed relative depletion of Nb, Ta, and Ti, along with relative enrichment in Ba and Pb observed in LT lavas is strikingly similar to that observed in the Pan African basement granite underlying the flood basalts (Rooney et al., 2018). However, similar enrichment and depletion is observed in arc-derived magmas where the mantle becomes enriched by fluids from the subducting slab. Therefore, the observed enrichment observed in LT basalts could be caused by melting of a metasomatically enriched SCLM as suggested by Beccaluva et al. (2009) or from recycled crust entrained in rising mantle plumes. Aside from variations in potential melt sources, fractionation of HFSE-

bearing oxide phases in the magma can also contribute to depletion of Nb, Ta, and Ti. Indeed, CFB lavas are not primary melts and have experienced significant differentiation within the lithosphere, therefore it is reasonable to assume some combination of the proposed enrichment/depletion trends typically observed in LT lavas. Understanding the origin of LT lavas thus requires a more detailed investigation of the lithospheric impact on the geochemistry of the magmatic system.

In the discussion that follows, we will attempt to 1) describe the geochemical changes that occur in Ethiopian LT lavas over time; 2) establish the depths of the polybaric plumbing system via MELTS using bulk-rock compositions as proxies for the liquid line of descent; 3) deconvolute the relative influence of lithospheric processes, such as fractionation, assimilation, recharge, and evacuation from the magma chamber (REAFC); and, 4) re-evaluate the conceptual model for evolution of the LT magmatic system in Ethiopia.

3.5.1 Insights from the Magmatic Stratigraphy

Before we can model differentiation trends in the LT lavas, we must first evaluate the occurrence of the new geochemical subgroups within the stratigraphy to determine if all three can be treated as products that can be modeled by differentiation. The high Cr/Ni lavas plot in the same ranges as the low Nb/La lavas with the exception of being higher in Cr/Ni. Stratigraphically, the high Cr/Ni subgroup is restricted to the upper portion of Middle group B and is associated primarily with aphyric flows with coarse-grained textures (ophitic and intergranular). The restricted range in composition observed in high Cr/Ni flows (Figure 3.2, Figure 3.3, Figure 3.4, Figure 3.5, and Supplementary Table 3.2) are consistent with the existing petrostratigraphic interpretation that these flows erupted during the apex of flood basalt volcanism (Krans et al., 2018). While the high Nb/La and low Nb/La subgroups occur

interspersed throughout the Middle flood basalt subgroups (Figure 3.5), the distribution is not entirely random. The low Nb/La subgroup, which comprises the majority of flows, is found throughout the stratigraphic section. However, the volumetrically less significant high Nb/La subgroup is highly concentrated near the beginning and ends of petrostratigraphic groups (e.g., Middle group A etc.), as well as when cumulate cargo is observed (clinopyroxene glomerocrysts and/or plagioclase megacrysts) (Figure 3.5). Since the High Nb/La lavas appear to share a common parental magma as the Low Nb/La (see convergence of Nb/La at MgO > 8.0 wt. % in Figure 3.2c), it is likely the case that these two subgroups diverge as a result of differentiation processes.

An increase in Nb/La with differentiation would require either fractionation of a phase that prefers La over Nb, or assimilation of a crustal component that has higher Nb/La. The former scenario would be difficult since the only observed phase that prefers La over Nb is plagioclase (see Supplementary Table C.1. and explanation of distribution coefficients in Appendix C). Since the difference in trace element compatibility between Nb ($D=0.01$) and La ($D=0.2$) in plagioclase is small, and that other phases like olivine, clinopyroxene, magnetite, and ilmenite would drive Nb/La down, this would require plagioclase to be the only phase fractionating to drive the Nb/La ratios up. It is unlikely that this is the case based on the observed modal mineralogy of the lavas (see section 2.3.2.2., Figure 2.4, and Figure 2.5 in Chapter 2). For the case of assimilation, measured crustal components tend to have lower Nb/La (0.19 – 0.65)(Pik et al., 1999; Rooney et al., 2018) than the high Nb/La LT lavas in this study (>0.7). A third possibility is that the high Nb/La signature could be related to solid-melt interaction between the crystal mush and residual liquid (Passmore et al., 2012). The association of high Nb/La lavas with cumulate cargo, and their placement in the stratigraphy is consistent

with periods of lower flux, and we propose they represent residual liquids chemically exchanging with the crystal mush. Since this is not a process, we can accurately evaluate using bulk rock geochemistry alone, we will omit the high Nb/La lavas while modeling in the remainder of this discussion.

Focusing now on the low Nb/La lavas, broad geochemical variations from Middle flood basalts are consistent with temporal changes in magmatic flux originally interpreted from petrostratigraphic evidence (Krans et al., 2018). Therefore, our initial conceptual model is that the LT lavas represent eruptions from a single magma chamber undergoing multiple recharge events from a similar parental magma source, and following each recharge event, the magma chamber evolves by a process of fractional crystallization. In this case, each flow erupted in sequence would represent a snapshot of the magmatic evolution of the chamber over time. In this simplified model, we could expect to see recharge events as abrupt increases in MgO, Ni, and Cr coupled with abrupt decreases in SiO₂, Al₂O₃, Na₂O, and K₂O. The subsequent differentiation of the magma chamber by fractional crystallization of mafic mineral phases (forsterite + diopside + anorthite) would show gradual depletion of MgO, Cr, and Ni coupled with gradual enrichment of SiO₂, Al₂O₃, Na₂O, and K₂O.

Beginning with Middle group A, we instead see a gradual increase in MgO, Ni, and Cr followed by an abrupt drop in these elements (Figure 3.5). Likewise, SiO₂, Al₂O₃, and Na₂O are gradually decreasing, followed by abrupt increases in these elements. These chemostratigraphic observations indicate the magma in the chamber becomes progressively more primitive over time, then abruptly transitions to more evolved lavas. These evolved lavas dominantly occur at the boundary between petrostratigraphic group (dashed lines in Figure 4.3), representing the first flows following a weathered horizon (i.e., paleosol prior to Middle group A, the unsampled

highly weathered basalt between Middle groups A and B, or the paleosol between Middle groups B and C; Figure 3.5). We suggest that a new pulse of flood basalt activity is stimulated by the recharge of more parental magmas, and initially expels the more evolved residual magma residing in the chamber after a hiatus. In this case, the residual magma would evolve during periods of low flux and low eruption. The gradual increase toward less evolved lavas over time can be explained by the continual removal of residual liquid being expelled from the magma chamber as the recharging magma progressively replaces the expelled liquid.

The above proposed simplified model for LT magma evolution has several inconsistencies if a single magma chamber undergoing recharge and fractional crystallization is assumed. The most notable inconsistency is the loss of clear evolutionary trends in Middle groups B and C (Figure 3.5). Additionally, elements such as Fe and Ti, which we only expect to fractionate significantly if the system is forming Fe-Ti oxides, are increasing in tandem with MgO in Middle group A (Figure 3.5a). This relationship between Fe, Ti, and MgO in Middle groups B and C seems to either disappear or become masked by other processes. By Middle group C, TiO₂ concentrations are at the highest observed in the LT basalts (~2.5 wt.%) while MgO is at the lowest (~4 wt. %) (Figure 3.5a). It is thus difficult to interpret the behavior of Mg, Fe, and Ti observed in the chemostratigraphy in terms of magma evolution within our initially hypothesized simplified model.

The inconsistencies in the liquid-line of descent outlined above require additional parameters to be added in our model. It is more likely that there are several staging chambers at various depths within the crust, each undergoing unique recharge and fractionation events (Bryan et al., 2010). In this case, individual flows within the magmatic stratigraphy may probe different regions of the magmatic plumbing system at various stages of differentiation. Flow-by-flow

interpretation of the magmatic stratigraphy would thus provide limited insight into the magmatic evolution of the LT flood basalts. However, the petrostratigraphic subgroups reveal broader changes in the magmatic plumbing system, and some of these changes can be seen within a subgroup (Krans et al., 2018). These petrostratigraphic groups temporally separate the LT flood basalts on the basis of broad petrological changes that indicate an overall shallowing of the magmatic plumbing system over time. We therefore examine the process of magmatic differentiation using these flow groups established on the basis of petrography and stratigraphy (Krans et al., 2018). We will first attempt to establish the range in crystallization depth for LT lavas using MELTS models (section 3.5.2). We will then apply FC, AFC, and REAFC models for deeper and shallower fractionating systems to resolve the upper and lower bounds of the geochemical range in LT lavas (section 3.5.3). Lastly, we will revise existing conceptual models for LT magma evolution in Ethiopia using the information gained from MELTS and REAFC modeling.

3.5.2 *MELTS Modeling*

Equilibrium crystallization modeling of the liquid line of descent for LT lavas was performed using the Excel version of rhyolite-MELTS v.1.1.x to estimate the range in depths that magma is being stalled and fractionated (Ghiorso and Sack, 1995; Gualda et al., 2012). While we presume many of the lavas have been chemically influenced by other lithospheric processes such as recharge, chamber evacuation, mixing, and assimilation, broad variations in depth of crystallization can still be inferred by capturing the lower and upper bounds of the LT lava.

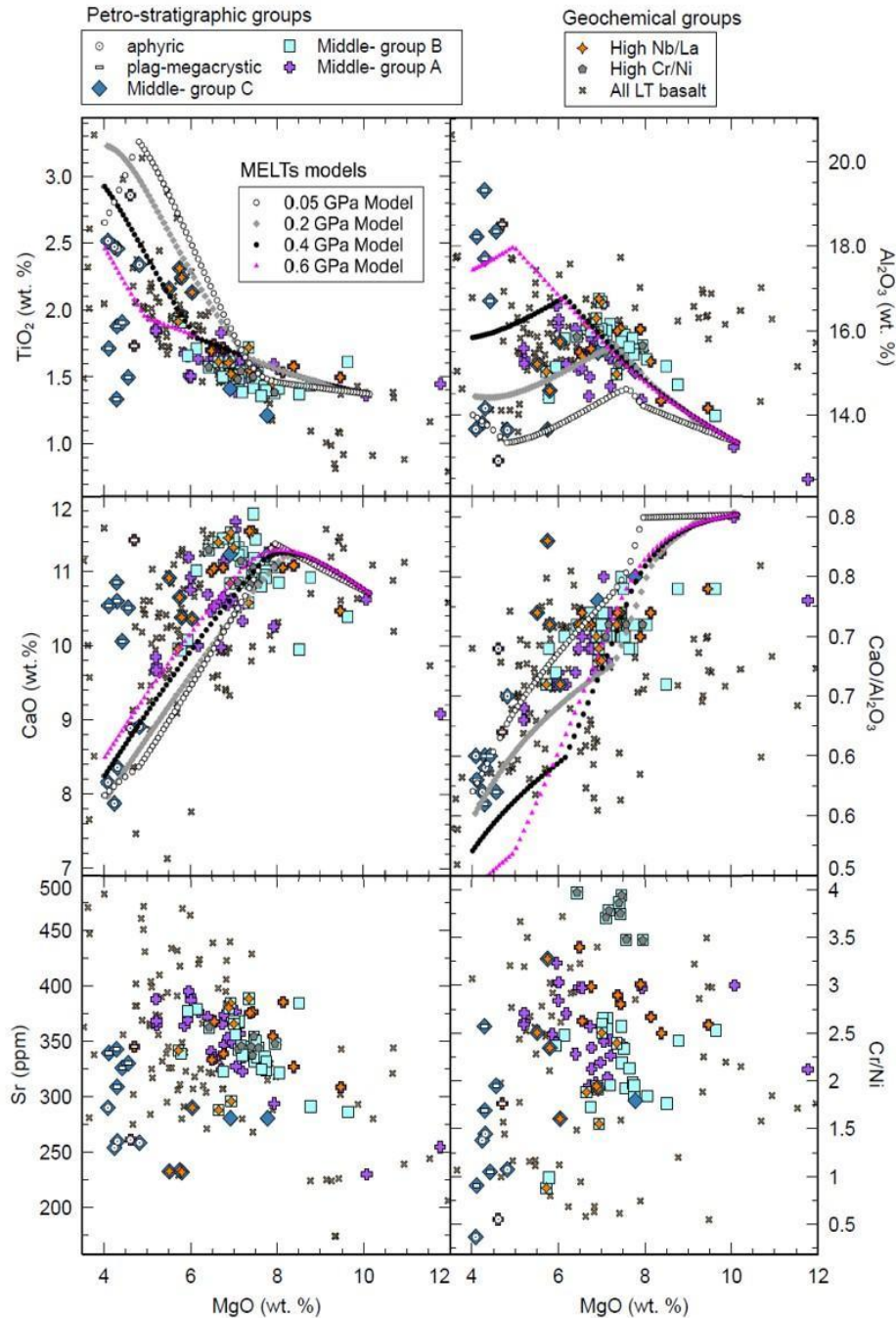
Models were run using a range of pressures, volatile contents, and oxygen fugacities reasonable for Ethiopian LT basalts (Figure 3.6). The most parental basalt (Sample 3383, MgO =

10.07 wt.%, Ni= 208 ppm, Cr= 625 ppm) lacking evidence of cumulates was selected from Middle group A to represent the starting composition in MELTS. Solutions were found using constant pressure models at 0.25 wt.% H₂O from 0.6 – 0.05 GPa (~middle to shallow crust). This is consistent with pressure ranges reported for coexisting LT dikes in the NW Ethiopian plateau (Rooney et al., 2018) and supports a polybaric plumbing system feeding the LT basalts (Krans et al., 2018). Initial runs predicted the crystallization of orthopyroxene which was not observed in thin section. We therefore suppressed the crystallization of orthopyroxene during model runs and re-ran all models. The suppression of orthopyroxene did not cause any noticeable changes to the liquid line of descent. All Middle groups (A-C) require a range of pressures to capture the majority of the dataset, with Middle group A generally trending deeper 0.4 – 0.6 GPa and Middle group C trending shallower (0.2 – 0.05 GPa).

While a subset of the LT basalt appears to be well predicted using the equilibrium crystallization models, no models (even when taken to extreme conditions) were able to capture the enriched CaO samples nor the TiO₂ and Fe₂O₃^T depleted samples. We suspect that buffering of the magmas as a result of recharge, along with melt-cumulate reactions may be causing the disparities we see in the MELTS models.

Given the differentiated character of the Ethiopian LT flood basalts (typically < 8 wt. % MgO) it is not surprising that a large portion of the data cannot be resolved using an equilibrium crystallization model. While the MELTS model is useful in showing relative variation in depth, the chemistry of the magmas is clearly influenced by processes within the lithosphere.

Figure 3.6. MELTS model results. Models were run in Excel Melts v.1.1x using a range in H_2O (0.1 – 1.0 wt.% H_2O) and pressures (0.05 – 1.0 GPa). Water estimates were limited to 1.0 wt. % since LT magmas in this region are considered to be ‘dry’ (Kieffer et al., 2004). Oxygen Fugacity was set to $QFM=0$ and was unconstrained during runs, as per Rooney (2018). Changing pressure models and constant pressure models were run. Orthopyroxene was predicted in MELTS but not observed petrographically, therefore we suppressed orthopyroxene in MELTS. The suppression of orthopyroxene did not yield a significant difference in liquid line of decent predicted by MELTS.



3.5.3 *Recharge, Evacuation, Assimilation, and Fractional Crystallization*

3.5.3.1 *RE AFC Model Construction*

The significance of recharge, eruption, and fractional crystallization on the chemical evolution of a magma chamber have been illustrated in numerous theoretical and numerical frameworks (O’Hara, 1977; DePaolo, 1981; O’Hara and Mathews, 1981; Albarede, 1985; O’Neill and Jenner, 2012; Lee et al., 2014). To date, very few studies have applied such models to CFB provinces (Yu et al., 2015; Grant et al., 2020; Davis et al., 2021), despite our understanding that LIPs have large magmatic plumbing systems that continually undergo recharge, eruption, and fractional crystallization.

We construct a series of constant mass Recharge-Evacuation-Assimilation-Fractional Crystallization (RE AFC) models using the formulation of Lee et al. (2014). We then compare these models to fractional crystallization models (FC) and combined assimilation and fractional crystallization models (AFC). Details on the equations used and how each parameter is defined can be found in Appendix C. The purpose of applying the RE AFC model is two-fold: 1) to place a quantitative (or semi-quantitative) constraint on the relative changes in magmatic flux over time by predicting the relative contribution of evacuation (i.e., eruption) on the LT system. We evaluate relative changes by evaluating the groups stratigraphically. 2) Estimate the relative percentage of crustal contamination needed to produce the low Nb/La ratio observed in LT lavas.

The RE AFC model applied herein treats a magma chamber as a box with a starting composition where each element has an initial concentration (C_{ch}^0). In reality, the plumbing system of a continental flood basalt province is more likely fed by a complex network of dikes and sills, so we will use the term “magma chamber” from here on to refer to the generalized

scenarios defined below. We generalize the LT plumbing system into a deeper network undergoing similar REAFC processes (deep system) and a shallower network undergoing similar processes (shallow system). The presence of a deep and shallow plumbing system (both interconnected and erupting in isolation) is supported by petrologic observations (Pik et al., 1998; Krans et al., 2018) and pressures determined by MELTS modeling (0.6 GPa to 0.05GPa; this study).

Deep system REAFC: Within the deep system, the starting composition and recharge composition are always the parental magma defined in the MELTS models (3383). This system can stall anywhere in the deep to middle crust (>0.5 GPa), where the fractionating phases are predominantly clinopyroxene and olivine with limited influence of plagioclase and Fe-Ti oxides (Supplementary Table C.2 in Appendix C).

Shallow system REAFC: Within the shallow system, the starting composition can vary from the original parental composition (3383) to any more evolved composition derived by REAFC from the parent (3383). However, without *a priori* information as to changes in the composition of the magma fluxing from deeper system, we apply an initial assumption that the composition equals that of the parent composition (3383). When attempts to find REAFC solutions using the original parent composition fail, we used the most parental composition from within the petrostratigraphic group being modeled (i.e., 3493 in group B, and 3497 in group C). We further require that any new starting composition must be derivable from the original parent composition by REAFC (Figure 3.8). Since this system is stalling in the shallower crust (<0.5 GPa), the fractionating phases are predominantly plagioclase and olivine with greater quantities of Fe-Ti oxides and limited to no influence from clinopyroxene (Supplementary Table C.2).

The concentration of each element evolves by cycles of time-integrated steps (ΔM_{re}) along the REAFC curve (C_{ch}^{REAFC}) as a function of the inputs (recharge and assimilation) and outputs (evacuation and fractional crystallization). This requires the concentration of each element in the crustal component involved in assimilation (C_{cc}) and the recharging magma (C_{re}) to be known. For the recharging magma, we assume a composition equal to the starting composition of the magma chamber. For the crustal component, we use the composition of a Pan African granite which underlies our basalts (Rooney et al., 2018). In addition, a bulk distribution coefficient for each element ($D_{solid/melt}$) must be estimated based on the modal mineralogy of crystallizing phases constrained by the deep versus shallow system (Supplementary Table C.1 and Supplementary Table C.2).

All of the above parameters can be realistically defined based on existing data and observations for the Ethiopian LT flood basalt province. This leaves three parameters to manipulate in the equation: the relative percentages of evacuation (α_e) crystallization (α_x), and the percentage of assimilation (α_{cc}) with respect to the recharge rate. If we assume that crustal assimilation cannot exceed 10 %, and that MELTS modeling provides an approximate constraint on α_x , then the most variation within the model occurs with the relative percent evacuated from the system during a given flow interval.

We selected elements to model that are most sensitive to the REAFC processes: (1) Elements compatible in the modelled mineral phases – Sr in plagioclase, Ni in olivine, and Cr in clinopyroxene. Ni and Cr are also highly sensitive to fractionation of Fe-Ti oxides (magnetite and ilmenite); (2) Elements incompatible in modelled mineral phases – Nb and La were selected due to their incompatibility and the unusually low Nb/La values reported for LT lavas that has classically been explained as resulting from crustal contamination (Pik et al., 1999).

3.5.3.2 *Model Results*

In our modelling, we sought to bracket the data between the deep and shallow models given the observation that both shallow and deep cumulate types are found intermittently throughout the Middle flood basalts, suggesting the LT lavas were derived from a combination of both a mid-crustal and shallow-crustal magmatic plumbing systems. The results of REAFC modeling can be seen in Figures 3.7 and 3.8. In Figure 3.7, the modeling results for a deep and shallow system by REAFC, AFC, and FC for Middle group A show the simultaneous solutions for multiple elements (Nb, La, Sr, Cr and Ni) varying as a function of differentiation (MgO).

AFC process could explain the observed data; however, this would require numerous AFC models with varying percentages of crustal assimilation to explain all observed data. In all cases, neither the FC nor AFC models were able to achieve the distinct decreasing Nb/La trends with decreasing MgO observed in the Middle LT flood basalts (Figure 3.8). In contrast, a single REAFC model can account for a larger subset of the lavas by simulating the observed curvature in the Nb/La vs. MgO. The REAFC models reported here predict between 3% and 10% assimilation of Pan African granite, with the majority of lavas falling between 3-4% crustal assimilation. The upper estimate for assimilation in this study is similar to a numerical estimate made by Kieffer et al. (2004) for the Ethiopian LT flood basalts (12 %) and is considerably less than what has been estimated for the conjugate Yemen flood-basalt province using isotopic AFC models (25 %; Baker, 2000).

Comparing REAFC temporally in the Middle flood basalts, we see the smallest contribution of crustal assimilation and the highest evacuation occurring in Middle group B (Figure 3.8). The greatest contribution of crustal assimilation occurs in Middle group C, which is coupled with the lowest evacuation (eruption). The REAFC model results are in strong

agreement with field, petrographic, and geochemical observations that indicate the LT magma system achieves an apex of flux in Middle group B, then begins to diminish during Middle group C. In addition, a deep REAFC system for Middle group B was found to be unnecessary since a shallow system model was entirely sufficient to fit the data (ignoring the one outlier near 8 wt.% MgO).

Figure 3.7. REAFC Model results for shallow and deep fractionating systems within Middle group A, Low Nb/La lavas. Each element is plotted against MgO (wt. %) to illustrate the enrichment trends modeled and observed in LT lavas. The right side of the figure shows elements compatible ($D > 1$; Supplementary Table C.1) within observed mineral phases in LT lavas; each element is uniquely sensitive to a dominant phase (e.g., Ni in olivine, Cr in clinopyroxene, and Sr in plagioclase). Both Ni and Cr are highly sensitive to fractionation of Fe-Ti oxides, also observed in the LT lavas, therefore we use small percentages of ilmenite and magnetite when calculating bulk D .

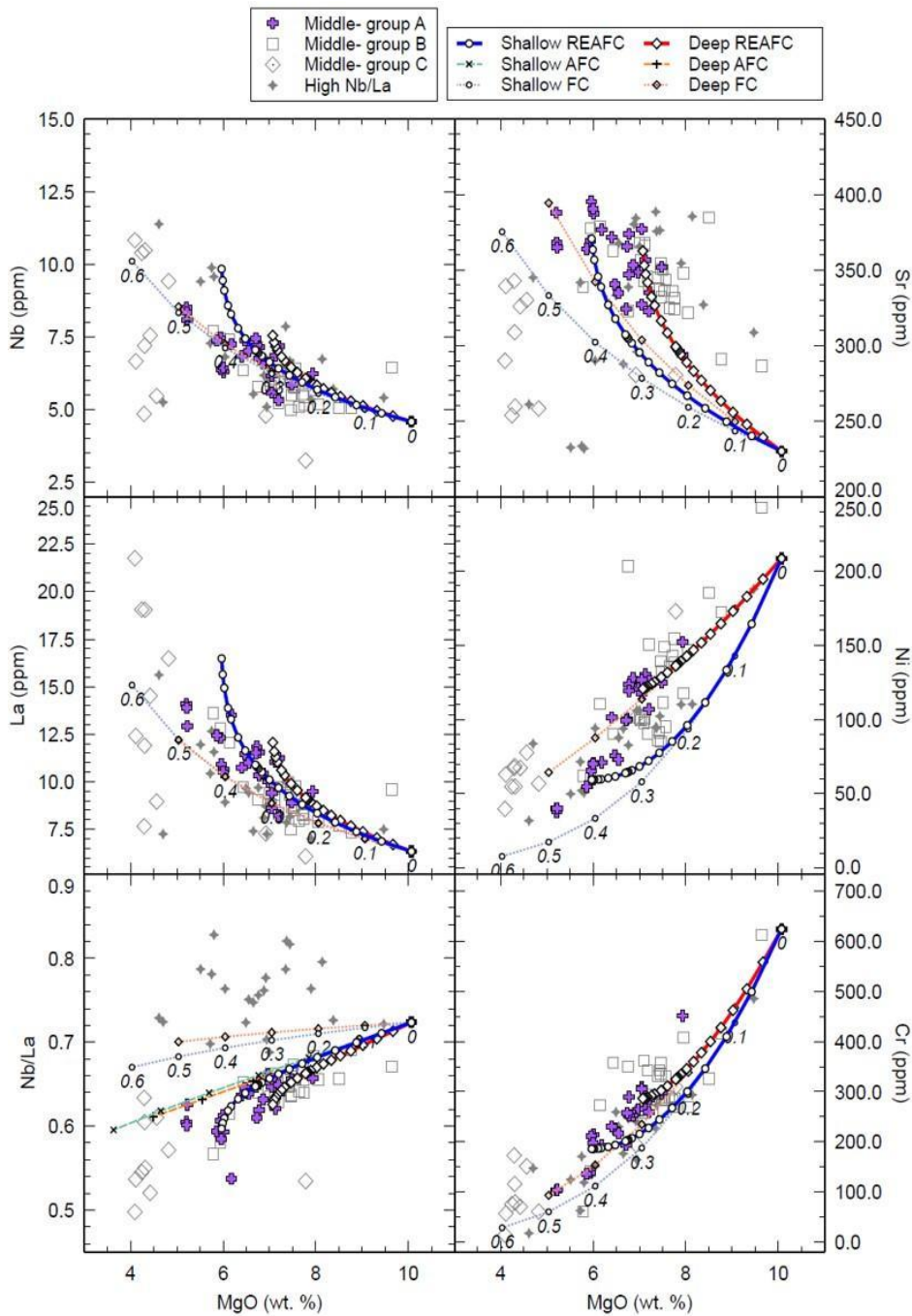


Figure 3.7. (cont'd)

The left side of the figure shows elements that are incompatible ($D < 1$; Supplementary Table C.1) within observed mineral phases in LT lavas, in particular, the HFSEs Nb and La. In addition, we have added Nb/La to illustrate how the commonly observed low Nb/La ratios in LT lavas can be achieved. The compatible elements (Sr, Ni, and Cr) vs. MgO must be satisfied by the REAFC model results prior to accepting the evacuation-assimilation-crystallization conditions—this provides an internal check that reduces the number of non-unique solutions that could fit Nb and La versus MgO. We have added the FC and AFC results to Nb/La versus MgO to emphasize the necessity for the addition of recharge and evacuation to model the Nb/La trends observed in LT basalts.

Figure 3.8. REAFC versus AFC and FC model results for Middle groups A, B, and C Low Nb/La lavas.

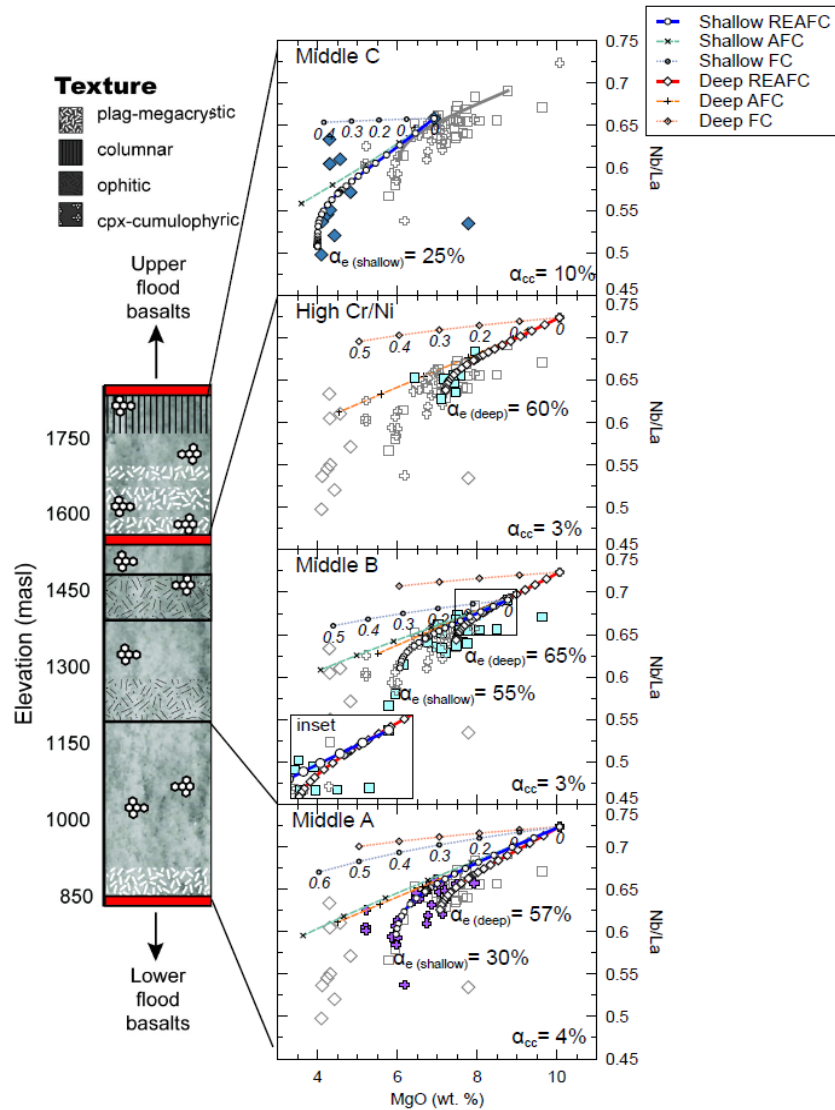


Figure 3.8. (cont'd)

High Cr/Ni lavas from group B (a sub-set within in the Low Nb/La geochemical group) have also been modeled as they are thought to occur as the system achieves an apex in eruption. The simplified petrostratigraphic section on the left side of figure is modified from Krans et al. (2018) and illustrates changes in cumulate textures that are indicative of fractionation depth of crystal mush zones. Numbers along FC curves denote decimal percentage of crystalized material with respect to remaining liquid. All deep REAFC systems have the same starting composition which is the parental composition (3383). There are at least three shallow systems with differing starting compositions: group A has a starting composition equal to the parental composition (3383), Middle B has a starting composition equal to an evolved output from the deep REAFC curve (see inset), and Middle C has a starting composition equal to an evolved output from the shallow REAFC system of group A (gray line). In general, the deeper system tends to have higher evacuation (α_e) by mass than the shallower system. In addition, evacuation by mass is greatest in Middle group B and lowest in Middle group C. Note the greatest amount of crustal assimilation (α_{cc}) occurs in group C, while the least crustal assimilation occurs in group B. An interesting note—there are three plag-megacrystic flows within Group C that lie between the FC and AFC curves, while all other lavas lie along the REAFC curve.

3.5.4 Improved Conceptual model for LT Magma Evolution

The results of the MELTS and REAFC models are in agreement with a polybaric plumbing system that progressively shallows over time. First, the MELTS models estimate that LT lavas were fractionating between 0.6 – 0.05 GPa (middle to shallow crust), and that both the deep and the shallow systems were contemporaneous throughout Middle flood basalt activity (Figure 3.6). Our observation that a deep and shallow REAFC model are required to fit the upper and lower bounds of the data further support the existence of a polybaric plumbing system. Second, the starting composition of the shallow REAFC system becomes progressively more evolved over time (from group A to C), while the percentage of material evacuating the shallow system increases (from A to B) and then decreases (from B to C) (Figure 3.8).

We suggest that the early plumbing system (Middle group A) is not well established in terms of volume and connectivity, therefore evacuating the chambers will be less efficient (Figure 3.9a). In this paradigm, magma stalls at multiple levels within the crust, permitting

different phase assemblages to control fractionation depending on the stalling depth. These different assemblages will impart a distinct trace element fingerprint on lavas erupted from the deeper versus shallower systems (Figure 3.9a). The cumulate material transported by various lavas reflects these different pressure regimes. During this phase, only a single parental composition (i.e., 3383) is required, with limited assimilation of the Pan African granitic crust.

The transition from Middle group A to Middle group B is coincident with the disappearance of plagioclase cumulates in flows. Despite the disappearance of plagioclase megacrysts, MELTS and REAFC models indicate the shallow system and deep system are both active. The more restricted geochemical ranges observed in the chemostratigraphy (Figure 3.5) as well as the higher evacuation percentages (Figures 3.7) predicted in both the shallow and deep REAFC models point to this phase as representing an apex in magmatic flux. The increase in magma supplying the deep and shallow system allows the plumbing system to mature and become more connected; this in turn, along with a shallowing of the plumbing system, permits more efficient magma evacuation (eruption) (Figure 3.9b).

Middle flood basalt group C occurs after a stratigraphically defined hiatus. REAFC models show no plausible solutions that incorporate a deep fractionating system, consistent with the interpretation of a dying magma system that once efficiently fed the Ethiopian flood basalts (Krans et al., 2018). The shallow system has again evolved in starting and recharge composition in comparison to earlier flow groups (A and B). Among all three Middle flood basalt groups, Middle group C exhibits the lowest relative proportion of magma erupting (25 %), and the highest proportion of assimilated Pan African crust (10%). As the magma supply entering the lower crust diminishes, less buffering from recharge and eruption results in the residual liquid in

the existing magma plumbing system being more impacted more profoundly by fractional crystallization and assimilation (Figure 3.9c).

Figure 3.9. Revised conceptual model for LT magma evolution in Ethiopia. Symbols used in figures are the same as in the REAFC constant mass magma chamber model parameters, where α_x = relative proportion of fractional crystallization, α_{cc} = relative proportion of assimilation, α_e = relative proportion of eruption/evacuation C_{ch}^0 = starting composition of the magma chamber, C_{re} = composition of recharging magma. a) Middle flood basalt group A is fed by a deep fractionating system and shallow system where the starting composition is equal to the recharging composition (in this case sample 3383 from Middle group A). The deep system would occur in the mid-crust (~0.6 GPa) where clinopyroxene and olivine are the dominant crystallizing phases. In the shallow system (~0.4 GPa), olivine and plagioclase are the dominant crystallizing phases, with a greater influence of Fe-Ti oxides than the deeper system. The deeper system has a higher relative proportion of erupted magma than the shallow system. This is not to say that the deeper plumbing system erupted a greater total volume of basalt, but rather that more of what entered the chamber via recharge was escaping to the surface. Assimilation of Pan African crust is less than 5% in both the deep and shallow system.

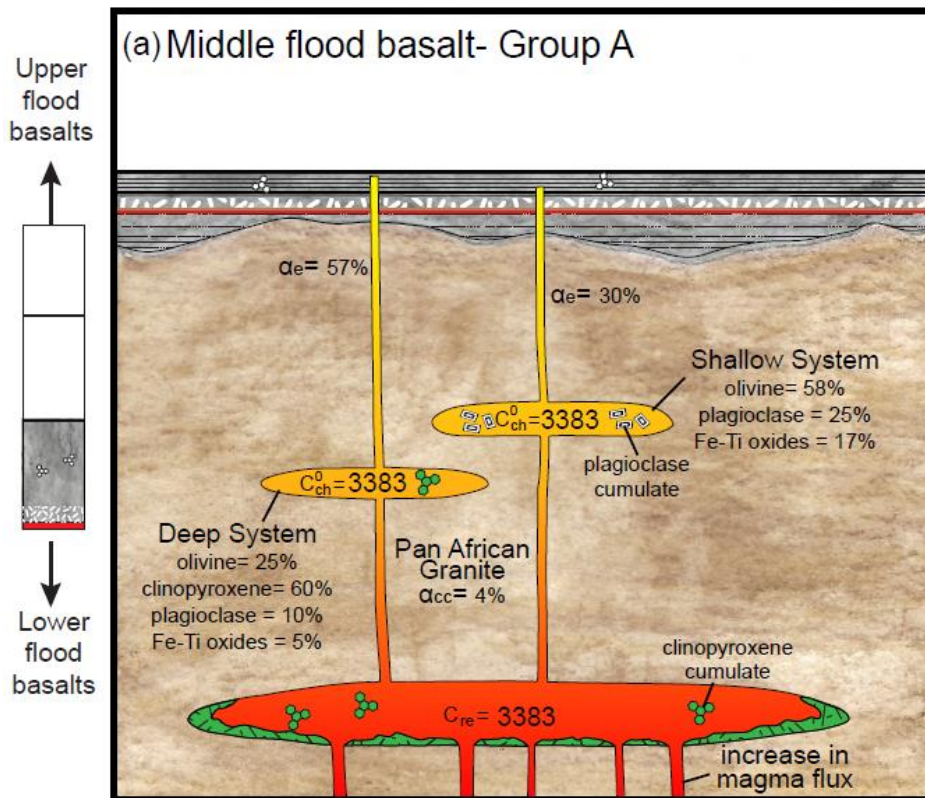


Figure 3.9. (cont'd)

b) Middle flood basalt group B is still fed by a deep and shallow system, but we are now seeing a more levels of stagnation in the crust. The deep system still has the same starting and recharging compositions as in Middle group A, but with an increase in olivine fractionation and absence of plagioclase fractionation in the High Cr/Ni subgroup (thought to represent the apex of flood volcanism). The shallow system has now evolved to a new starting composition, which could be residual liquid from earlier eruptions or a mixed liquid from multiple pathways—we use sample 3493 as the new starting composition and recharging composition for the shallow system. Both the deep and shallow system experience elevated relative proportions of erupted magma compared to Middle group A. Assimilation of Pan African crust is still less than 5%. c) Middle flood basalt group C occurs after a hiatus. REAFC models show no plausible solutions when attempting to use a deep fractionating system. The shallow system, again, has a starting composition that is evolved in comparison to earlier flow groups (A and B)—here we use sample 3497 as the starting and recharging composition. The relative proportion of magma erupting from this system is the lowest it has been in all three Middle flood basalt groups (25 %). In addition, the relative proportion of assimilated Pan African crust is at its highest of all the three Middle flood basalt groups (10%).

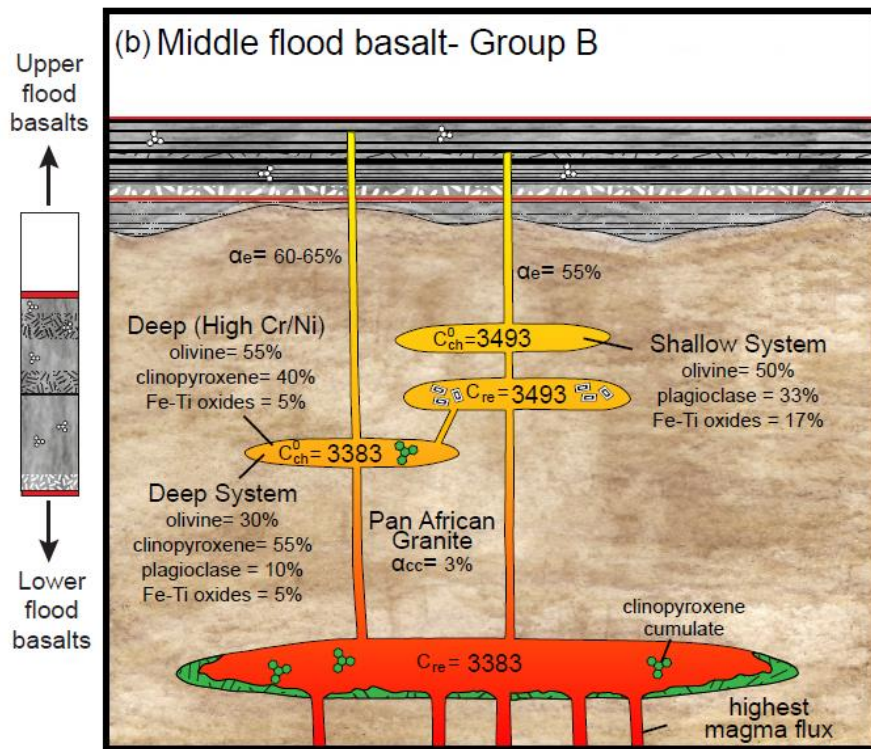
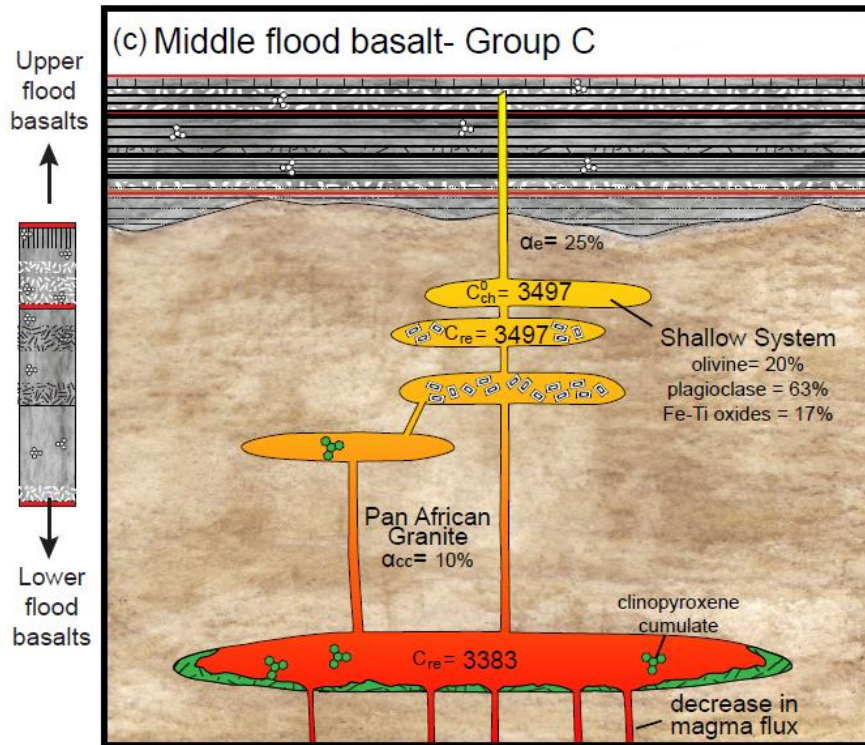


Figure 3.9. (cont'd)



3.6 CONCLUSIONS

When combined with existing petrostratigraphic observations (Krans et al., 2018), our results provide an internally consistent model describing the magmatic evolution of a continental flood basalt. MELTS modeling reported in this study are consistent with previous interpretations based on mineralogy (Pik et al., 1998; Krans et al., 2018), and show a range in crystallization pressures from mid-crust (0.6 GPa) to shallow crust (0.05 GPa). We furthermore find that this polybaric magmatic system shallows over time.

Our REAFC modelling estimates refine our understanding of the relative role of different components of this polybaric magmatic system during the evolution of the province. The main phase of LT flood volcanism began with lower relative proportions of evacuation from both the

deep and shallow system in Middle group A, followed by an increase in evacuation in both the deep and shallow system in Middle group B, and finally a loss of evacuation from the deep system in Middle group C. These results are interpreted as representing a complete magmatic cycle that evolves through an initially immature system, transitioning to a more mature system with high magma flux, and finally moving towards a terminal system with significantly decreased magma supply.

We show that the combined effects of REAFC have significant leverage on the incompatible element enrichment of a continental flood basalt. Such enrichment processes have direct relevance in the interpretation of the crustal contamination, with larger implications in the interpretation of radiogenic isotopes in such systems. We show that within the Ethiopian-Yemen LIP, the proportion of crustal assimilation (3-10 %) necessary to accommodate the data is markedly lower than previously estimated values (10 - 25 %; Baker, 2000; Meshesha and Shinjo, 2007).

Our models help clarify several geochemical observations within the LT flood basalts in the NW Ethiopian plateau. For starters, the remarkable homogeneity in major elements (Figure 3.5) and trace element patterns (Rooney, 2017; Figure 3.4 in this chapter) can be explained by a magmatic system undergoing simultaneous recharge-evacuation-assimilation-fractional crystallization approaching steady state conditions (i.e. becoming more efficient at moving new magma input through the system and erupting at the surface). The wide variability in geochemistry observed in flows near petrostratigraphic boundaries (Figure 3.5) is consistent with a magmatic system experiencing revived magmatic flux after a period of quiescence. The decreasing Nb/La in LT lavas does not require significant contribution from a crustal component but can in fact occur as a result of fractionating phases (Figure 3.7). Furthermore, a non-linear

decrease in Nb/La with decreasing MgO cannot be achieved by FC nor AFC alone and requires recharge and evacuation to be included parameters in modeling (Figures 3.7 and 3.8). The results of these models have profound implications for future studies of CFB magma evolution and may in turn bring us closer to identifying the primary magma composition in some of the largest volcanic provinces on Earth.

4. MODELING THE ORIGIN OF THE ISOTOPIC SIGNATURE FOR LT MAGMAS IN THE ETHIOPIAN CONTINENTAL FLOOD BASALT PROVINCE

4.1 INTRODUCTION AND BACKGROUND

Continental flood basalt (CFB) provinces typically erupt two distinct basalt compositions—Low-Ti (LT) basalts and High-Ti (HT) basalts. In the Ethiopian Flood Basalt province, LT and HT lavas erupted contemporaneously in spatially adjacent provinces with very little overlap between LT and HT lavas (Pik et al., 1998, 1999; Kieffer et al., 2004). The clear geochemical and spatial distinction between LT and HT lava types has led to investigations of their magmatic origins using geochemical and isotopic datasets (Pik et al., 1999; Kieffer et al., 2004; Beccaluva et al., 2009; Natali et al., 2016). While the source of HT lavas has been attributed to melting of the Afar plume (Pik et al., 1999; Natali et al., 2016), the origin of LT lavas remains a topic of debate (Pik et al., 1999; Kieffer et al., 2004; Beccaluva et al., 2009). An outstanding question about Ethiopian Flood Basalt Province is whether the compositional zoning of erupted lavas reflects compositional zoning in the Afar plume, differences in plume vs. non-plume source components (e.g., depleted mantle and sub-continental lithospheric mantle), or varying influence from crustal contamination.

Low-Ti basalts are thought to be easily susceptible to crustal contamination due to the overall depletion in incompatible elements (Pik et al., 1999), however their homogeneous composition (tight grouping on trace element diagrams) requires an efficient magma plumbing system with high melt input at low residence time (Lee et al., 2014: Chapter 3). Trace element modeling using REAFC in the Middle flood basalts of the northwestern Ethiopian plateau

(Chapter 3) suggest that 3 – 10 % contamination from local Pan African granite is expected, but this only accounts for mid to shallow crustal contamination because a deeper crustal component is suspected, but due to difficulty in direct sampling of the lower crust, and the differentiated nature of the LT basalts, this could not be modeled effectively using REAFC. Isotopic constraints are needed resolve a more complete picture of the lithospheric role in the formation of LT magmas.

On the Yemen- conjugate margin, Sr-Nd-Pb isotopes were used to estimate ~20-30% crustal assimilation by AFC in contemporaneous LT flood basalts (Baker et al., 1996b). This estimate was reduced to ~20% crustal assimilation with the additional analysis of oxygen isotopes (Baker et al., 2000). These insights provide an interesting contrast to the REAFC modelling presented in chapter 3, which suggest less than half of this assimilation value is necessary. However, direct comparison between the magmatic system beneath the northwest Ethiopian plateau and Yemen are complicated by quite distinct lithosphere in both regions. The crustal terranes beneath Yemen are old Archean lithospheric fragments (Baker et al., 1996b), while the Ethiopian lithosphere is comprised of Late Proterozoic mafic accreted arc terranes (Pik et al., 1999). These differences are important factors when considering potential lithospheric assimilation.

The concept of lithospheric assimilation should not be viewed as synonymous with crustal assimilation. Indeed, differentiating between contributions to the radiogenic isotope budget of a magma of a crustal versus SCLM origin is non-trivial. Many previous studies have suggested that LT lavas in CFB provinces experienced some contribution from the SCLM (Hawkesworth et al., 1984; Hergt et al., 1989; Lightfoot et al., 1993; Shirey et al., 1994; Yan et al., 2007). There are two known types of SCLM in East Africa—an enriched type and a depleted type. It has been

proposed that LT lavas were generated through interaction with depleted SCLM (CITE). The depleted SCLM type, identified in xenolith studies, is thought to reflect the depleted residual portion of the mantle (Bianchini et al., 2014). This depleted mantle is depleted in basalt forming elements such that it is difficult to extract significant volumes of further melt in order to form the LT flood basalts; such difficulties have typically resulted in other studies suggesting SCLM contribution to flood basalts to instead consider SCLM that has been subsequently re-enriched (e.g. Shirey et al., 1994; Shirey, 1997).

The enriched type of SCLM in East Africa is thought to be comprised of metasomes – regions of the SCLM that have been re-enriched since the original stabilization of the lithosphere with percolating fluids/melts. When melted, these metasomes produce some of the most incompatible trace element enriched, silica under-saturated lavas known in East Africa, and often possess HIMU-like isotopic signatures (Rooney et al., 2014). These magmas correspond to the Type IIb magmas in East Africa (Rooney, 2017), and are profoundly different to the tholeiitic LT lavas, which are also among the most incompatible trace element depleted magmas in East Africa (Type Ia; Rooney, 2017).

Constraints on the potential SCLM origin for the LT magmas can come from radiogenic isotope compositions. Specifically, both SCLM types, enriched and depleted, have distinct isotopic signatures in ϵHf - ϵNd space that plot off the mantle array. The enriched SCLM component plots below the ϵHf - ϵNd mantle array, and the depleted component plots above the mantle array (Rooney et al., 2014; Bianchini et al., 2014). Despite the utility of coupled Hf and Nd isotopes in resolving the SCLM question, no well-constrained Hf isotope dataset exists for the LT flood basalts in this region.

In this chapter, we will attempt to resolve the SCLM debate for LT lavas in East Africa by using Hf-isotopes in tandem with Sr-Nd-Pb isotopic systems. Succinctly, if LT lavas fall above or below $\epsilon\text{Hf}-\epsilon\text{Nd}$ mantle array, then contribution from the SCLM is plausible as a source component. We will also evaluate the source component mixing that formed LT basalts by evaluating the relative contribution from major reservoirs in East Africa: 1) the Afar Plume, 2) the depleted mantle (DM), 3) the sub-continental lithospheric mantle (SCLM), and 4) the continental crust.

Here we present Sr-Nd-Pb-Hf isotopes from parental to evolved lavas from multiple stratigraphic levels in the LT stratigraphy. We apply multiple binary mixing models between various components, and finally model the potential effect of assimilation-fractional crystallization (AFC) on the LT isotopic signature, informed by modelling undertaken in Chapter 3. We find that the source of LT magmas is at least a three-component system that is dominantly DM, with 10-30% Afar Plume, and a 10-20% lithospheric component, with no apparent contribution from the SCLM. The Upper flood basalts have a greater influence from DM than the Middle and Lower flood basalts, while Middle flood basalts show greater lithospheric overprint. The precise lithospheric component is still unclear due to the limited data constraints available for composition of the lower crust and lithospheric mantle, but $^{207}\text{Pb}/^{204}\text{Pb}$ and ϵHf observed in LT lavas would suggest a lithospheric component with $^{207}\text{Pb}/^{204}\text{Pb}$ around 15.5 and ϵHf concentrations that are elevated from the current estimate for PAL (-15; Rooney et al., 2012a). The transition toward more DM component and less Afar Plume component over time is consistent with thermo-mechanical erosion of the lithospheric mantle as a result of the impinging plume head beneath East Africa (Rooney et al., 2012a; Furman et al., 2016)

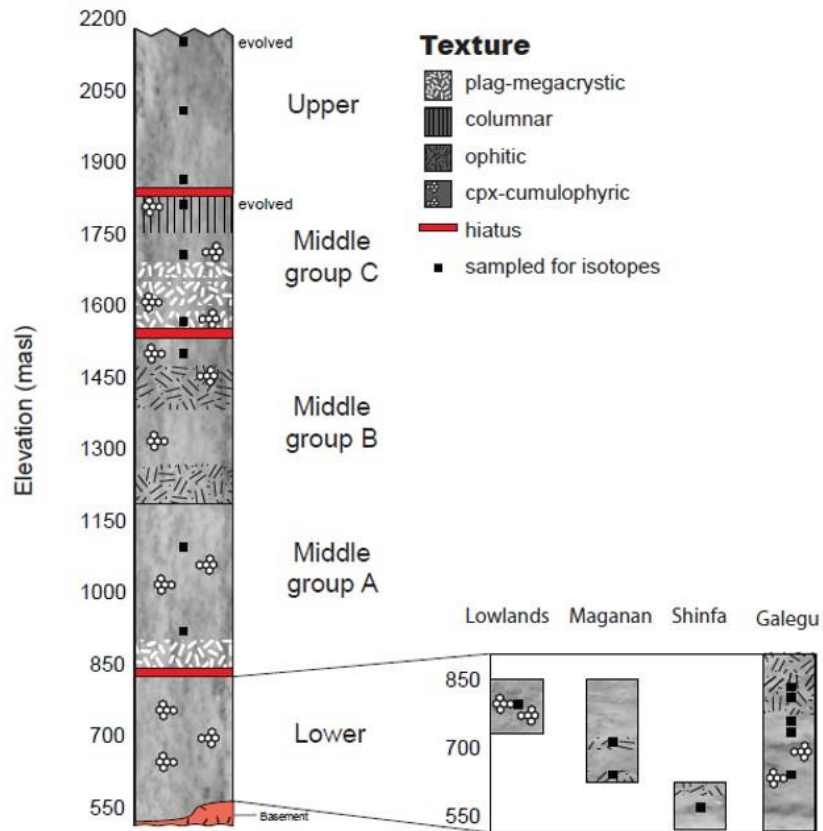
4.2 METHODS

A total of 18 samples were selected from the Lower (n=9), Middle (n=6), and Upper (n=3) LT flood basalt sequence. Sampling criteria was used to target the following: 1) representative flows from each flood basalt group, 2) lavas that represent liquid composition (phenocryst-poor) when possible, 3) lavas with MgO >7.0 wt.% to represent parental magmas, and 4) lavas with MgO <5.0 wt. % to represent evolved magmas as a potential vector of contamination (Figure 4.1).

Samples were crushed using a ceramic plate jaw crusher, and rock chips were handpicked to minimize the impact of alteration and large crystals. Samples were acid-leached, processed, and analyzed for Sr-Nd-Pb-Hf radiogenic isotopes at the University of Hawai'i at Manoa following procedure outlined in Finlayson et al (2018). Pb, Nd, and Hf were analyzed by MC-ICP-MS, while Sr was measured via TIMS as detailed in Finlayson et al (2018). Results for measured isotopes are compiled in Supplementary Table D.1.

Measured Sr-Nd-Pb-Hf isotopes were age-corrected to initial values using an age of 30 Ma (See Appendix C).

Figure 4.1. Stratigraphic sampling of select Lower, Middle and Upper LT lavas for Sr-Nd-Pb-Hf isotope analysis. Simplified stratigraphic section after Krans et al. (2018) (See Figure 2.5 in Chapter 2). A total of 18 samples were analyzed for Sr-Nd-Pb-Hf isotopes (three Upper, six Middle, and nine Lower). Two evolved samples (MgO, 5.0 wt.%) were selected from the Upper flood basalt group and the Middle group C flood basalt group. Lower flood basalt lavas are from discontinuous sections in the Ethiopia lowlands, west of Lake Tana (See figure 2.1b in Chapter 2 for spatial distribution of sections).



4.3 RESULTS

All LT lavas in this study plot within the expected Sr-Nd-Pb isotopic ranges for LT flood basalts in Ethiopia (Figure 4.2). A weak negative correlation is observed between MgO (wt. %) and $^{87}\text{Sr}/^{86}\text{Sr}$ (Figure 4.3). Likewise, a weak positive correlation is observed between MgO (wt. %) and $^{143}\text{Nd}/^{144}\text{Nd}$ (Figure 4.3). These two observations combined suggest a shift in isotopic

composition as a result of magma differentiation which will be addressed later in the discussion. The Hf and Pb isotopic ratios do not appear to be correlated with MgO (Figure 4.3).

Isotopic ratios were also plotted against Nb/La since this has been shown to decrease with REAFC as the magmatic system evolves and may be a more sensitive index of magma differentiation since MgO becomes buffered during high flux (See Chapter 3, Figure 3.7). We see a stronger negative correlation between Nb/La and $^{87}\text{Sr}/^{86}\text{Sr}$ than between MgO and $^{87}\text{Sr}/^{86}\text{Sr}$. Likewise, we see a stronger positive correlation is observed between Nb/La and $^{143}\text{Nd}/^{144}\text{Nd}$ (Figure 4.4). Additionally, $^{206}\text{Pb}/^{204}\text{Pb}$ is positively correlated with Nb/La (Figure 4.4). These observations suggest that the isotopic composition of LT magmas might be shifting as a result of REAFC. We will test this using AFC modeling in the discussion.

Figure 4.2. Sr-Nd-Pb-Hf isotopic plots for Ethiopian LT lavas. Upper flood basalts (red circles), Middle flood basalts (blue diamonds), and lower LT flood basalts (green triangles) are new data from this study. Published LT, HT1, and HT2 flood basalt data for Ethiopian Plateau (Pik et al., 1999; Kieffer et al., 2004; Teklay et al., 2005; Beccaluva et al., 2009; Rooney et al., 2018). Pan African Lithosphere (PAL), Afar Plume, and depleted mantel (DM) components as defined in Rooney et al. (2012a). Upper crust (UC) and Lower crust (LC) components as defined by Pik et al. (1999). Gerba Guracha are lavas from a metasomatic component from Rooney et al. (2014). Lithospheric mantle xenoliths from the African and Arabian plates (Shaw et al., 2007). Note that LT lavas lay on or slightly above the northern hemisphere reference line (NHRL) in $^{206}\text{Pb}/^{204}\text{Pb} - ^{207}\text{Pb}/^{204}\text{Pb}$ isotopic space. In addition, LT lavas lay on or slightly above the mantle array (gray line) in $\epsilon_{\text{Nd}} - \epsilon_{\text{Hf}}$ isotopic space.

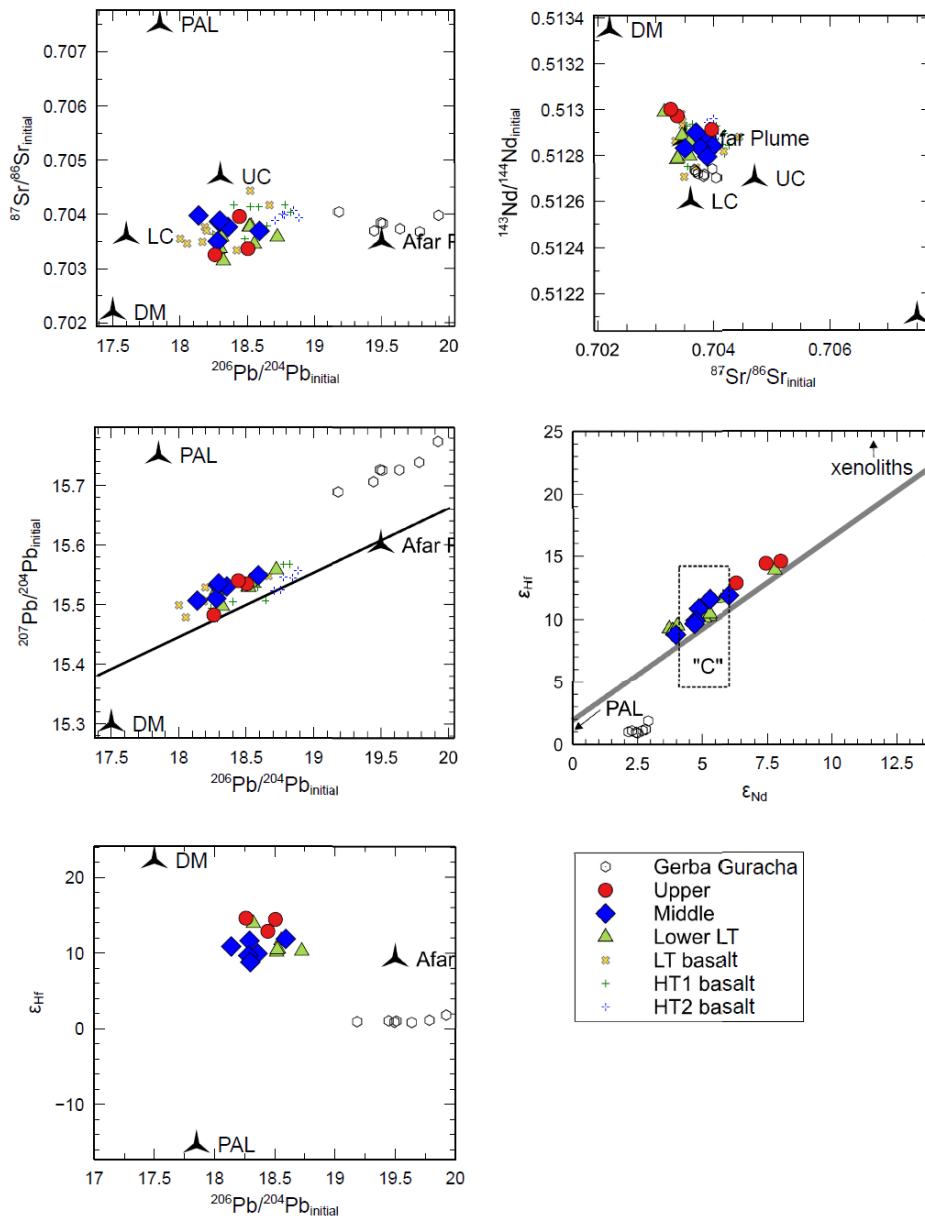


Figure 4.3. Sr-Nd-Pb-Hf Isotopic plots for Ethiopian LT lavas as a function of MgO (wt.%). All other symbols same as in Figure 4.2. Note, there appears to be a slight increase in $^{87}\text{Sr}/^{86}\text{Sr}$ (a) and decrease in $^{143}\text{Nd}/^{144}\text{Nd}$ (b) with decreasing MgO (wt.%), which would be consistent with an increase in crustal contamination as magma evolves. The relationship between differentiation (decreasing MgO) and the other isotopic systems is unclear.

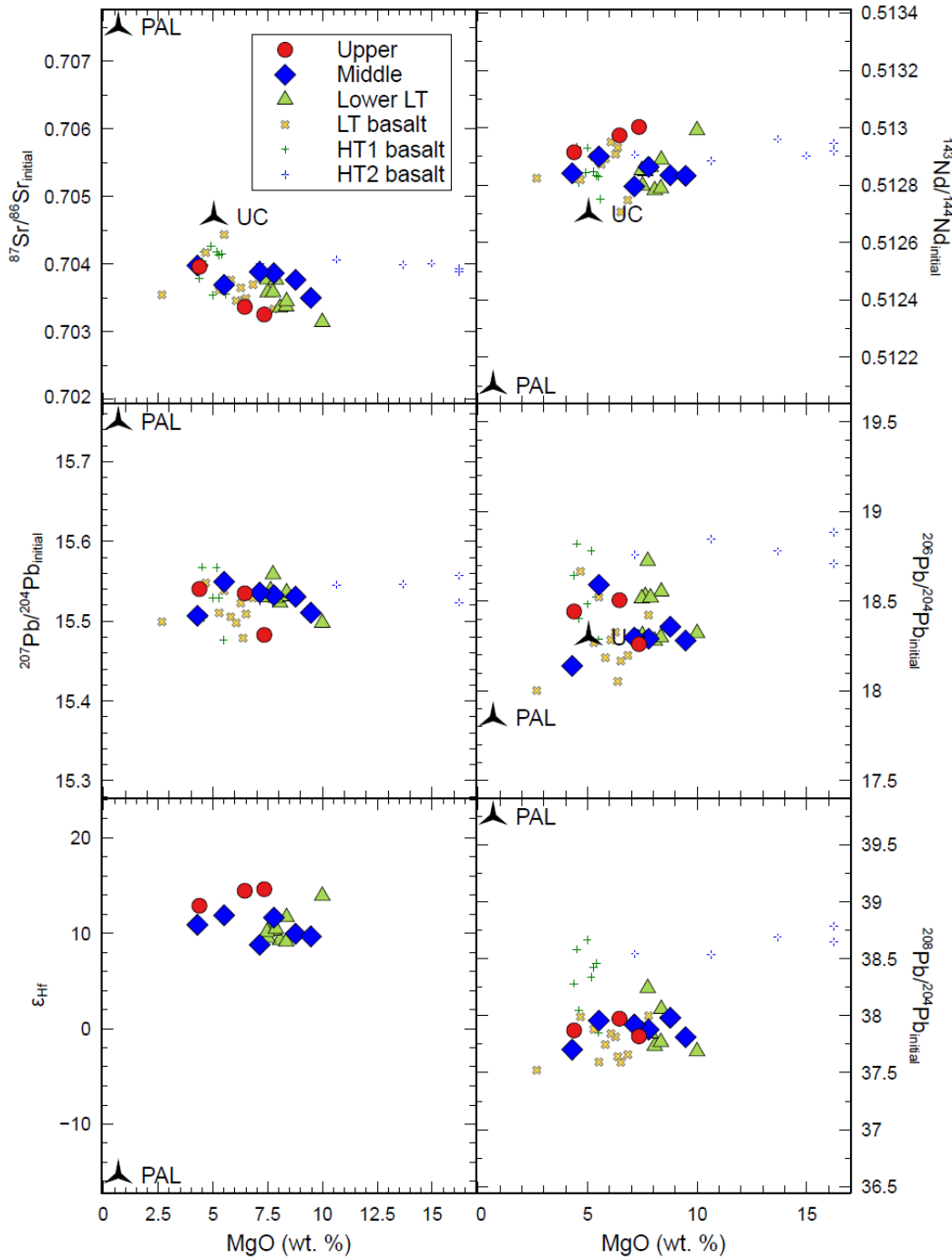
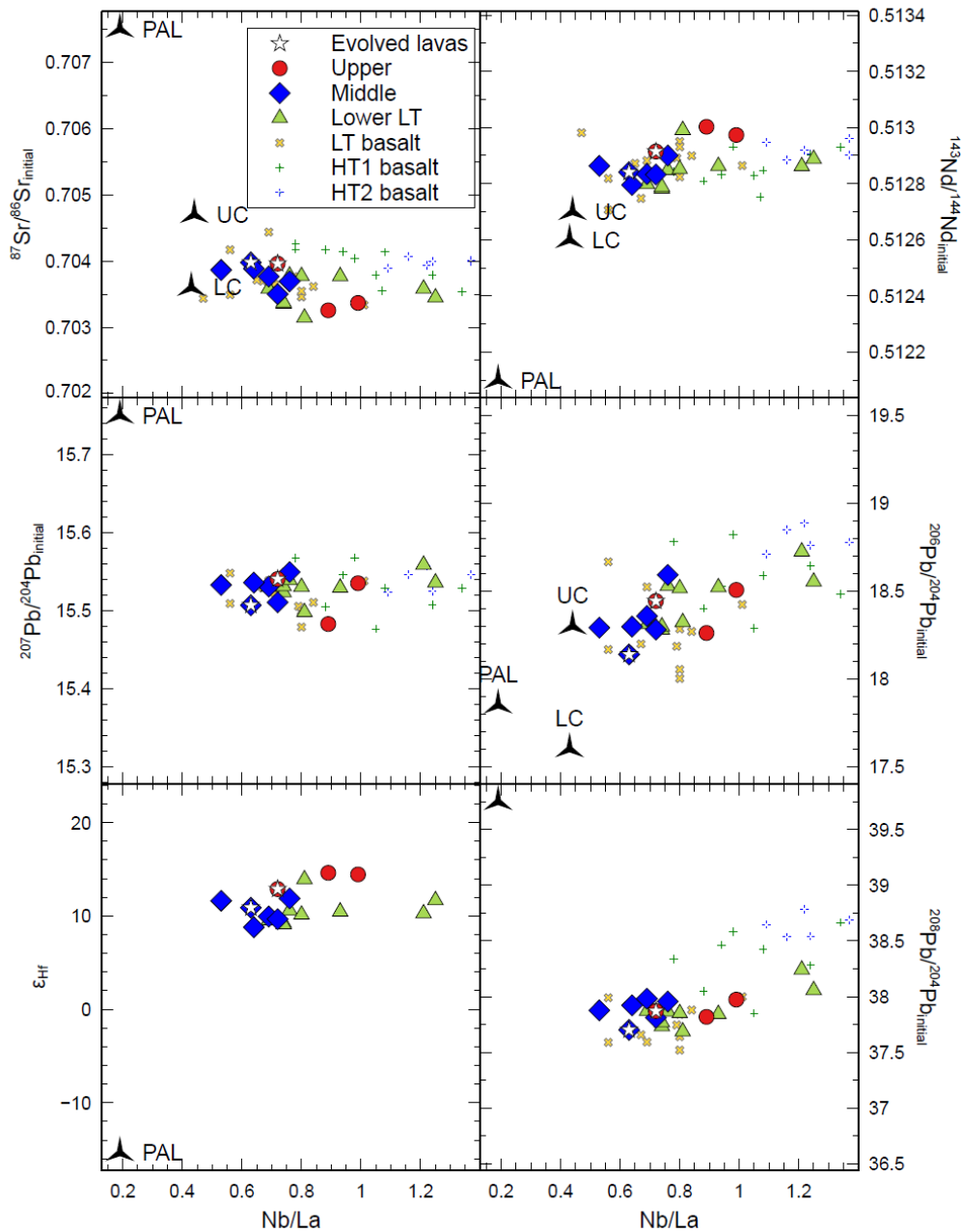


Figure 4.4. Sr-Nd-Pb-Hf isotopic plots for Ethiopian LT lavas as a function of Nb/La. White stars over symbols indicate evolved samples ($MgO < 5.0$ wt. %). All other symbols same as in Figure 4.2. Note that we again observe an increase in $^{87}Sr/^{86}Sr$ and decrease in $^{143}Nd/^{144}Nd$ with decreasing Nb/La. In addition, we observe a decrease in $^{206}Pb/^{204}Pb$ with decreasing Nb/La. In Sr-Nd- ^{206}Pb isotopic spaces, a decrease in Nb/La correlates with isotopic compositions trending toward lithospheric components (PAL, UC, and LC). We however do not see a relationship between decreasing Nb/La and $^{207}Pb/^{204}Pb$, and arguably no relationship ϵ_{Hf} and Nb/La. Unlike the PAL, $^{207}Pb/^{204}Pb$ and ϵ_{Hf} are not well-defined for upper crust and lower crust components in Ethiopia.



4.4 DISCUSSION

4.4.1 Assimilation-Fractional Crystallization (AFC)

Previous trace element modeling via REAFC suggests between 4 -10 % crustal assimilation from Pan Africa lithosphere (PAL) (See Chapter 3, Figure 3.7 and related text). To test how AFC might influence the isotopic signature of the LT magmas, we will combine previously constrained parameters from REAFC (Chapter 3) and apply them in the AFC model from DePaolo (1981):

$$IC_m^{AFC} = \frac{\left(\frac{r}{r-1}\right) \left(\frac{C_a}{Z}\right) (1 - F^{-z}) IC_a + C_0^f F^{-z} IC_0}{\left(\frac{r}{r-1}\right) \left(\frac{C_a}{Z}\right) (1 - F^{-z}) + C_0^f F^{-z}} \quad \text{Eq. 4.1}$$

IC_m^{AFC} = Isotopic composition of a magma undergoing AFC

IC_a = Isotopic ratio of assimilant

IC_0 = Isotopic ratio of initial magma

C_a = Concentration of element in assimilant

C_0 = Concentration of element in initial magma

r = relative ratio of assimilated material to crystallized material; where r

$$= \frac{\alpha_{cc}}{\alpha_x}$$

α_{cc}

= % assimilated assuming constant mass chamber determined from REAFC

α_x = % crystalized assuming constant mass chamber determined from REAFC

$z = \frac{r + D_0 - 1}{r - 1}$, where D_0 = bulk partition coefficient of trace element

F = fraction of liquid remaining, relative to initial mass (0.1 to 1.0; step = 0.1)

This equation estimates the isotopic composition of a magma undergoing AFC by relating the isotopic composition and corresponding trace element compositions in the parental magma and assimilant with the simultaneous removal of crystallizing phases (parameters defined above).

The starting parental magma composition was chosen from the Lower flood basalt group based on it being the furthest away from the PAL component in Sr-Nd and Sr-Pb space and being relatively high in MgO (7.7 wt. %) (Supplementary Table E.1). We use the Pan African lithosphere (PAL) as described in Rooney et al. (2012a) as the assimilation component (Supplementary Table E.1). The bulk partition coefficients are based on the mineral assemblages used in REAFC models (Supplementary Table E.1, Chapter 3- Supplementary Table C.1 and Supplementary Table C.2).

We ran a Deep AFC model and Shallow AFC model to cover the minimum and maximum conditions concluded from REAFC models in Chapter 3. The parameters for these models can be found in Supplementary Table E.2. The Deep AFC model is dominated by clinopyroxene and olivine fractionation with only 4% assimilation of PAL. The Shallow AFC model is dominated by olivine and plagioclase fractionation and 10 % assimilation of PAL. The results of both models are shown in Figure 4.5.

The AFC models indicate that it is possible to capture a range in compositions simply through AFC of a single parental magma. In addition, both the shallow and the deep model can achieve the observed variation in LT lavas, indicating that the observed variation in LT lavas does not require a significant amount of crust—only 4 – 10 % PAL is needed, as opposed to the 12-25% estimated by others (Baker et al., 2000; Kieffer et al., 2004). Still, not all LT lavas are predicted from a single parental magma mixing with PAL. The $^{207}\text{Pb}/^{204}\text{Pb}$ versus $^{206}\text{Pb}/^{204}\text{Pb}$ (Figure 4.5) would indicate that the PAL used in our AFC model may not be the most

appropriate vector of contamination for LT lavas. The evolved lavas (white stars) in Figure 4.5 suggest a possible vector of contamination, pointing toward lower $^{207}\text{Pb}/^{204}\text{Pb}$ (~15.5).

Recall that in the REAFC model (Chapter 3), we used a locally exposed Pan African Granite which would represent contamination in the mid-shallow crust. REAFC modeling of Middle LT flood basalts indicate 3-10% contamination of PAL in the mid to shallow crust (Figure 3.8). We do not know how much contamination occurred in the lower crust. It is possible that the unknown lithospheric component resides in the lower crust, and the potential contamination vector indicated by $^{207}\text{Pb}/^{204}\text{Pb}$ suggests a lower $^{207}\text{Pb}/^{204}\text{Pb}$ component (Figure 4.5). It should also be noted that the parental magma used in the AFC models is not along the binary mixing line between DM and Afar Plume components (Figure 4.5). In the next section, we will evaluate the relative contribution of mantle and lithospheric components imprinting LT magmas.

Figure 4.5. Isotope AFC models for Ethiopian LT lavas. The two evolved lavas from the Middle and Upper flood basalt groups are identified by the white stars to indicate a contamination vector. Solid line represents binary mixing between the depleted mantle (DM) and Afar plume components (discussed in section 4.2.2) and is included here to illustrate the parental magma does not plot on the binary mixing line for mantle endmembers.

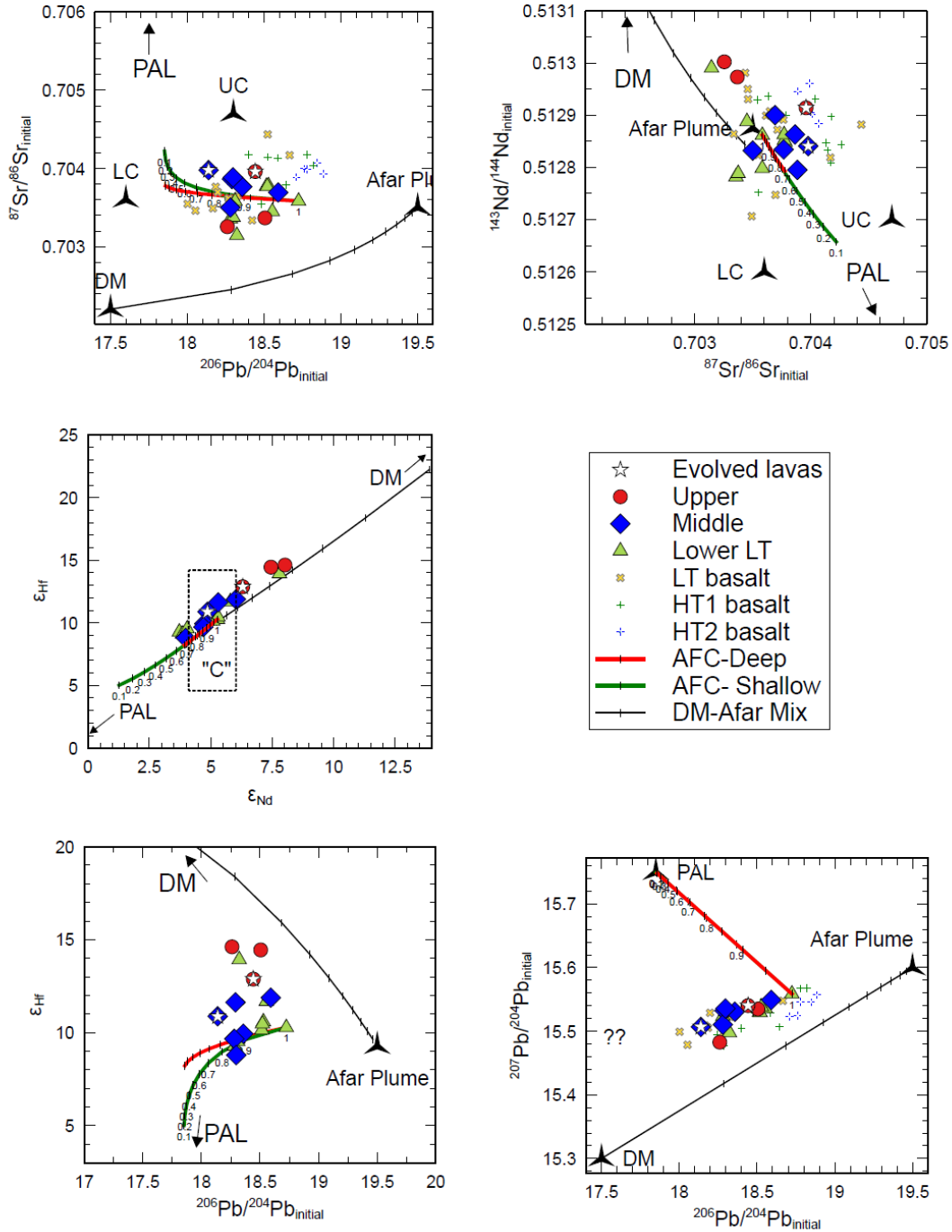


Figure 4.5. (cont'd)

A Deep AFC model was run using the bulk distribution coefficients determined for a mid-crustal fractionating system as determined from REAFC (Supplementary Table E.2; also see Chapter 3). A Shallow AFC model was run using the bulk distribution coefficients determined for a shallow-crustal fractionating system as determined from REAFC (Supplementary Table E.2; also see Chapter 3). The relative percentage of 4% assimilation (AFC-Deep) and 10% assimilation (AFC-shallow) was used and is based off the estimated value from REAFC (see Chapter 3). All other symbols same as in Figure 4.2. Note the disparity between the AFC models and observed data in $^{206}\text{Pb}/^{207}\text{Pb}$ space.

4.4.2 Mixing

We used the following mixing model by Powell (1984) to first test binary mixing between the Afar Plume and depleted upper Mantle (DM) reservoirs as a potential source for LT lavas:

$$IC_m = IC_a \left(\frac{C_a X}{C_m} \right) + IC_b \left(\frac{C_b (1 - x)}{C_m} \right) \quad \text{Eq. 4.2}$$

Where,

IC_a = Isotopic ratio of element in source 1

IC_b = Isotopic ratio of element in source 2

IC_m = Isotopic ratio of element in mixed source

C_a = concentration of element in source 1

C_b = concentration of element in source 2

C_m = concentration of element in mixed source

x = degree of mixing (0.1 to 1.0)

This equation estimates the isotopic composition of a mixed two-component system by relating the isotopic ratio and corresponding trace element composition in each component at a given degree of mixing. The specific compositions of the DM and Afar Plume components can be

found in Supplementary Table E.2. We varied the degree of mixing between 10 – 100 % (0.1 – 1.0) at 10% increments. The results of this mixing model are shown in Figure 4.6. We found that a DM-Afar Plume hybrid source with 10 -30% Afar Plume is a likely source of the LT flood basalts, but that a third component is necessary to capture the data in Hf-Pb, Pb-Pb, Sr-Pb, and Hf-Nd isotopic space (Figure 4.6).

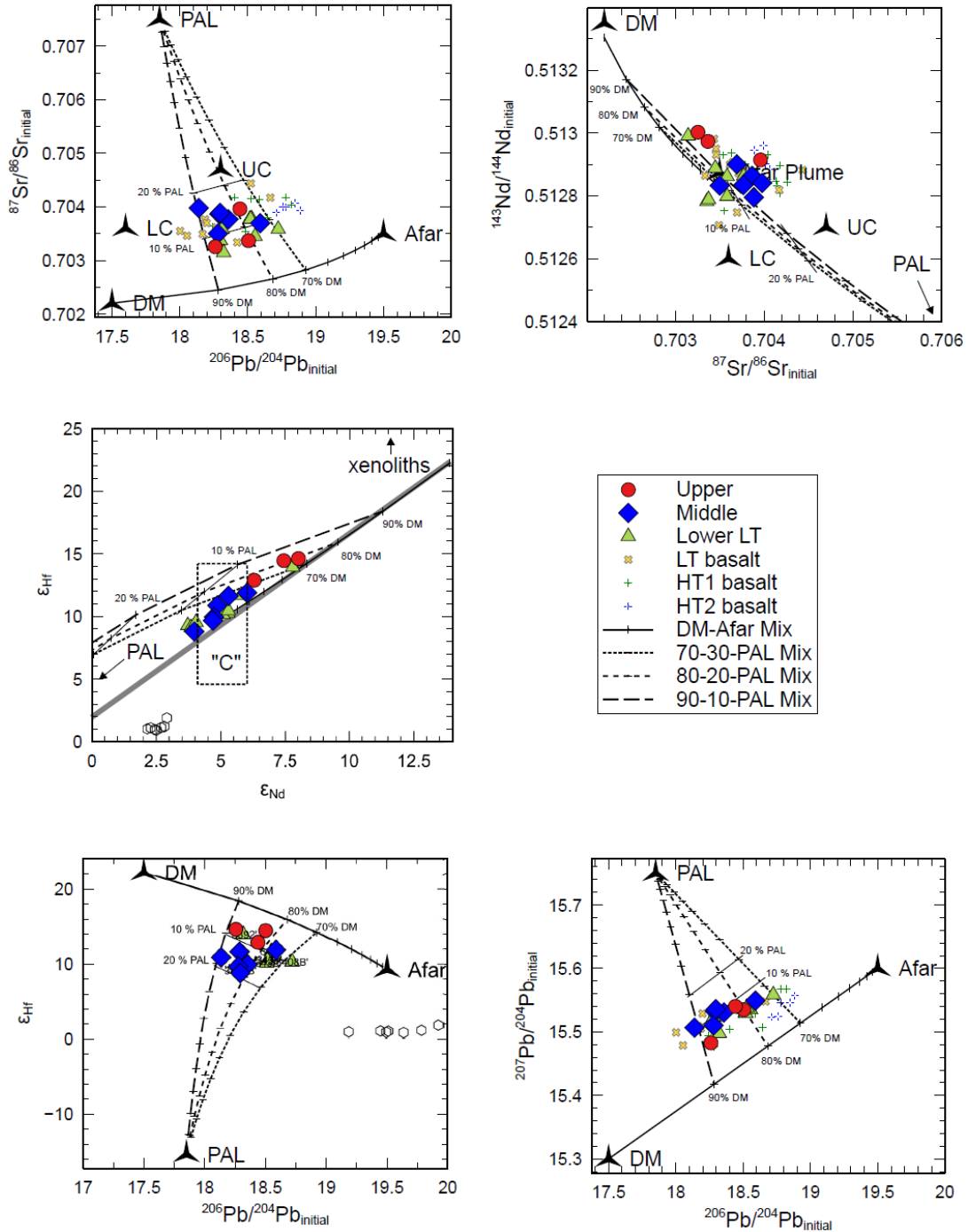
Next, we used the DM-Afar Plume hybrid compositions estimated from the first mixing model with Pan African Lithosphere (PAL) to test the relative lithospheric contribution on LT lavas (See Supplementary Table E.2 for specific details). We again varied the degree of mixing between 10 – 100 % (0.1 – 1.0) at 10% increments. We find that most LT flood basalts can be explained by mixing a DM-Afar Plume hybrid source with 10- 20 % PAL. There is however some disagreement to the estimated % PAL in ϵHf - ϵNd isotopic space, where the amount of PAL is estimated around only 5%. This inconsistency is not surprising considering what we observed in the AFC models in the previous section—again further evidence that there is an unknown lithospheric component that is yet to be defined.

Despite not having a well-defined lithospheric component in all isotopic spaces, the AFC and mixing models presented here, along with the REAFC modeling from Chapter 3, are clear indicators that a lithospheric component is indeed present in LT magmas. Recall that in Chapter 3, the only way to capture the trend of decreasing Nb/La with MgO in LT lavas was to include about 3-10 % crustal contamination in the REAFC model (Figure 3.8). We can explore this idea further by comparing the isotopic compositions of the LT lavas using similar indices of differentiation (decreasing MgO and decreasing Nb/La). Note in Figure 4.3 how $^{87}\text{Sr}/^{86}\text{Sr}$ increases toward PAL and the upper crustal (UC) component with decreasing MgO. Likewise, $^{143}\text{Nd}/^{144}\text{Nd}$ decreases toward PAL and UC with differentiation (Figure 4.3). The same

relationship can be seen with decreasing Nb/La in Figure 4.4, where $^{87}\text{Sr}/^{86}\text{Sr}$ increases toward PAL and UC with decreasing Nb/La and $^{143}\text{Nd}/^{144}\text{Nd}$ decreases toward PAL and UC with decreasing Nb/La. Not only does this support a lithospheric component influencing the LT magmas, but that the lithospheric component is most likely in the crust—where the magma undergoes differentiation.

The isotopic ratios plotted against MgO and Nb/La offer insight as to what the potential crustal contamination vector could be in isotopic space. While it is similar to the PAL component defined by Schilling et al. (1992) and Rooney et al. (2012a) and the upper crustal component defined by Pik et al. (1999), the lack of change in $^{207}\text{Pb}/^{204}\text{Pb}$ with differentiation suggests the component has similar $^{207}\text{Pb}/^{204}\text{Pb}$ as the parental magma (closer to 15.5) as opposed to the PAL component (15.75) (Figure 4.3 and 4.4). This point is further exemplified when attempting to model PAL as a contamination vector by AFC (Figure 4.5).

Figure 4.6. Isotope mixing models for Ethiopian LT lavas. Solid line represents binary mixing between the depleted mantle (DM) and Afar plume components. Majority of LT lavas appear to be related to a DM-Afar plume hybrid that has 90 – 70% DM and 10 – 30% Afar Plume. Dashed lines are binary mixing models between a DM-Afar plume hybrid and Pan African lithosphere (PAL) component. LT lavas typically fall between 10 – 20 % mixing with PAL. All other symbols same as in Figure 4.2.



4.4.3 *Temporal Variation in Source Components*

According to the mixing models, there is considerable overlap in Lower, Middle, and Upper LT flood basalts in terms of contribution from PAL (Figure 4.7). However, the Upper flood basalt appear to be the least contaminated by PAL (<10 %), while the most contaminated samples occur in the Middle flood basalt (10 – 20 %; Figure 4.7). Recall that in Chapter 3, the modeled assimilation by REAFC increased from 3 – 4 % to 10 % near the end of the Middle flood basalt sequence (Figure 3.8). It is important to keep in mind that the Pan African Granite used in the REAFC model is a direct sample of the crust underlying the LT province for which major and trace element chemistry was measured (Rooney et al., 2018), while the PAL isotopic component has been inferred from 3-component mixing vectors (Schilling et al., 1992; Rooney et al., 2012a). Furthermore, it was concluded in section 4.4.2 that while the PAL component used in AFC models works in Sr-Nd-Hf space, it is too high in $^{207}\text{Pb}/^{204}\text{Pb}$ to be the correct lithospheric component for modeling (Figure 4.5).

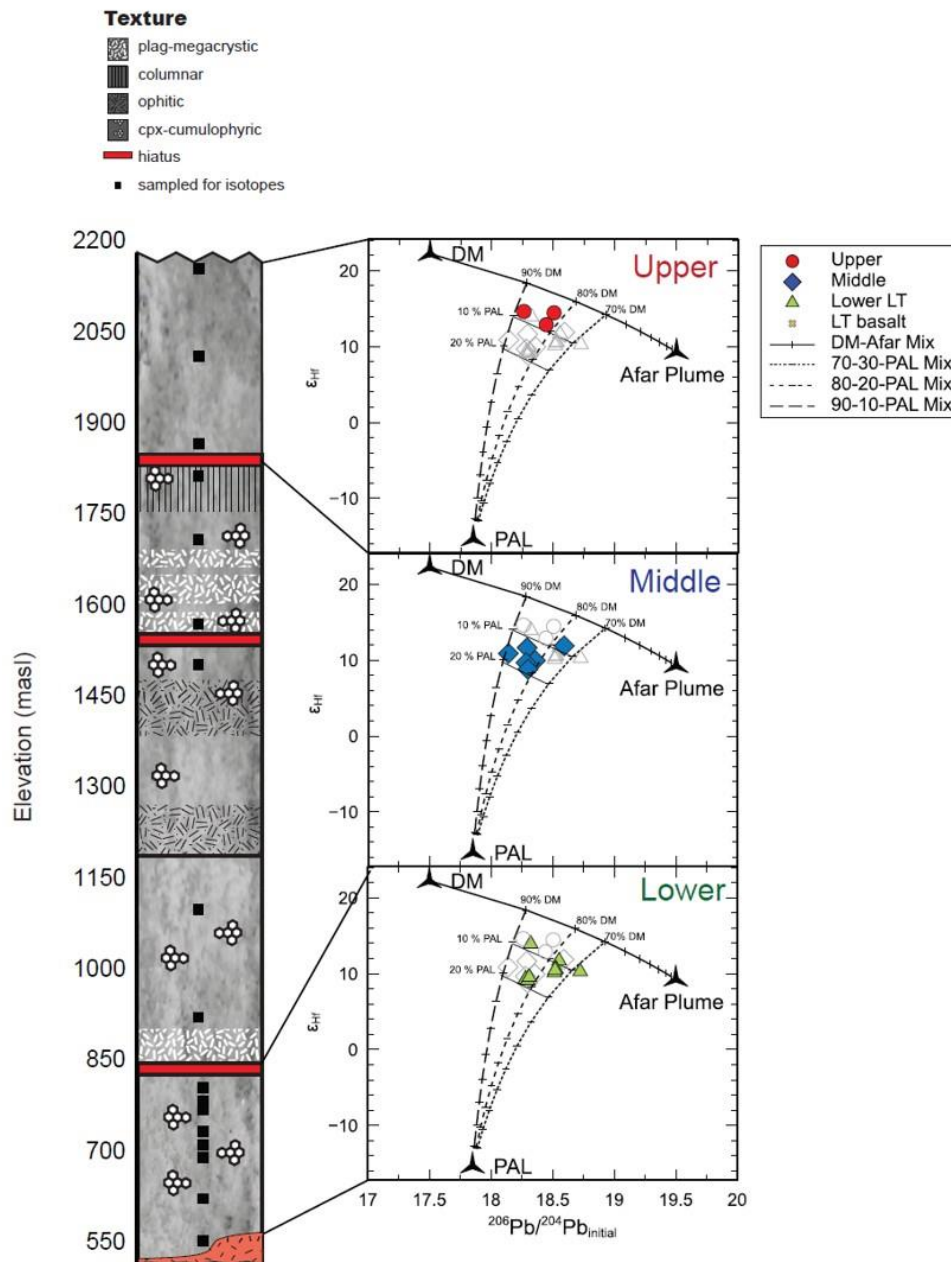
Despite the disparity in the exact values between the trace element REAFC models and the isotopic mixing models, both tell a similar story in terms of a temporal transition in the role of continental lithosphere in the evolution of the LT magmas. If we consider this in terms of the conceptual model for LT magma evolution (Chapter 2- section 2.5.2; revised in Chapter 3- section 3.5.5), it makes sense that the Middle flood basalts would have the highest influence of crustal contamination despite being part of the main-stage of flood volcanism. This is in part because the main phase of volcanism was not a continuous outpouring of lavas at constant frequency—it pulses, waxes, and wanes throughout the main phase. There are two key processes occurring during the main-phase of flood volcanism that would contribute to higher contamination from the crust: 1) High rates of magma flux caused by increased melt generation

is continuously supplying heat to the crust which in turn raises the geotherm and facilitate assimilation (Blundy and Annen, 2016); 2) We have shown through REAFC that the highest rate of assimilation occurs toward the end of the main phase (Middle group C) as the system begins to shut down (Figure 3.8 and section 2.5.2). As the rate of new magma supplying the plumbing system slows, heat flux would eventually decrease and reduce the volume of eruptible magma (Blundy and Annen, 2016), as supported by the decrease in evacuation shown in the REAFC model (Figure 3.8). With lower rates of evacuation, the contribution from assimilation and fractional crystallization on magma evolution become more pronounced, as they are no longer diluted by magma recharging and leaving the system (Lee et al., 2014). It has been shown that the locus of magmatism has migrated from below the LT province to below the HT province over time (Rooney et al., 2018). As the magmatic plumbing system migrated eastward, the magmatic system below the LT province likely experienced a decrease in magmatic flux that eventually led to a decrease in volcanic activity from the large outpourings of flood basalt lavas shield activity and more felsic magmatism in the region (Ayalew et al., 1999, 2002; Ukstins et al., 2002; Kieffer et al., 2004; Krans et al., 2018).

The temporal variation in the source shows a stronger contribution from the Afar Plume in the Lower flood basalt sequence and increasing contribution from the DM in the Middle and Upper flood basalt sequences. It is possible that the Upper flood basalts are derived from a greater contribution of the depleted mantle due to decompression of ambient mantle as a result of thermo-mechanical erosion of the lithosphere associated with the Afar plume (Rooney et al., 2012a). In this case, a higher plume component would be expected in the earlier erupted lavas as a result of adiabatic melting of the impinging plume head (Beccaluva et al., 2009). Over time, elevated mantle potential temperatures in the depleted upper mantle surrounding the plume

would cause an increase in melt contribution from the depleted mantle (Beccaluva et al., 2009; Rooney et al., 2012a).

Figure 4.7. Temporal changes in ϵ_{Hf} - $^{206}Pb/^{204}Pb_{initial}$ isotopic space from Lower to Middle to Upper LT flood basalts. Mixing models and symbols are the same as in Figure 4.6. According to the mixing models, the Upper flood basalt show the least influence from Pan African Lithosphere (PAL), and the Middle flood basalt show the most influence of PAL. Over time, there is less contribution from the Afar Plume and more from depleted mantle (DM). Simplified stratigraphic section after Krans et al. (2018) (See Figure 2.5 in Chapter 2).



4.5 CONCLUSIONS

We find that the majority of LT flood basalts can be explained by a three-component mix between DM, Afar Plume, and a lithospheric component, and that contribution from the SCLM is not likely (Figure 4.2). An initial binary mixing model found a hybrid DM-Afar plume source with 10 – 30% Afar Plume and 90 – 70% depleted mantle, however 10- 20 % PAL was needed as a third mixing component to resolve the isotopic variation in LT lavas (Figure 4.6). Over time, the relative contribution from the depleted mantle increases from ~70 % in the Lower flood basalt sequence to ~90 % in the Upper flood basalt sequence. This increase in contribution from the depleted mantle is consistent with a rising geothermal gradient caused by the impinging plume head beneath East Africa (Beccaluva et al., 2009; Rooney et al., 2012c).

The greatest contribution from a lithospheric component occurs during the main-phase of flood volcanism (Middle group C) and this is consistent with previous conceptual models regarding magma evolution in the Ethiopian LT flood basalt province (Krans et al., 2018; see also Chapter 2 and Chapter 3)The exact lithospheric component driving LT magmas away from a two-component DM-Afar Plume source, either by AFC or by source mixing is yet to be constrained, but a lower crustal origin is likely. Isotopic ratios plotted against indices of differentiation (MgO and Nb/La) clearly point toward a crustal component for contamination that is similar to the PAL component previously defined (Schilling et al., 1992; Rooney et al., 2012a), but with lower $^{207}\text{Pb}/^{204}\text{Pb}$ (Figures 4.3 and 4.4).

APPENDICES

APPENDIX A: Detailed sample information

Sample locations, flow elevations and thickness, and general outcrop notes can be found in Supplementary Table A.1. Location information is reported using WGS84 in decimal degrees latitude and longitude (DD Lat and DD Long, respectively). Elevations are reported in meters above sea level. Minimum and maximum elevation reported when contacts between flows were observed in the field (unless specified otherwise). Flow thickness determined from minimum and maximum thickness.

Petro-graphic information for individual samples can be found in Supplementary Table A.2. Textures and mode (modal mineralogy) are as described in results sections 2.1.1.1 and 2.1.1.2, respectively. The total volume % phenocrysts are approximations from visual inspection of thin sections and hand sample. The % An for plagioclase was determined petrographically by Michel Lévy method. NS= no sample collected.

APPENDIX B: Major and trace element data and standards

Major and trace element analysis of Ethiopian LT basalt are presented in Supplementary Table B.1. This Table is subdivided by petrostratigraphic groups as follows: Middle group A (Table B.1_a), Middle group B (Table B.1_b), Middle group C (Table B.1_c), and Upper (Table B.1_d). Standard analysis for XRF can be found in Supplementary Table B.2. ICPMS standards, detection limits, and extrapolation standards can be found in Supplementary Table B.3. Geochemical means and ranges by petrostratigraphic group can be found in Supplementary Table B.4

All flows in this table are classified as LT lavas as defined by Pik et al, 1998) with the exception of 13 samples from the Lower flood basalts that were described as “transitional” by Krans et al. (2018) (See Chapter 2.3.2). These transitional flows do not fit into LT, HT1, nor HT2 geochemical classifications as defined by Pik et al, 1998 and require more detailed treatment of the dataset that is beyond the scope of this dissertation

APPENDIX C: Trace element modeling parameters

REAFc Model

We use the constant mass REAFc model from Lee et al. (2014).

$$C_{ch}^{REAFc} = \frac{C_{re} + \alpha_{cc}C_{cc}}{D\alpha_x + \alpha_e} - \left[\frac{C_{re} + \alpha_{cc}C_{cc}}{D\alpha_x + \alpha_e} - C_{ch}^0 \right]^{[-\Delta\bar{M}_{re}(D\alpha_x + \alpha_e)]}$$

C_{ch}^0 = Initial concentration of element in magma chamber (user defined). We use the composition of the most parental basalt (high MgO, Ni, and Cr) from each petrostratigraphic group (Middle group A, B, and C) suited to represent a liquid composition (free of cumulates) (Supplementary Table C.2). We assume that each petrostratigraphic group denotes a change in the magmatic plumbing system which requires reevaluation of the starting composition in the magma chamber in order to effectively execute the REAFc model.

C_{ch}^{REAFc} = concentration of element in magma chamber (model output). The model outputs a percentage of change from initial concentrations of the element in the magma chamber based on the user defined inputs in the REAFc model. This percentage of change is then multiplied by the starting concentration of the element in the magma chamber to determine the final concentration of the element at a given step (see definition of overturn ($\Delta\bar{M}_{re}$) below).

C_{cc} = concentration of element in the crustal assimilant (user defined). We use the composition of a Pan African granite reported in Rooney et al. (2018) (Supplementary Table C.2).

C_{re} = concentration of element in the recharging magma (user defined). In all cases we use a recharge composition equivalent to the starting composition in each model (Supplementary Table C.2).

α_x = proportion of crystallization relative to recharge rate (user defined).

α_{cc} = proportion of assimilation relative to recharge rate (user defined).

α_e = proportion of evacuation relative to recharge rate (user defined).

The sum of the mass inputs (recharge and assimilation) and outputs (evacuation and fractional crystallization) of an element must be equal to the change in total amount of the element in a magma chamber in order to maintain constant mass. Assimilation of continental crust was run between 0 and 10%, while evacuation and crystallization were free to vary as any combination that summed to 100%.

D = bulk distribution coefficient between crystallizing phases and melt (user defined; see Supplementary Table C.1) Elements that are compatible in particular phases ($D > 1$) include Sr, Ni, and Cr (Supplementary Table C.1). Within each petrostratigraphic model, a bulk distribution coefficient for a deeper fractionating system and shallower fractionating system was determined on the basis of modal mineralogy observed in lavas from that group (Supplementary Table C.1) and pressures determined from MELTS modeling (0.6 – 0.05 GPa). In general, the ‘deep’ fractionation system (> 0.5 GPa) favors the crystallization of clinopyroxene over plagioclase, while the ‘shallow’ fractionation system (< 0.5 GPa) favors the crystallization of plagioclase over clinopyroxene. The prediction of Sr, Cr, and Ni enrichment/depletion trends with respect to MgO must be satisfied using realistic modal percentages of phases prior to accepting the prediction of Nb and La. Without this modal constraint, the REAFC prediction of highly incompatible elements such as Nb and La would yield several non-unique solutions achieved by a combination of % crystallization, % assimilation, and % evacuation.

$\Delta \bar{M}_{re}$ = Number of overturns for a constant mass magma chamber (step function). This is not to be confused with the petrologic term ‘overturn’. In this equation, an overturn is a time-

integrated step function as a system achieves steady state. An incompatible element ($D < 1$) will require more overturns in a chamber undergoing recharge to achieve steady state than a compatible element ($D > 1$). This relationship is responsible for the inflection in the REAFC curve when plotting results for two elements with different compatibility (Figures 5.3 and 5.4.) The number of overturns can be related to residence time of the magma in the chamber if the recharge rate is known (Lee et al., 2014). When recharge rate is not known, relative difference in REAFC parameters can still be assessed to illustrate how a magmatic plumbing system changes over time. $\Delta \bar{M}_{re}$ was run from 0 to 100, though most elements achieved steady state. FC and AFC models were run along-side REAFC models.

FC Model

We adapt the Rayleigh fractionation model from Rayleigh (1986) using the parameters defined in Lee et al. (2014).

$$C_{ch}^{FC} = C_{ch}^0 F^{(D-1)}$$

C_{ch}^{FC} = Concentration of element in residual melt during fractional crystallization.

F = Fraction of melt remaining during crystallization, where $F = 1 - \Delta \bar{M}_{re}$. FC models terminate when $\Delta \bar{M}_{re} = 1$ (1 overturn), as this would equal 100% crystallization since it assumes no melt is being added to the system.

*All other variables defined in REAFC parameters.

AFC Model

We adapt the AFC model from DePaolo (1981) using the parameters defined in Lee et al. (2014).

$$C_{ch}^{AFC} = \frac{C_{ch}^0 r \alpha_x + C_{ch}^{FC} (1 - \alpha_x)}{F}$$

C_{ch}^{AFC} = Concentration of element in residual melt during combined assimilation and fractional crystallization.

r = relative ratio of assimilated material to crystallizing material, where $r = \left(\frac{\alpha_{cc}}{\alpha_x} \right)$

*All other variables defined in REAFC parameters.

AFC models also terminate when $\Delta \bar{M}_{re} = 1$ (1 overturn), as they also assume no melt is being added to the system.

APPENDIX D: Sr-Nd-Pb-Hf isotope data and standards

Measured Sr-Nd-Pb-Hf isotopes for Lower, Middle, and Upper LT flood basalts, NW Ethiopian plateau can be found in Supplementary Table D.1.

APPENDIX E: Isotope modeling parameters

Isotope AFC model endmembers and parameters can be found in Supplementary Table E.1. The Pan African Lithosphere (PAL) component is as defined in Rooney et al (2012a). Parental magma (3408 B) is a Lower flood basalt from this study. α_{cc} =relative proportion of assimilation, α_x =relative proportion of crystallization, similar to REAFC results in Chapter 3. D_{Sr} , D_{Nd} , D_{Pb} , D_{Hf} are bulk distribution coefficients for elements used in Isotopic AFC models and are derived from mineral assemblages determined for deep and shallow fractionating systems in Chapter 3.

Isotope mixing model endmembers can be found in Supplementary Table E.2. The Pan African Lithosphere (PAL), Afar Plume, and depleted mantle (DM) components are as defined in Rooney et al (2012a). Hf concentrations for DM are assumed similar to N-MORB, and Hf concentrations for Afar plume are assumed similar to OIB (Sun and McDunough, 1989). The DM-Afar Plume hybrid compositions are out-puts from the DM-Afar Plume binary mixing model.

REFERENCES

REFERENCES

- Abbate, E., Bruni, P., Ferretti, M.P., Delmer, C., Laurenzi, M.A., Hagos, M., Bedri, O., Rook, L., Sagri, M., and Libsekal, Y., 2014, The East Africa Oligocene intertrappean beds: Regional distribution, depositional environments and Afro/Arabian mammal dispersals: *Journal of African Earth Sciences*, v. 99, p. 463–489.
- Albarede, F., 1985, Regime and trace-element evolution of open magma chambers: *Nature*, v. 318, p. 356–358, doi:10.1038/318356a0.
- Anderson, F.W., and Dunham, K.C., 1966, *The geology of northern Skye*: Edinburgh, HM Stationery Office, v. 80.
- Anderson, A.T., and Greenland, L.P., 1969, Phosphorus fractionation diagram as a quantitative indicator of crystallization differentiation of basaltic liquids: *Geochimica et Cosmochimica Acta*, v. 33, p. 493–505.
- Annels, R., 1973, Proterozoic flood basalts of eastern Lake Superior: the Keweenaw volcanic rocks of the Mamainse Point area, Ontario: Ottawa, Department of Energy, Mines and Resources, doi:10.4095/102486.
- Arndt, N.T., Czamanske, G.K., Wooden, J.L., and Fedorenko, V.A., 1993, Mantle and crustal contributions to continental flood volcanism: *Tectonophysics*, v. 223, doi:10.1016/0040-1951(93)90156-E.
- Ayalew, D., Barbey, P., Marty, B., Reisberg, L., Yirgu, G., and Pik, R., 2002, Source, genesis, and timing of giant ignimbrite deposits associated with Ethiopian continental flood basalts: *Geochim Cosmochim Acta*, v. 66, doi:10.1016/S0016-7037(01)00834-1.
- Ayalew, D., Yirgu, G., and Pik, R., 1999, Geochemical and isotopic (Sr, Nd and Pb) characteristics of volcanic rocks from southwestern Ethiopia: *J Afr Earth Sci*, v. 29, doi:10.1016/S0899-5362(99)00104-9.
- Baker, J.A., 2000, Resolving Crustal and Mantle Contributions to Continental Flood Volcanism, Yemen; Constraints from Mineral Oxygen Isotope Data: *Journal of Petrology*, v. 41, p. 1805–1820, doi:10.1093/petrology/41.12.1805.
- Baker, J., Macpherson, C., Menzies, M., Thirlwall, M., Al-Kadasi, M., and Matthey, D., 2000, Resolving crustal and mantle contributions to continental flood volcanism, Yemen; constraints from mineral oxygen isotope data: *J Petrol*, v. 41, doi:10.1093/petrology/41.12.1805.
- Baker, J., Snee, L., and Menzies, M., 1996a, A brief Oligocene period of flood volcanism in Yemen: implications for the duration and rate of continental flood volcanism at the Afro-

- Arabian triple junction: *Earth and Planetary Science Letters*, v. 138, p. 39–55, doi:10.1016/0012-821X(95)00229-6.
- Baker, J.A., Thirlwall, M.F., and Menzies, M.A., 1996b, Sr–Nd–Pb isotopic and trace element evidence for crustal contamination of plume-derived flood basalts: Oligocene flood volcanism in western Yemen: *Geochimica et Cosmochimica Acta*, v. 60, p. 2559–2581, doi:10.1016/0016-7037(96)00105-6.
- Barry, T., Self, S., Kelley, S., Reidel, S., Hooper, P., and Widdowson, M., 2010, New ⁴⁰Ar/³⁹Ar dating of the Grande Ronde lavas, Columbia River Basalts, USA: implications for duration of flood basalt eruption episodes: *Lithos*, v. 118, doi:10.1016/j.lithos.2010.03.014.
- Bartels, K.S., Kinzler, R.J., and Grove, T.L., 1991, High pressure phase relations of primitive high-alumina basalts from Medicine Lake volcano, northern California: *Contrib Miner Petrol*, v. 108, doi:10.1007/BF00285935.
- Beane, J., Turner, C., Hooper, P., Subbarao, K., and Walsh, J., 1986, Stratigraphy, composition and form of the Deccan basalts, Western Ghats, India: *Bull Volcanol*, v. 48, doi:10.1007/BF01073513.
- Beccaluva, L., Bianchini, G., Natali, C., and Siena, F., 2009, Continental Flood Basalts and Mantle Plumes: a Case Study of the Northern Ethiopian Plateau: *Journal of Petrology*, v. 50, p. 1377–1403, doi:10.1093/petrology/egp024.
- Bennett, E.N., Lissenberg, C.J., and Cashman, K.V., 2019, The significance of plagioclase textures in mid-ocean ridge basalt (Gakkel Ridge, Arctic Ocean): *Contributions to Mineralogy and Petrology*, v. 174, p. 49, doi:10.1007/s00410-019-1587-1.
- Berg, J.H., and Klewin, K.W., 1988, High-MgO lavas from the Keweenawan midcontinent rift near Mamainse Point: *Ontario Geology*, v. 16.
- Bianchini, G., Bryce, J.G., Blichert-Toft, J., Beccaluva, L., and Natali, C., 2014, Mantle dynamics and secular variations beneath the East African Rift: Insights from peridotite xenoliths (Mega, Ethiopia): *Chemical Geology*, v. 386, p. 49–58, doi:10.1016/j.chemgeo.2014.07.024.
- Blundy, J.D., and Annen, C.J., 2016, Crustal Magmatic Systems from the Perspective of Heat Transfer: *Elements*, v. 12, p. 115–120, doi:10.2113/gselements.12.2.115.
- Bohrson, W.A., and Spera, F.J., 2001, Energy-constrained open-system magmatic processes II: application of energy-constrained assimilation–fractional crystallization (EC-AFC) model to magmatic systems: *Journal of Petrology*, v. 42, p. 1019–1041.
- Bohrson, W.A., Spera, F.J., Ghiorso, M.S., Brown, G.A., Creamer, J.B., and Mayfield, A., 2014, Thermodynamic Model for Energy-Constrained Open-System Evolution of Crustal Magma Bodies Undergoing Simultaneous Recharge, Assimilation and Crystallization:

- the Magma Chamber Simulator: *Journal of Petrology*, v. 55, p. 1685–1717, doi:10.1093/petrology/egu036.
- Bondre, N.R., Duraiswami, R.A., and Dole, G., 2004, Morphology and emplacement of flows from the Deccan Volcanic Province, India: *Bull Volcanol*, v. 66, doi:10.1007/s00445-003-0294-x.
- Bondre, N.R., and Hart, W.K., 2008, Morphological and textural diversity of the Steens Basalt lava flows, Southeastern Oregon, USA: implications for emplacement style and nature of eruptive episodes: *Bull Volcanol*, v. 70, doi:10.1007/s00445-007-0182-x.
- Borges, M.R., Sen, G., Hart, G.L., Wolff, J.A., and Chandrasekharam, D., 2014, Plagioclase as recorder of magma chamber processes in the Deccan Traps: Sr-isotope zoning and implications for Deccan eruptive event: *Journal of Asian Earth Sciences*, v. 84, p. 95–101, doi:10.1016/j.jseaes.2013.10.034.
- Bowen, N.L., 1928, *The Evolution of the Igneous Rocks*: Princeton University Press.
- Boynton, W.V., 1984, Cosmochemistry of the Rare Earth Elements: Meteorite Studies, *in* *Developments in Geochemistry*, Elsevier, v. 2, p. 63–114, doi:10.1016/B978-0-444-42148-7.50008-3.
- Brown, F.H., and Mcdougall, I., 2011, Geochronology of the Turkana depression of northern Kenya and southern Ethiopia: *Evolutionary Anthropology: Issues, News, and Reviews*, v. 20, p. 217–227.
- Bryan, S.E., Peate, I.U., Peate, D.W., Self, S., Jerram, D.A., Mawby, M.R., Marsh, J.S. (Goonie), and Miller, J.A., 2010, The largest volcanic eruptions on Earth: *Earth-Science Reviews*, v. 102, p. 207–229, doi:10.1016/j.earscirev.2010.07.001.
- Camp, V.E., Ross, M.E., Duncan, R.A., Jarboe, N.A., Coe, R.S., Hanan, B.B., and Johnson, J.A., 2013, The Steens basalt: Earliest lavas of the Columbia River basalt group: *Geol Soc Am Spec Pap*, v. 497.
- Chenet, A., Fluteau, F., Courtillot, V., Gérard, M., and Subbarao, K., 2008, Determination of rapid Deccan eruptions across the cretaceous–tertiary boundary using paleomagnetic secular variation: results from a 1200-m-thick section in the Mahabaleshwar escarpment: *J Geophys Res Solid Earth*, v. 113, doi:10.1029/2006JB004635.
- Cheng, L., Yang, Z., Zeng, L., Wang, Y., and Luo, Z., 2014, Giant plagioclase growth during storage of basaltic magma in Emeishan Large Igneous Province, SW China: *Contrib Miner Petrol*, v. 167, doi:10.1007/s00410-014-0971-0.
- Chorowicz, J., Collet, B., Bonavia, F., Mohr, P., Parrot, J., and Korme, T., 1998, The Tana basin, Ethiopia: intra-plateau uplift, rifting and subsidence: *Tectonophysics*, v. 295, doi:10.1016/S0040-1951(98)00128-0.

- Cornwell, D., Mackenzie, G., England, R., Maguire, P., Asfaw, L., and Oluma, B., 2006, Northern Main Ethiopian Rift crustal structure from new high-precision gravity data: *Geological Society of London*, v. 259, p. 307–321, doi:<https://doi.org/10.1144/GSL.SP.2006.259.01.23>.
- Cornwell, D., Maguire, P., England, R., and Stuart, G., 2010, Imaging detailed crustal structure and magmatic intrusion across the Ethiopian Rift using a dense linear broadband array: *Geochem Geophys Geosyst*, v. 11, doi:[10.1029/2009GC002637](https://doi.org/10.1029/2009GC002637).
- Courtillot, V., Besse, J., Vandamme, D., Montigny, R., Jaeger, J., and Cappetta, H., 1986, Deccan flood basalts at the cretaceous/tertiary boundary? *Earth Planet Sci Lett*, v. 80, doi:[10.1016/0012-821X\(86\)90118-4](https://doi.org/10.1016/0012-821X(86)90118-4).
- Cox, K.G., 1980, A Model for Flood Basalt Vulcanism: *Journal of Petrology*, v. 21, p. 629–650, doi:<https://doi.org/10.1093/petrology/21.4.629>.
- Davaille, A., Stutzmann, E., Silveira, G., Besse, J., and Courtillot, V., 2005, Convective patterns under the Indo-Atlantic «box»: *Earth Planet Sci Lett*, v. 239, doi:[10.1016/j.epsl.2005.07.024](https://doi.org/10.1016/j.epsl.2005.07.024).
- Davis, W.R., Collins, M.A., Rooney, T.O., Brown, E.L., Stein, C.A., Stein, S., and Moucha, R., 2021, Geochemical, petrographic, and stratigraphic analyses of the Portage Lake Volcanics of the Keweenaw CFBP: implications for the evolution of Main stage volcanism in Continental Flood Basalt Provinces: *Geological Society, London, Special Publications*, v. 518, doi:[10.1144/SP518-2020-221](https://doi.org/10.1144/SP518-2020-221).
- DePaolo, D.J., 1981, Trace element and isotopic effects of combined wallrock assimilation and fractional crystallization: *Earth and Planetary Science Letters*, v. 53, p. 189–202, doi:[10.1016/0012-821X\(81\)90153-9](https://doi.org/10.1016/0012-821X(81)90153-9).
- Duraiswami, R.A., Bondre, N.R., Dole, G., Phadnis, V.M., and Kale, V.S., 2001, Tumuli and associated features from the western Deccan Volcanic Province, India: *Bull Volcanol*, v. 63, doi:[10.1007/s004450100160](https://doi.org/10.1007/s004450100160).
- Ebinger, C., Yemane, T., Woldegabriel, G., Aronson, J., and Walter, R., 1993, Late Eocene—recent volcanism and faulting in the southern main Ethiopian rift: *J Geol Soc*, v. 150, doi:[10.1144/gsjgs.150.1.0099](https://doi.org/10.1144/gsjgs.150.1.0099).
- Emeleus, C.H., and Bell, B.R., 2005, *British regional geology: the palaeogene volcanic districts of Scotland*: Keyworth, Nottingham, British Geological Survey.
- Ernst, R.E., 2014, *Large igneous provinces*: Cambridge University Press.
- Ernst, R., Grosfils, E., and Mège, D., 2001, Giant Dike Swarms: Earth, Venus, and Mars: *Annual Review of Earth and Planetary Sciences*, v. 29, p. 489–534, doi:[10.1146/annurev.earth.29.1.489](https://doi.org/10.1146/annurev.earth.29.1.489).

- Farentani, C.G., Richard, M., and Ghiorso, M.S., 1996, Petrological models of magma evolution and deep crustal structure beneath hotspots and flood basalt provinces: *Earth and Planetary Science Letters*, v. 143, p. 81–94, doi:[https://doi.org/10.1016/0012-821X\(96\)00138-0](https://doi.org/10.1016/0012-821X(96)00138-0).
- Feig, S.T., Koepke, J., and Snow, J.E., 2006, Effect of water on tholeiitic basalt phase equilibria: an experimental study under oxidizing conditions: *Contrib Miner Petrol*, v. 152, doi:[10.1007/s00410-006-0123-2](https://doi.org/10.1007/s00410-006-0123-2).
- Finlayson, V.A., Konter, J.G., Konrad, K., Koppers, A.A.P., Jackson, M.G., and Rooney, T.O., 2018, Sr–Pb–Nd–Hf isotopes and $^{40}\text{Ar}/^{39}\text{Ar}$ ages reveal a Hawaii–Emperor-style bend in the Rurutu hotspot: *Earth and Planetary Science Letters*, v. 500, p. 168–179, doi:[10.1016/j.epsl.2018.08.020](https://doi.org/10.1016/j.epsl.2018.08.020).
- Furman, T., Bryce, J., Rooney, T., Hanan, B., Yirgu, G., and Ayalew, D., 2006, Heads and tails: 30 million years of the Afar plume: *Geological Society of London*, v. 259, p. 95–119, doi:<https://doi.org/10.1144/GSL.SP.2006.259.01.09>.
- Furman, T., Nelson, W.R., and Elkins-Tanton, L.T., 2016, Evolution of the East African rift: Drip magmatism, lithospheric thinning and mafic volcanism: *Geochimica et Cosmochimica Acta*, v. 185, p. 418–434, doi:[10.1016/j.gca.2016.03.024](https://doi.org/10.1016/j.gca.2016.03.024).
- George, R., and Rogers, N., 2002, Plume dynamics beneath the African plate inferred from the geochemistry of the Tertiary basalts of southern Ethiopia: *Contrib Miner Petrol*, v. 144, doi:[10.1007/s00410-002-0396-z](https://doi.org/10.1007/s00410-002-0396-z).
- George, R., Rogers, N., and Kelley, S., 1998, Earliest magmatism in Ethiopia: evidence for two mantle plumes in one flood basalt province: *Geology*, v. 26, <https://doi.org/10.1130/G23CO2>.
- Ghiorso, M.S., and Sack, R.O., 1995, Chemical mass transfer in magmatic processes IV. A revised and internally consistent thermodynamic model for the interpolation and extrapolation of liquid-solid equilibria in magmatic systems at elevated temperatures and pressures: *Contributions to Mineralogy and Petrology*, p. 197–212, doi:<https://doi.org/10.1007/BF00307281>.
- Gibson, S.A., Thompson, R.N., Dickin, A.P., and Leonardos, O.H., 1995, High-Ti and low-Ti mafic potassic magmas: Key to plume-lithosphere interactions and continental flood-basalt genesis: *Earth and Planetary Science Letters*, v. 136, p. 149–165, doi:[10.1016/0012-821X\(95\)00179-G](https://doi.org/10.1016/0012-821X(95)00179-G).
- Grant, T.B., Larsen, R.B., Brown, E.L., Muller, A.B., and McEnroe, S., 2020, Mixing of heterogeneous, high-MgO, plume-derived magmas at the base of the crust in the Central Iapetus Magmatic Province (Ma 610–550): Origin of parental magmas to a global LIP event: *Lithos*, v. 364, p. 105535, doi:[10.1016/j.lithos.2020.105535](https://doi.org/10.1016/j.lithos.2020.105535).
- Green, D.H., 1971, Composition of basaltic magmas as indicators of conditions of origin: application to oceanic volcanism: *Philosophical Transactions for the Royal Society of London. Series A, Mathematical and Physical Sciences*, p. 707–725.

- Grove, T.L., Kinzler, R.J., Baker, M.B., Donnelly-Nolan, J.M., and Leshner, C.E., 1988, Assimilation of granite by basaltic magma at Burnt Lava flow, Medicine Lake volcano, northern California: Decoupling of heat and mass transfer: *Contributions to Mineralogy and Petrology*, v. 99, p. 320–343, doi:10.1007/BF00375365.
- Gualda, G.A.R., Ghiorso, M.S., Lemons, R.V., and Carley, T.L., 2012, Rhyolite-MELTS: a Modified Calibration of MELTS Optimized for Silica-rich, Fluid-bearing Magmatic Systems: *Journal of Petrology*, v. 53, p. 875–890, doi:10.1093/petrology/egr080.
- Hansen, H., and Grönvold, K., 2000, Plagioclase ultraphyric basalts in Iceland: the mush of the rift: *Journal of Volcanology and Geothermal Research*, v. 98, p. 1–32.
- Hawkesworth, C., Mantovani, M., and Peate, D., 1988, Lithosphere Remobilization during Parana CFB Magmatism: *Journal of Petrology*, v. Special_Volume, p. 205–223, doi:10.1093/petrology/Special_Volume.1.205.
- Hawkesworth, C.J., Marsh, J.S., Duncan, A.R., Erlank, A.J., and Norry, M.J., 1984, The role of continental lithosphere in the generation of the Karoo volcanic rocks: evidence from combined Nd-and Sr-isotopes studies: *Geol. Soc. South Afr. Spec. Publ.*, v. 13, p. 341–354.
- Heinonen, J.S., Luttinen, A.V., and Bohrsen, W.A., 2016, Enriched continental flood basalts from depleted mantle melts: modeling the lithospheric contamination of Karoo lavas from Antarctica: *Contributions to Mineralogy and Petrology*, v. 171, p. 9, doi:10.1007/s00410-015-1214-8.
- Hergt, J.M., Chappell, B.W., McCulloch, M.T., McDougall, I., and Chivas, A.R., 1989, Geochemical and isotopic constraints on the origin of the Jurassic dolerites of Tasmania: *Journal of Petrology*, v. 30, p. 841–883.
- Herzberg, C., and Asimow, P.D., 2008, Petrology of some oceanic island basalts: PRIMELT2. XLS software for primary magma calculation: *Geochem Geophys Geosyst*, v. 9, doi:10.1029/2008GC002057.
- Higgins, M.D., and Chandrasekharam, D., 2007, Nature of sub-volcanic magma chambers, Deccan Province, India: evidence from quantitative textural analysis of plagioclase megacrysts in the Giant Plagioclase Basalts: *Journal of Petrology*, v. 48, p. 885–900.
- Hofmann, C., Courtillot, V., Feraud, G., Rochette, P., Yirgu, G., Ketefo, E., and Pik, R., 1997, Timing of the Ethiopian flood basalt event and implications for plume birth and global change: *Nature*, v. 389, p. 838–841.
- Hofmann, A.W., Jochum, K.P., Seufert, M., and White, W.M., 1986, Nb and Pb in oceanic basalts: new constraints on mantle evolution: *Earth and Planetary Science Letters*, v. 79, p. 33–45, doi:10.1016/0012-821X(86)90038-5.

- Holm, P.M., and Prægel, N., 2006, Cumulates from primitive rift-related East Greenland Paleogene magmas: petrological and isotopic evidence from the ultramafic complexes at Kælvegletscher and near Kærven: *Lithos*, v. 92, doi:10.1016/j.lithos.2006.03.036.
- Hooper, P., Subbarao, K., and Beane, J., 1988, The giant plagioclase basalts (GPBs) of the western Ghats, Deccan Traps: *Deccan Flood Basalts Mem Geol Soc India*, v. 10.
- Huber, N., 1973, The Portage lake volcanics (Middle Keweenawan) on Isle Royale, Michigan: *USGS Professional Paper 754-C*.
- Ivanov, A.V., Demonterova, E.I., Rasskazov, S.V., and Yasnygina, T.A., 2008, Low-Ti melts from the southeastern Siberian Traps Large Igneous Province: Evidence for a water-rich mantle source? *Journal of Earth System Science*, v. 117, p. 1–21, doi:10.1007/s12040-008-0008-z.
- Jean, M., 2013, Geochemical and paleomagnetic variation in basalts from the Wendell Regional Aquifer Systems Analysis (RASA) drill core: Evidence for magma recharge and assimilation-fractional crystallization from the central Snake River Plain, Idaho: *Geosphere*, v. 9, p. 1319, doi:10.1130/GES00914.1.
- Jerram, D.A., Dobson, K.J., Morgan, D.J., and Pankhurst, M.J., 2018, The Petrogenesis of Magmatic Systems: Using Igneous Textures to Understand Magmatic Processes, *in* *Volcanic and Igneous Plumbing Systems*, Elsevier, p. 191–229, doi:10.1016/B978-0-12-809749-6.00008-X.
- Jerram, D.A., Mountney, N., Howell, J., Long, D., and Stollhofen, H., 2000, Death of a sand sea: an active aeolian erg systematically buried by the Etendeka flood basalts of NW Namibia: *J Geol Soc*, v. 157, doi:10.1144/jgs.157.3.513.
- Jerram, D.A., and Stollhofen, H., 2002, Lava–sediment interaction in desert settings; are all peperite-like textures the result of magma–water interaction? *J Volcanol Geotherm Res*, v. 114, doi:10.1016/S0377-0273(01)00279-7.
- Jerram, D.A., and Widdowson, M., 2005, The anatomy of Continental Flood Basalt Provinces: geological constraints on the processes and products of flood volcanism: *Lithos*, v. 79, p. 385–405, doi:10.1016/j.lithos.2004.09.009.
- Jourdan, F., Bertrand, H., Schärer, U., Blichert-Toft, J., Féraud, G., and Kampunzu, A.B., 2007, Major and Trace Element and Sr, Nd, Hf, and Pb Isotope Compositions of the Karoo Large Igneous Province, Botswana–Zimbabwe: Lithosphere vs Mantle Plume Contribution: *Journal of Petrology*, v. 48, p. 1043–1077, doi:10.1093/petrology/egm010.
- Kappelman, J., Tewabe, D., Todd, L., Feseha, M., Kay, M., Kocurek, G., Nachman, B., Tabor, N., and Yadeta, M., 2014, Another unique river: a consideration of some of the characteristics of the trunk tributaries of the Nile River in northwestern Ethiopia in relationship to their aquatic food resources: *J Hum Evol*, v. 77, doi:10.1016/j.jhevol.2014.03.008.

- Kieffer, B. et al., 2004, Flood and Shield Basalts from Ethiopia: Magmas from the African Superswell: *Journal of Petrology*, v. 45, p. 793–834, doi:10.1093/petrology/egg112.
- Kimura, J., and Kawabata, H., 2015, Ocean Basalt Simulator version 1 (OBS1): trace element mass balance in adiabatic melting of a pyroxenite-bearing peridotite: *Geochem Geophys Geosyst*, v. 16, doi:10.1002/2014GC005606.
- Kogiso, T., Hirschmann, M.M., and Frost, D.J., 2003, High-pressure partial melting of garnet pyroxenite: possible mafic lithologies in the source of ocean island basalts: *Earth Planet Sci Lett*, v. 216, doi:10.1016/S0012-821X(03)00538-7.
- Krans, S.R., Rooney, T.O., Kappelman, J., Yirgu, G., and Ayalew, D., 2018, From initiation to termination: a petrostratigraphic tour of the Ethiopian Low-Ti Flood Basalt Province.: *Contributions to Mineralogy & Petrology*, v. 173, p. 1–1.
- Lee, C.-T.A., Lee, T.C., and Wu, C.-T., 2014, Modeling the compositional evolution of recharging, evacuating, and fractionating (REFC) magma chambers: Implications for differentiation of arc magmas: *Geochimica et Cosmochimica Acta*, v. 143, p. 8–22.
- Lightfoot, P.C., Hawkesworth, C.J., Hergt, J., Naldrett, A.J., Gorbachev, N.S., Fedorenko, V.A., and Doherty, W., 1993, Remobilisation of the continental lithosphere by a mantle plume: major-, trace-element, and Sr-, Nd-, and Pb-isotope evidence from picritic and tholeiitic lavas of the Noril'sk District, Siberian Trap, Russia: *Contributions to Mineralogy and Petrology*, v. 114, p. 171–188, doi:10.1007/BF00307754.
- Lightfoot, P.C., Naldrett, A.J., Gorbachev, N.S., Doherty, W., and Fedorenko, V.A., 1990, Geochemistry of the Siberian Trap of the Noril'sk area, USSR, with implications for the relative contributions of crust and mantle to flood basalt magmatism: *Contributions to Mineralogy and Petrology*, v. 104, p. 631–644, doi:10.1007/BF01167284.
- Mackenzie, G., Thybo, H., and Maguire, P., 2005, Crustal velocity structure across the Main Ethiopian Rift: results from two-dimensional wide-angle seismic modelling: *Geophys J Int*, v. 162, doi:10.1111/j.1365-246X.2005.02710.x.
- Mahoney, J.J., Sheth, H.C., Chandrasekharam, D., and Peng, Z.X., 2000, Geochemistry of Flood Basalts of the Toranmal Section, Northern Deccan Traps, India: Implications for Regional Deccan Stratigraphy: *Journal of Petrology*, v. 41, p. 1099–1120, doi:10.1093/petrology/41.7.1099.
- Mammo, T., 2013, Crustal structure of the flood basalt province of Ethiopia from constrained 3-D gravity inversion: *Pure Appl Geophys*, v. 170, doi:10.1007/s00024-013-0663-0.
- McIntire, W.L., 1963, Trace element partition coefficients—a review of theory and applications to geology: *Geochimica et Cosmochimica Acta*, v. 27, p. 1209–1264.
- Mège, D., and Korme, T., 2004, Dyke swarm emplacement in the Ethiopian large igneous province: not only a matter of stress: *J Volcanol Geotherm Res*, v. 132, doi:10.1016/S0377-0273(03)00318-4.

- Melluso, L., Beccaluva, L., Brotzu, P., Gregnanin, A., Gupta, A.K., Morbidelli, L., and Traversa, G., 1995, Constraints on the Mantle Sources of the Deccan Traps from the Petrology and Geochemistry of the Basalts of Gujarat State (Western India): *Journal of Petrology*, v. 36, p. 1393–1432, doi:10.1093/petrology/36.5.1393.
- Melluso, L., Mahoney, J.J., and Dallai, L., 2006, Mantle sources and crustal input as recorded in high-Mg Deccan Traps basalts of Gujarat (India): *Lithos*, v. 89, p. 259–274, doi:10.1016/j.lithos.2005.12.007.
- Meshesha, D., and Shinjo, R., 2007, Crustal contamination and diversity of magma sources in the northwestern Ethiopian volcanic province: *Journal of Mineralogical and Petrological Sciences*, v. 102, p. 272–290, doi:10.2465/jmps.061129.
- Miller, J.D., and Ripley, E.M., 1996, Layered intrusions of the Duluth complex, Minnesota, USA, *in* *Developments in Petrology*, Elsevier, v. 15, p. 257–301.
- Mohr, P., 1983, Volcanotectonic aspects of Ethiopian rift evolution: *Bull Cent Rech Explor Prod Elf-Aquitaine*, v. 7.
- Mohr, P., and Zanettin, B., 1988, The Ethiopian flood basalt province, *in* Macdougall, J.D. ed., *Continental flood basalts*, Dordrecht, Springer, doi:10.1007/978-94-015-7805-9_3.
- Morley, C.K., Wescott, W., Stone, D., Harper, R., Wigger, S., and Karanja, F., 1992, Tectonic evolution of the northern Kenyan Rift: *J Geol Soc*, v. 149, doi:10.1144/gsjgs.149.3.0333.
- Morse, S.A., 1980, *Basalts and phase diagrams: an introduction to the quantitative use of phase diagrams in igneous petrology*: New York, Springer, doi:10.1007/978-1-4612-6081-3.
- Natali, C., Beccaluva, L., Bianchini, G., Ellam, R.M., Savo, A., Siena, F., and Stuart, F.M., 2016, High-MgO lavas associated to CFB as indicators of plume-related thermochemical effects: the case of ultra-titaniferous picrite–basalt from the Northern Ethiopian–Yemeni Plateau: *Gondwana Research*, v. 34, p. 29–48.
- Nishimura, K., 2009, A trace-element geochemical model for imperfect fractional crystallization associated with the development of crystal zoning: *Geochimica et Cosmochimica Acta*, v. 73, p. 2142–2149.
- Nishimura, K., 2013, AIFCCalc: An Excel spreadsheet for modeling simultaneous assimilation and imperfect fractional crystallization: *Computers and Geosciences*, v. 51, p. 410–414.
- O’Hara, M.J., 1977, Geochemical evolution during fractional crystallisation of a periodically refilled magma chamber: *Nature*, v. 266, p. 503–507, doi:10.1038/266503a0.
- O’Hara, M.J., and Herzberg, C., 2002, Interpretation of trace element and isotope features of basalts: relevance of field relations, petrology, major element data, phase equilibria, and magma chamber modeling in basalt petrogenesis: *Geochim Cosmochim Acta*, v. 66, doi:10.1016/S0016-7037(02)00852-9.

- O'Hara, M.J., and Mathews, R.E., 1981, Geochemical evolution in an advancing, periodically replenished, periodically tapped, continuously fractionated magma chamber: *Journal of the Geological Society*, v. 138, p. 237–277, doi:10.1144/gsjgs.138.3.0237.
- O'Neill, H.S.C., and Jenner, F.E., 2012, The global pattern of trace-element distributions in ocean floor basalts: , p. 8.
- Óskarsson, B.V., Andersen, C.B., Riishuus, M.S., Sørensen, E.V., and Tegner, C., 2017, The mode of emplacement of Neogene flood basalts in Eastern Iceland: The plagioclase ultraphyric basalts in the Grænavatn group: *J Volcanol Geotherm Res*, v. 332, doi:10.1016/j.jvolgeores.2017.01.006.
- Passmore, E., MacLennan, J., Fitton, G., and Thordarson, T., 2012, Mush Disaggregation in Basaltic Magma Chambers: Evidence from the ad 1783 Laki Eruption: *Journal of Petrology*, v. 53, p. 2593–2623, doi:10.1093/petrology/egs061.
- Peate, I.U., and Bryan, S.E., 2008, Re-evaluating plume-induced uplift in the Emeishan large igneous province: *Nature Geoscience*, v. 1, p. 625–629.
- Peate, D.W., and Hawkesworth, C.J., 1994, Lithospheric to asthenospheric transition in Low-Ti flood basalts from southern Paraná & Brazil: *Chemical Geology*, p. 24.
- Peng, Z., Mahoney, J., Hooper, P., Harris, C., and Beane, J., 1994, A role for lower continental crust in flood basalt genesis? Isotopic and incompatible element study of the lower six formations of the western Deccan Traps: *Geochim Cosmochim Acta*, v. 58, doi:10.1016/0016-7037(94)90464-2.
- Piccirillo, E.M., 1988, Continental flood volcanism from the Paraná Basin (Brazil), *in* Macdougall, J.D. ed., *Continental flood basalts*, Dordrecht, Springer, doi:10.1007/978-94-015-7805-9_6.
- Pik, R., Deniel, C., Coulon, C., Yirgu, G., Hofmann, C., and Ayalew, D., 1998, The northwestern Ethiopian Plateau flood basalts: Classification and spatial distribution of magma types: *Journal of Volcanology and Geothermal Research*, v. 81, p. 91–111, doi:10.1016/S0377-0273(97)00073-5.
- Pik, R., Deniel, C., Coulon, C., Yirgu, G., and Marty, B., 1999, Isotopic and trace element signatures of Ethiopian flood basalts: evidence for plume–lithosphere interactions: *Geochimica et Cosmochimica Acta*, v. 63, p. 2263–2279, doi:10.1016/S0016-7037(99)00141-6.
- Powell, R., 1984, Inversion of the assimilation and fractional crystallization (AFC) equations; characterization of contaminants from isotope and trace element relationships in volcanic suites: *Journal of the Geological Society*, v. 141, p. 447–452.
- Prave, A.R., 2016, Geology and geochronology of the Tana Basin, Ethiopia: LIP volcanism, super eruptions and Eocene–Oligocene environmental change: *Earth and Planetary Science Letters*, p. 8.

- Rayleigh, Lord, 1896, L. *Theoretical considerations respecting the separation of gases by diffusion and similar processes*: The London, Edinburgh, and Dublin Philosophical Magazine and Journal of Science, v. 42, p. 493–498, doi:10.1080/14786449608620944.
- Reidel, S.P., Camp, V.E., Tolan, T.L., and Martin, B.S., 2013, The Columbia River flood basalt province: stratigraphy, areal extent, volume, and physical volcanology: *Geol Soc Am Sp Pap*, v. 497.
- Renne, P.R., and Basu, A.R., 1991, Rapid eruption of the Siberian Traps flood basalts at the Permo-Triassic boundary: *Science*, v. 253, doi:10.1126/science.253.5016.176.
- Ridley, V.A., and Richards, M.A., 2010, Deep crustal structure beneath large igneous provinces and the petrologic evolution of flood basalts: *Geochem Geophys Geosyst*, v. 11, doi:10.1029/2009GC002935.
- Rochette, P., Tamrat, E., Féraud, G., Pik, R., Courtillot, V., Ketefo, E., Coulon, C., Hoffmann, C., Vandamme, D., and Yirgu, G., 1998, Magnetostratigraphy and timing of the Oligocene Ethiopian traps: *Earth and Planetary Science Letters*, v. 164, p. 497–510.
- Roeder, P.L., and Emslie, R.F., 1970, Olivine-liquid equilibrium: *Contributions to Mineralogy and Petrology*, v. 29, p. 275–289, doi:10.1007/BF00371276.
- Rollinson, H., 1993, *Using geochemical data: Evaluation, Presentation, Interpretation*: London, Longman, v. 1, 352 p.
- Rooney, T.O., 2017, The Cenozoic magmatism of East-Africa: Part I—Flood basalts and pulsed magmatism: *Lithos*, v. 286, p. 264–301.
- Rooney, T.O., Hanan, B.B., Graham, D.W., Furman, T., Blichert-Toft, J., and Schilling, J.-G., 2012a, Upper Mantle Pollution during Afar Plume–Continental Rift Interaction: *Journal of Petrology*, v. 53, p. 365–389, doi:10.1093/petrology/egr065.
- Rooney, T.O., Hart, W.K., Hall, C.M., Ayalew, D., Ghiorso, M.S., Hidalgo, P., and Yirgu, G., 2012b, Peralkaline magma evolution and the tephra record in the Ethiopian Rift: *Contributions to Mineralogy and Petrology*, v. 164, p. 407–426, doi:10.1007/s00410-012-0744-6.
- Rooney, T.O., Herzberg, C., and Bastow, I.D., 2012c, Elevated mantle temperature beneath East Africa: *Geology*, v. 40, p. 27–30.
- Rooney, T.O., Krans, S.R., Mege, D., Arnaud, N., Korme, T., Kappelman, J., and Yirgu, G., 2018, Constraining the magmatic plumbing system in a zoned continental flood basalt province: *Geochemistry, Geophysics, Geosystems*, v. 19, p. 3917–3944.
- Rooney, T.O., Lavigne, A., Svoboda, C., Girard, G., Yirgu, G., Ayalew, D., and Kappelman, J., 2017, The making of an underplate: pyroxenites from the Ethiopian lithosphere: *Chem Geol*, v. 455, doi:10.1016/j.chemgeo.2016.09.011.

- Rooney, T.O., Mohr, P., Dosso, L., and Hall, C., 2013, Geochemical evidence of mantle reservoir evolution during progressive rifting along the western Afar margin: *Geochimica et Cosmochimica Acta*, v. 102, p. 65–88.
- Rooney, T.O., Morell, K.D., Hidalgo, P., and Fraceschi, P., 2015, Magmatic consequences of the transition from orthogonal to oblique subduction in P anama: *Geochemistry, Geophysics, Geosystems*, v. 16, p. 4178–4208, doi:10.1002/2015GC006150.
- Rooney, T.O., Nelson, W.R., Dosso, L., Furman, T., and Hanan, B., 2014, The role of continental lithosphere metasomes in the production of HIMU-like magmatism on the northeast African and Arabian plates: *Geology*, v. 42, p. 419–422, doi:10.1130/G35216.1.
- Schilling, J.-G., Kingsley, R.H., Hanan, B.B., and McCully, B.L., 1992, Nd-Sr-Pb isotopic variations along the Gulf of Aden: Evidence for Afar Mantle Plume-Continental Lithosphere Interaction: *Journal of Geophysical Research*, v. 97, p. 10927, doi:10.1029/92JB00415.
- Self, S., Thordarson, T., and Keszthelyi, L., 1997, Emplacement of Continental Flood Basalt Lava Flows, *in* Mahoney, J. and Coffin, M. eds., *Large igneous provinces: continental, oceanic, and planetary flood volcanism*, Geophysical Monograph Series, <https://doi.org/10.1029/GM100p0381>.
- Sen, G., 2001, Generation of Deccan trap magmas: *Journal of Earth System Science*, v. 110, p. 409–431.
- Sen, G., Borges, M., and Marsh, B.D., 2006, A case for short duration of Deccan Trap eruption: *Eos Trans Am Geophys Union*, v. 87, doi:10.1029/2006EO200001.
- Shaw, J.E., Baker, J.A., Kent, A.J.R., Ibrahim, K.M., and Menzies, M.A., 2007, The Geochemistry of the Arabian Lithospheric Mantle--a Source for Intraplate Volcanism? *Journal of Petrology*, v. 48, p. 1495–1512, doi:10.1093/petrology/egm027.
- Sheldon, N.D., 2003, Pedogenesis and geochemical alteration of the Picture Gorge subgroup, Columbia River basalt, Oregon: *Geol Soc Am Bull*, v. 115, doi:10.1130/B25223.1.
- Sheth, H., 2016, Giant plagioclase basalts: continental flood basalt-induced remobilization of anorthositic mushes in a deep crustal sill complex: *Geol Soc Am Bull*, v. 128, doi:10.1130/B31404.1.
- Sheth, H.C., Mahoney, J.J., and Chandrasekharam, D., 2004, Geochemical stratigraphy of Deccan flood basalts of the Bijasan Ghat section, Satpura Range, India: *Journal of Asian Earth Sciences*, v. 23, p. 127–139, doi:10.1016/S1367-9120(03)00116-0.
- Shi, P., and Libourel, G., 1991, The effects of FeO on the system CMAS at low pressure and implications for basalt crystallization processes: *Contrib Miner Petrol*, v. 108, doi:10.1007/BF00307332.

- Shirey, S.B., 1997, Re-Os isotopic compositions of Midcontinent rift system picrites: implications for plume–lithosphere interaction and enriched mantle sources: *Canadian Journal of Earth Sciences*, v. 34, p. 489–503.
- Shirey, S.B., Berg, J.H., and Carlson, R.W., 1994, Temporal changes in the sources of flood basalts: isotopic and trace element evidence from the 1100 Ma old Keweenaw Mamainse Point Formation, Ontario, Canada: *Geochimica et Cosmochimica Acta*, v. 58, p. 4475–4490.
- Spera, F.J., and Bohron, W.A., 2001, Energy-constrained open-system magmatic processes I: General model and energy-constrained assimilation and fractional crystallization (EC-AFC) formulation: *Journal of Petrology*, v. 42, p. 999–1018.
- Stuart, G., Bastow, I., and Ebinger, C., 2006, Crustal structure of the northern Main Ethiopian Rift from receiver function studies: *Geological Society of London*, v. 259, p. 253–267, doi:<https://doi.org/10.1144/GSL.SP.2006.259.01.20>.
- Sweeney, R.J., Duncan, A.R., and Erlank, A.J., 1994, Geochemistry and Petrogenesis of Central Lebombo Basalts of the Karoo Igneous Province: *Journal of Petrology*, v. 35, p. 95–125, doi:[10.1093/petrology/35.1.95](https://doi.org/10.1093/petrology/35.1.95).
- Teklay, M., Asmerom, Y., and Toulkeridis, T., 2005, Geochemical and Sr-Nd isotope ratios in Cenozoic basalts from Eritrea: evidence for temporal evolution from low-Ti tholeiitic to high-Ti alkaline basalts in Afro-Arabian Continental Flood Basalt Province: , p. 17.
- Thordarson, T., and Self, S., 1998, The Roza Member, Columbia River Basalt Group: a gigantic pahoehoe lava flow field formed by endogenous processes? *J Geophys Res Solid Earth*, v. 103, doi:[10.1029/98JB01355](https://doi.org/10.1029/98JB01355).
- Ukstins, I.A., Renne, P.R., Wolfenden, E., Baker, J., Ayalew, D., and Menzies, M., 2002, Matching conjugate volcanic rifted margins: 40 Ar/39 Ar chrono-stratigraphy of pre-and syn-rift bimodal flood volcanism in Ethiopia and Yemen: *Earth Planet Sci Lett*, v. 198, doi:[10.1016/S0012-821X\(02\)00525-3](https://doi.org/10.1016/S0012-821X(02)00525-3).
- Vanderkluyzen, L., Mahoney, J.J., Hooper, P.R., Sheth, H.C., and Ray, R., 2011, The Feeder System of the Deccan Traps (India): Insights from Dike Geochemistry: *Journal of Petrology*, v. 52, p. 315–343, doi:[10.1093/petrology/egq082](https://doi.org/10.1093/petrology/egq082).
- Villiger, S., 2004, The Liquid Line of Descent of Anhydrous, Mantle-Derived, Tholeiitic Liquids by Fractional and Equilibrium Crystallization--an Experimental Study at 1 {middle dot}0 GPa: *Journal of Petrology*, v. 45, p. 2369–2388, doi:[10.1093/petrology/egh042](https://doi.org/10.1093/petrology/egh042).
- Walker, J.A., Gmitro, T.T., and Berg, J.H., 2002, Chemostratigraphy of the Neoproterozoic Alona Bay lavas, Ontario: *Canadian Journal of Earth Sciences*, v. 39, p. 1127–1142.
- Wolff, J., and Ramos, F., 2013, Source materials for the main phase of the Columbia River Basalt Group: geochemical evidence and implications for magma storage and transport: *Geol Soc Am Spec Pap*, v. 497.

- Wright, T.L., and Doherty, P.C., 1970, A Linear Programming and Least Squares Computer Method for Solving Petrologic Mixing Problems: Geological Society of America Bulletin, v. 81, p. 1995, doi:10.1130/0016-7606(1970)81[1995:ALPALS]2.0.CO;2.
- Xu, Y., Chung, S.-L., Jahn, B., and Wu, G., 2001, Petrologic and geochemical constraints on the petrogenesis of Permian–Triassic Emeishan flood basalts in southwestern China: Lithos, v. 58, p. 145–168, doi:10.1016/S0024-4937(01)00055-X.
- Yan, Z., Huang, Z., Xu, C., Chen, M., and Zhang, Z., 2007, Signatures of the source for the Emeishan flood basalts in the Ertan area: Pb isotope evidence: Chinese Journal of Geochemistry, v. 26, p. 207–213, doi:10.1007/s11631-007-0207-3.
- Yu, X., Chen, L.-H., and Zeng, G., 2015, Growing magma chambers control the distribution of small-scale flood basalts: Scientific Reports, v. 5, p. 16824, doi:10.1038/srep16824.
- Zanettin, B., Justin Visentin, E., Bellieni, G., Piccirillo, E., and Francesca, R., 1983, The volcanism of the North Turkana Basin, Kenya; age, succession and structural evolution: Bulletin des Centres de Recherches Exploration Production Elf-Aquitaine, v. 7.
- Zanettin, B., Justin-Visentin, E., Nicoletti, M., Piccirillo, E., and Carrelli, A., 1980, Correlations among Ethiopian volcanic formations with special references to the chronological and stratigraphical problems of the “Trap Series”: Atti Convegna Lincei, v. 47.
- Zhang, Z., Mahoney, J.J., Mao, J., and Wang, F., 2006, Geochemistry of picritic and associated basalt flows of the western Emeishan flood basalt province, China: J Petrol, v. 47, doi:10.1093/petrology/egl034.